

# Non-Abelian Atom Optics

Von der Fakultät für Mathematik und Physik der  
Gottfried Wilhelm Leibniz Universität Hannover  
zur Erlangung des Grades

**Doktor der Naturwissenschaften**

– **Dr. rer. nat.** –

genehmigte

**Dissertation**

von

**Dipl.-Phys. Andreas Jacob**

geboren am 12. Oktober 1976 in Kyritz

2009

Referent: Prof. Dr. Luis Santos

Korreferent: Prof. Dr. Ernst M. Rasel

Tag der Promotion: 25. 6. 2009

# Abstract

Although neutral atoms do not naturally present electromagnetism, artificial gauge fields may be induced by different means. This thesis is particularly concerned with the physics of cold atomic gases in the presence of artificial electromagnetism, and more specifically with those situations in which atoms experience a non-Abelian gauge field. This thesis hence brings together two rather disparate areas, namely cold gases and non-Abelian gauge fields, towards what we have called non-Abelian atom optics.

Gauge potentials, and gauge theories in general, are crucial for the understanding of fundamental forces between subatomic particles. The simplest example of a gauge potential is the vector potential in the theory of electromagnetism. In this example the different vector components are scalars, and hence they commute with each other, i.e. the gauge field is Abelian. Non-Abelian situations, where the gauge potential is a matrix whose vector components do not commute, are surprisingly scarce in nature. So far, candidates have mainly been restricted to molecular systems which are largely approachable only by means of spectroscopy. Other systems are liquid crystals which show the required non-Abelian symmetries.

An elegant derivation and description of the emergence of non-Abelian gauge potentials has been presented by Wilczek and Zee [WZ84]. These authors showed that in the presence of a general adiabatic motion of a quantum system with degenerate states, gauge potentials will appear which are traditionally only encountered in high energy physics to describe the interactions between elementary particles. Ultracold atomic clouds are particularly promising candidates for realising such scenarios, since the access to physical parameters is, from an experimental point of view, unprecedented. In this sense, it was recently proposed that properly tailored laser beams, coupled to degenerate internal electronic states of a tripod configuration, can be employed to induce non-Abelian gauge fields in the center of mass motion of cold atoms [RJOF05]. With the implementation of these proposals, ultracold atoms would offer a unique testbed for the analysis of non-trivial effects on the properties of multicomponent cold atomic systems in the presence of non-Abelian gauge fields.

This thesis is devoted to both the detailed analysis of the generation of artificial non-Abelian fields, as well as to the discussion of the novel physics expected for cold gases in the presence of these fields. After introducing some fundamentals of atom optics in chapter 1, we discuss in chapter 2 some simple laser arrangements that allow the creation of non-Abelian gauge potentials for atoms with a tripod level scheme. We describe a simple experimental scheme to achieve a constant, but non-Abelian gauge field in detail. Furthermore we investigate non-Abelian generalizations of both the Landau and the symmetric gauge in detail and discuss how these may be generated by means of realistically feasible lasers in a tripod scheme.

In chapter 3 we study the wave packet dynamics of a cloud of ultracold atoms in the presence of non-Abelian gauge fields. First, we discuss the perspectives for the observation of a non-Abelian Aharonov-Bohm effect in non-commutative interferometric arrangements. We propose a possible optical tweezer experiment including a non-Abelian flux, for which the population transfer crucially depends on the path taken. In the second part of this chapter we discuss

---

intrinsic non-Abelian effects in the dynamics of cold atomic wavepackets.

Chapter 4 deals with the energy levels of the non-Abelian Hamiltonians, i.e. the Landau levels of cold atomic gases in non-Abelian gauge fields are analyzed. In particular we identify effects on the energy spectrum and density distribution which remarkably are due purely to the non-Abelian character of the fields.

Another approach to understand these systems is to study their dispersion relation and its effects. In chapter 5 we show that in the presence of a constant but non-Abelian gauge, the dispersion law of the system presents a quasi-relativistic character (given by the appearance of a Dirac cone-anticone) similar to that recently found for electrons in graphene. Again, as for electrons in graphene, we show the possibility to achieve Veselago-type superlensing. As another consequence of the particular dispersion relation we show in chapter 6, that atom reflection shows unusual features, since an incident wave may split into two reflected waves at a barrier, an ordinary specular reflection and an additional non-specular one. Remarkably, the latter wave can exhibit negative reflection and may become evanescent if the angle of incidence exceeds a critical value. These reflection properties are crucial for future designs in non-Abelian atom optics.

In the outlook chapter 7 we discuss the inclusion of the interactions in these systems and possible remarkable features which may occur in Bose-Einstein condensates in non-Abelian gauge fields, as e.g. the possibility of creating a bright soliton with positive scattering lengths.

**keywords:** atom optics, non-Abelian gauge fields, artificial electromagnetism

# Zusammenfassung

Obwohl neutrale Atome auf herkömmliche Art keinen Elektromagnetismus zeigen, ist es dennoch möglich künstliche Eichfelder mit verschiedenen Mitteln zu erzeugen. Diese Arbeit beschäftigt sich vor allem mit der Physik kalter Gase in der Anwesenheit künstlicher elektromagnetischer Felder, insbesondere wenn die Atome nicht-Abelschen Eichfeldern ausgesetzt sind. Diese Dissertation verbindet damit zwei bisher unabhängig betrachtete Gebiete der Physik, nämlich kalte Gase und nicht-Abelsche Eichfelder, die wir zusammengeführt nicht-Abelsche Atomoptik nennen möchten.

Eichtheorien im Allgemeinen sind entscheidend für das Verständnis der Kräfte zwischen subatomaren Teilchen. Das einfachste Beispiel eines Eichpotentials ist das Vektorpotential in der Theorie des Elektromagnetismus. In diesem Beispiel sind die verschiedenen Vektorkomponenten Skalare und kommutieren deswegen miteinander, d.h. das Eichfeld ist Abelsch. Nicht-Abelsche Fälle, in denen das Eichpotential ein Matrix ist, dessen Vektorkomponenten nicht miteinander kommutieren, sind überraschend selten in der Natur zu finden. Bislang waren Kandidaten hauptsächlich auf Molekülsysteme beschränkt, die größtenteils nur mit spektroskopischen Methoden zugänglich sind. Ein weiteres Beispiel sind Flüssigkristalle, welche ebenfalls die erforderlichen nicht-Abelschen Symmetrien aufweisen.

Eine elegante Herleitung und Beschreibung der Entstehung nicht-Abelscher Eichpotentiale wurde durch Wilczek und Zee [WZ84] aufgezeigt. Diese Autoren bewiesen, dass während der adiabatischen Bewegung eines entarteten Quantensystems Eichpotentiale auftreten, die normalerweise nur in der Hochenergiephysik angetroffen werden, um Wechselwirkungen zwischen Elementarteilchen zu beschreiben. Ultrakalte Atomwolken sind insbesondere Kandidaten für die Verwirklichung solcher Szenarien, weil die Zugriffsmöglichkeiten auf die physikalischen Parameter aus experimenteller Sicht beispiellos ist. In dieser Hinsicht wurde vor kurzem vorgeschlagen, dass entsprechend abgestimmte und mit entarteten internen elektronischen Zuständen eines Tripod-Termschemas gekoppelte Laserstrahlen verwendet werden können, um nicht-Abelsche Eichfelder für die Bewegung des Massenschwerpunktes zu erzeugen [RJOF05]. Mit der Verwirklichung dieser Vorschläge würden ultrakalte Atome eine einmalige Testumgebung für die Untersuchung dieser nichttrivialen Effekte an mehrkomponentigen Systemen in Gegenwart nicht-Abelscher Eichfelder bieten.

Diese Dissertation widmet sich sowohl der detaillierten Untersuchung der Erzeugung nicht-Abelscher Eichfelder, als auch der Diskussion neuartiger Physik, die man für kalte Gase in diesen Feldern erwartet. Nach einer Einführung in die Grundlagen der Atomoptik in Kapitel 1 erörtern wir in Kapitel 2 einige einfache Laseranordnungen, die die Erzeugung nicht-Abelscher Eichfelder für Atome mit Tripod-Termschema erlauben. Wir beschreiben im Detail ein einfaches experimentelles Schema, um ein konstantes, aber nicht-Abelsches Eichfeld zu erzeugen. Die nicht-Abelsche Verallgemeinerung sowohl der Landau-Eichung, als auch der symmetrischen Eichung werden ebenfalls untersucht. Auch für diese Fälle erörtern wir, wie man sie mit realistischen Laserkonfigurationen in einem Tripod-Termschema erzeugen kann.

In Kapitel 3 erforschen wir die Dynamik von Wellenpaketen einer Wolke ultrakalter Atome

---

unter dem Einfluss nicht-Abelscher Eichfelder. Zuerst diskutieren wir hier das Auftreten eines nicht-Abelschen Aharonov-Bohm Effektes in nicht-kommutierenden interferometrischen Anordnungen. Wir schlagen weiterhin ein mögliches Experiment mit optischen Pinzetten vor, dass zu einem nicht-Abelschen Fluss führt. In diesem hängt die Änderung der Besetzungszahlen entscheidend vom eingeschlagenen Pfad ab. Im zweiten Teil dieses Kapitels diskutieren wir weitere immanente nicht-Abelsche Effekte in der Dynamik kalter atomarer Wellenpakete.

Kapitel 4 beschäftigt sich mit den Energieniveaus (Landau-Niveaus) nicht-Abelscher Hamiltonfunktionen kalter atomarer Gase. Insbesondere identifizieren wir Auswirkungen auf das Energiespektrum und die Dichteverteilung, die einzig durch den nicht-Abelschen Charakter des Feldes entstehen.

Ein anderer Zugang zu diesen Systemen ist die Untersuchung der Dispersionsrelation und ihrer Auswirkungen. Im Kapitel 5 zeigen wir, dass in Gegenwart eines konstanten aber nicht-Abelschen Eichfeldes die Dispersionsrelation, wie unlängst auch in Graphen gefunden, einen quasi-relativistischen Charakter (angesichts des Auftretens eines Dirac Doppelkegels) annimmt. Ferner, wie für Elektronen in Graphen, demonstrieren wir die Möglichkeit eine Veselago-Superlinse zu erzeugen. Als eine weitere Auswirkung dieser speziellen Dispersionsrelation zeigen wir in Kapitel 6, dass atomare Reflektion besondere Eigenschaften hat. Eine einfallende Welle kann sich an einer Barriere in zwei reflektierte Wellen aufteilen, eine normale, symmetrisch gespiegelte Reflektion und eine zusätzliche, nicht symmetrisch gespiegelte. Bemerkenswerterweise kann letztere negative Reflektion aufweisen und sogar evaneszent werden, wenn der Einfallswinkel einen kritischen Wert überschreitet. Diese Reflektionseigenschaften sind entscheidend für die zukünftige Entwicklung nicht-Abelscher Atomoptik.

Im Ausblick in Kapitel 7 beschreiben wir die Einführung von Wechselwirkungen in diesen Systemen. Wir diskutieren bemerkenswerte Eigenschaften die in Bose-Einstein-Kondensaten in nicht-Abelschen Eichfeldern auftreten können, wie z.B. die Möglichkeit der Erzeugung heller Solitonen mit positiver Streulänge.

**Schlagwörter:** Atomoptik, nicht-Abelsche Eichfelder, künstlicher Elektromagnetismus

# Contents

<b>1</b>	<b>Introduction</b>	<b>1</b>
1.1	Overview	1
1.2	Atom-Light-Interaction	1
1.2.1	Two-level atom	1
1.2.2	Laser Cooling	3
1.2.3	Dark states	4
1.2.4	Trapping of neutral atoms	5
1.3	Atom Optics	7
1.3.1	Thermal de Broglie wavelength	7
1.3.2	Atom Mirror	7
1.3.3	Atom Interferometry	8
1.3.4	Optical Lattices	8
1.4	Bose-Einstein condensation	10
1.4.1	Interactions in BECs: Introduction into the GPE	11
1.4.2	Solitons	12
<b>2</b>	<b>Artificial Electromagnetism</b>	<b>13</b>
2.1	Introduction	13
2.2	Rotation	14
2.3	Discrete Systems: Lattices	15
2.4	Continuous Systems: Lambda and Tripod schemes	20
2.4.1	Effective gauge fields for non-degenerate eigenstates	20
2.4.2	Effective gauge fields for degenerate eigenstates	22
2.4.3	Artificial Abelian fields: Three-level $\Lambda$ -systems	25
2.4.4	Non Abelian electromagnetism: Four-level tripod-systems	26
2.5	General conditions for non-Abelian gauges	33
2.5.1	Constant non-Abelian gauge	33
2.5.2	Landau Gauge	36
2.5.3	Symmetric Gauge	38
2.6	Summary	39
<b>3</b>	<b>Non-Abelian Atom Optics</b>	<b>41</b>
3.1	Introduction	41
3.2	Laser-induced non-Abelian gauge fields	41
3.3	Non-Abelian Aharonov-Bohm effect	42
3.4	Wavepackets in free space	46
3.5	Summary	52

<b>4</b>	<b>Non-Abelian Landau Levels</b>	<b>53</b>
4.1	Introduction . . . . .	53
4.2	Landau Levels . . . . .	53
4.3	Fock-Darwin spectrum . . . . .	55
4.4	Laser-induced non-Abelian Gauge fields . . . . .	56
4.4.1	Constant intensities . . . . .	56
4.4.2	Landau-like gauge . . . . .	56
4.4.3	Symmetric gauge . . . . .	57
4.5	Constant non-Abelian gauge . . . . .	57
4.6	Landau-like Non-Abelian gauge . . . . .	57
4.6.1	Periodic boundary conditions . . . . .	57
4.6.2	Absorbing boundary conditions . . . . .	60
4.6.3	de Haas-van Alphen-Effect . . . . .	63
4.6.4	Modified de Haas-van Alphen-Effect . . . . .	64
4.7	Symmetric gauge . . . . .	66
4.8	Summary . . . . .	69
<b>5</b>	<b>Quasi-Relativistic Physics with Cold Gases. Veselago Lensing</b>	<b>71</b>
5.1	Introduction . . . . .	71
5.2	Laser-induced non-Abelian gauge fields . . . . .	71
5.3	Dispersion relation . . . . .	73
5.4	Veselago lensing . . . . .	75
5.5	Summary . . . . .	77
<b>6</b>	<b>Negative Reflection under Non-Abelian Gauge Fields</b>	<b>79</b>
6.1	Introduction . . . . .	79
6.2	Laser arrangement . . . . .	79
6.3	Dispersion law . . . . .	80
6.4	Double and negative reflection of atoms . . . . .	81
6.5	Summary . . . . .	87
<b>7</b>	<b>Trapped and Interacting Bose Gases in Non-Abelian Gauge Fields</b>	<b>89</b>
7.1	Trapped gas in the presence of a “simple” non-Abelian gauge: Single branch case	89
7.2	Trapped gas in the presence of a “simple” non-Abelian gauge: Two branch case	92
7.3	Interaction Hamiltonian in the tripod system . . . . .	92
7.4	Effects of interactions in trapped condensates in the presence of the “simple” gauge	97
7.5	Solitons in 1D systems in the presence of the “simple” non-Abelian gauge . . .	98
<b>8</b>	<b>Conclusions</b>	<b>103</b>
	<b>Bibliography</b>	<b>104</b>
	<b>List of Publications</b>	<b>117</b>
	<b>Acknowledgements</b>	<b>119</b>



# Chapter 1

## Introduction

### 1.1 Overview

Over the last few decades atom optics has become one of the most active and interesting research fields in atomic physics. In atom optics, compared to conventional photon optics, the roles of light and matter are often reversed, using light to manipulate atomic matter waves. In this chapter we give a brief overview of basic atom optics ideas. Section 1.2 is devoted to an introduction to atom-light interaction as the fundamental principle for cooling and manipulating cold atoms. In section 1.3 we discuss a selection of some atom optics basics which are relevant for this thesis, such as the ideas of atomic mirror, atom interferometer and periodic potentials for atoms. In section 1.4 we study the effects of a gradual decrease in temperatures down to nK, and discuss the consequences of reaching the Bose-Einstein condensation regime.

### 1.2 Atom-Light-Interaction

#### 1.2.1 Two-level atom

To describe the basic effects of atom-light interaction it is sufficient to consider a two-level atom in a monochromatic light field, including the spontaneous emission  $\gamma$  of light as a dissipative effect, see fig. 1.1.

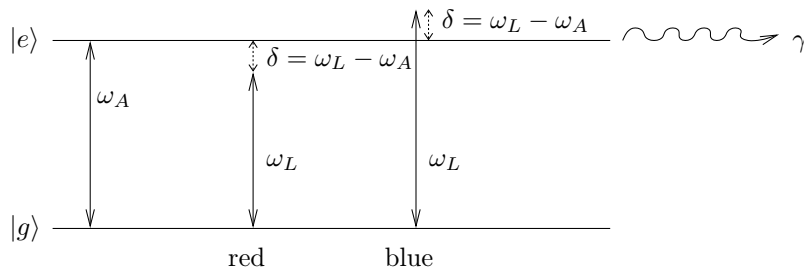


Fig. 1.1: Atomic scheme for a two-level atom.  $\delta = \omega_L - \omega_A$  is the detuning of the laser from the atomic transition. The laser can have less energy than the transition (red detuned,  $\delta < 0$ ), or more energy than the transition (blue detuned,  $\delta > 0$ ) or it can be resonant ( $\delta = 0$ ).

The interaction between the atom and the laser light induces a mechanical force acting on

the center of mass of the atom. Without entering into all calculational details (for a rigorous discussion see e.g. ref. [Mey01]) we just mention that the resulting average force exerted by the light on the atom acquires the form:

$$F = \hbar q_i \gamma \rho_{ee} - 2\hbar q_r \delta \rho_{ee} \quad (1.1)$$

where  $\delta$  is the laser detuning (laser frequency minus transition frequency),  $\gamma$  is the spontaneous emission rate,  $\Omega(z) = -e\mathbf{E}(z)\mathbf{d}/\hbar$  is the Rabi frequency (with  $\mathbf{E}(z)$  the electric field and  $\mathbf{d}$  the electric dipole associated to the two-level transition),  $q_r + iq_i = \frac{1}{\Omega} \frac{\partial \Omega}{\partial z}$  and  $\rho_{ee} = \langle e|\rho|e\rangle$  is the stationary population of the excited state.

The force eq. (1.1) consists clearly of two parts. The first term on the rhs is the radiation pressure force,  $F_{rp}$ , which may be explained on the grounds of absorption-spontaneous emission cycles. The net force from spontaneous emission is 0 (since the photons are emitted spontaneously in arbitrary directions) whereas the net force induced by the momenta of the absorbed lasers photons is given by  $F = \hbar\kappa\gamma\rho_{ee}$  where  $\hbar\kappa$  is the momentum transfer per absorbed photon. The radiation pressure force is a dissipative force because the action of spontaneous emission cannot be reversed, since the associated recoil gives a kick in a random direction. Hence, the radiation pressure force can be used for cooling.

The second term on the rhs in eq. (1.1) is called dipole force and it is induced by the spatial dependence of the laser intensity. The dipole force can be explained by recalculation of the energies of the ground and excited state of a two level atom up to 2nd order in perturbation theory. This leads to a force acting on ground-state atoms that corresponds to the left term on the rhs in eq. (1.1). The dipole force is a conservative force and can therefore be used for trapping atoms without any heating (as long as the detuning  $|\delta| \gg \gamma$ ). For red detuning ( $\delta < 0$ ) the atom in the ground state is driven towards regions of larger intensities (and it may be trapped there) whereas for blue detuning ( $\delta > 0$ ) the atom is driven towards regions of lower intensities (the laser repels the atoms), see fig. 1.2.

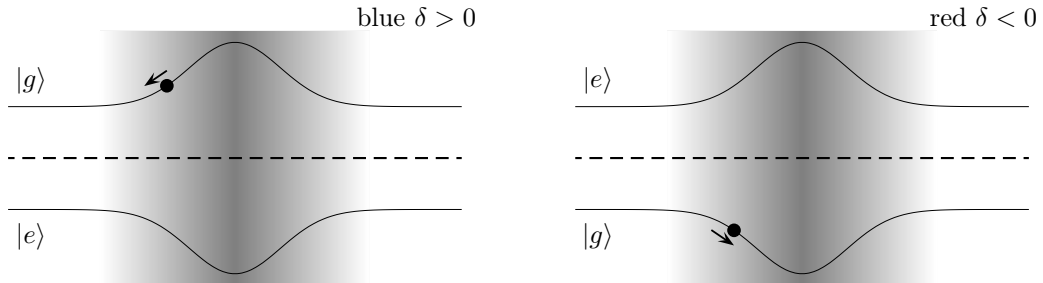


Fig. 1.2: Energy shifts through the dipole force: for blue detuning ( $\delta > 0$ ) the atoms are expelled from the laser beam, for red detuning ( $\delta < 0$ ) the atoms are attracted towards the high intensity

The relative role of the radiation pressure and the dipole force depends on the particular case considered. For laser plane waves there is no dipole force (since the laser intensity is constant) but the absorption of  $\hbar\mathbf{k}$  from the plane wave leads to a radiation pressure force. On the other hand, for a laser standing wave the radiation pressure force  $\mathbf{F}_{rp}$  vanishes, but the minima and

maxima of the standing wave create a space-dependent dipole force. As mentioned above, the radiation pressure is crucial in cooling techniques, whereas the dipole force (and the associated dipole potential) is fundamental for the manipulation of atoms, e.g. by optical tweezers or in the so-called optical lattices (see section 1.3.4).

### 1.2.2 Laser Cooling

As an example of the mechanical effects induced by radiation pressure on atoms we would like to comment briefly on laser cooling. Laser cooling has been a prerequisite for the intensive studies in the field of atom optics over the last few years. The importance of these techniques was recognized with the Nobel prize in 1997 [Chu98, CT98, Phi98]. In this section we briefly mention the simplest (and first proposed) laser cooling technique, i.e. Doppler cooling [HS75, WD75]. For a more detailed introduction to laser cooling see [MdS99].

As the name suggests, Doppler cooling is based on the fact that the Doppler shift ( $-\mathbf{k} \cdot \mathbf{v}$ ) leads to a velocity-dependent detuning. One may consider a two-level atom as the one discussed previously and two counterpropagating lasers with the same frequency ( $\omega_L$ ) and intensity (fig. 1.3). It is clear from fig. 1.4 that if the detuning  $\delta < 0$  then counterpropagating photons are closer to resonance, and hence are absorbed with larger probability. After the photon absorption, a spontaneous emission may occur in a random direction, leading to an atom recoil in the opposite direction. This absorption-emission cycle will lead to a net viscous force, which for  $\mathbf{v}$  in the vicinity of 0 acquires the form  $-\eta\mathbf{v}$ , with  $\eta$  the friction coefficient, which depends on the parameters of the system. The friction force is indeed very strong and this arrangement has accordingly been called “optical molasses”.

The random recoil following a spontaneous emission and the randomness in the light absorption lead to a momentum diffusion, which sets a limit to the temperature reachable using this technique:  $T_{\text{Doppler}} = \frac{\hbar\gamma}{2k_B}$ , which for e.g.  $^{23}\text{Na}$  amounts for approximately  $240 \mu\text{K}$ . A first experimental demonstration of Doppler cooling is discussed in refs. [PM82, ABLM82]. Lower temperatures, down to tens of recoil temperature  $T_{\text{rec}} = \hbar k^2/2mk_B$ , are possible by means of polarization gradient techniques, such as Sisyphus cooling [LWWP88, DCT89]. But these techniques are limited by  $T_{\text{rec}}$ .

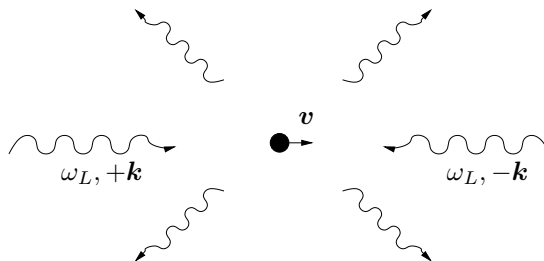


Fig. 1.3: Doppler cooling is based on the Doppler effect, see the atomic level scheme in fig. 1.4. The momentum transfer during the absorption leads to slowing down of the atom, whereas the phonon emission in a random direction averages out over time.

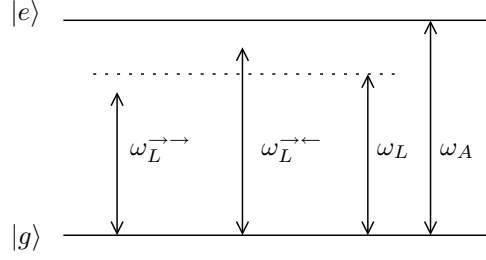


Fig. 1.4: Doppler cooling for a red detuned laser ( $\omega_L < \omega_A$ ). Atoms counterpropagating to the laser will see it with a higher frequency  $\omega_L^{\rightarrow\leftarrow} = \omega_L + \mathbf{k} \cdot \mathbf{v}$  and are more likely to absorb a photon because they are closer to resonance. Atoms co-propagating with the laser will see it with a frequency  $\omega_L^{\rightarrow\rightarrow} = \omega_L - \mathbf{k} \cdot \mathbf{v}$ .

### 1.2.3 Dark states

In the previous sections we discussed the simplified case of a two-level atom. However, many relevant systems involve more than two levels. Multilevel atoms lead to interesting novel physics induced by quantum interference, and in particular to the key concept of dark states, which plays a crucial role at many points of this thesis.

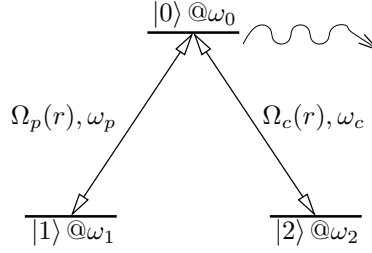


Fig. 1.5: Three levels  $\Lambda$ -system with laser transitions as described by the Hamiltonian (1.2) (except spontaneous emission from  $|0\rangle$ )

In this section we consider the case of a  $\Lambda$ -form three-level atom with two ground states ( $|1\rangle$  and  $|2\rangle$ ) and one excited state ( $|0\rangle$ ) which are coupled as shown in fig. 1.5 by the so-called control laser (with corresponding Rabi frequency  $\Omega_C(r)$  and frequency  $\omega_C$ ) and the so-called probe laser (with Rabi frequency  $\Omega_P(r)$  and frequency  $\omega_P$ ). The system is described by the Hamiltonian

$$H = H_{CM} + \sum_{j=0}^2 \hbar \omega_j |j\rangle \langle j| + \hbar (\Omega_P e^{-i\omega_P t} |0\rangle \langle 1| + \text{H.c.}) + \hbar (\Omega_C e^{-i\omega_C t} |0\rangle \langle 2| + \text{H.c.}), \quad (1.2)$$

where  $H_{CM}$  denotes the Hamiltonian for the center of mass motion. At this point, to simplify the discussion of the dark state concept [AO76], we do not consider the center of mass motion, although we may already anticipate that it plays a fundamental role in important laser cooling techniques and also at many points in this thesis.

Solving the Schrödinger equation  $i\hbar|\dot{\Psi}\rangle = H|\Psi\rangle$ , we obtain for each component of  $|\Psi\rangle = \sum_{j=0}^2 \Psi_j(\mathbf{r}, t)|j\rangle$  a set of coupled equations:

$$i\hbar\dot{\Psi}_0 = \hbar\omega_0\Psi_0 + \hbar(\Omega_P e^{-i\omega_P t}\Psi_1 + \Omega_C e^{-i\omega_C t}\Psi_2), \quad (1.3)$$

$$i\hbar\dot{\Psi}_1 = \hbar\omega_1\Psi_1 + \hbar\Omega_P^* e^{i\omega_P t}\Psi_0, \quad (1.4)$$

$$i\hbar\dot{\Psi}_2 = \hbar\omega_2\Psi_2 + \hbar\Omega_C^* e^{i\omega_C t}\Psi_0. \quad (1.5)$$

We remove the explicit time-dependence of the Hamiltonian by transforming

$$\Psi_0 = \Phi_0 e^{-i(\omega_1 + \omega_P)t}, \quad (1.6)$$

$$\Psi_1 = \Phi_1 e^{-i\omega_1 t}, \quad (1.7)$$

$$\Psi_2 = \Phi_2 e^{-i(\omega_1 + \omega_P - \omega_C)t}, \quad (1.8)$$

obtaining

$$i\hbar\dot{\Phi}_0 = \epsilon_{01}\Phi_0 + \hbar\Omega_C\Phi_2 + \hbar\Omega_P\Phi_1, \quad (1.9)$$

$$i\hbar\dot{\Phi}_1 = \hbar\Omega_P^*\Phi_0, \quad (1.10)$$

$$i\hbar\dot{\Phi}_2 = \epsilon_{21}\Phi_2 + \hbar\Omega_C^*\Phi_0, \quad (1.11)$$

where  $\epsilon_{21} = \hbar(\omega_2 - \omega_1 + \omega_C - \omega_P)$  is the detuning from the 2-photon resonance ( $|1\rangle \leftrightarrow |2\rangle$ ) and  $\epsilon_{01} = \hbar(\omega_0 - \omega_1 - \omega_P)$  is the detuning from the single photon resonance ( $|1\rangle \leftrightarrow |0\rangle$ ). In the following we consider the resonant case  $\epsilon_{21} = 0$ . From the form of the equations it becomes clear that the state

$$|D\rangle = \frac{1}{\Omega}(\Omega_C|1\rangle - \Omega_P|2\rangle) \quad \Omega^2 = \Omega_C^2 + \Omega_P^2 \quad (1.12)$$

is not coupled to  $|0\rangle$ . As shown in fig. 1.6, the original  $\Lambda$  system reduces to an uncoupled dark state  $|D\rangle$ , and two coupled states, namely  $|0\rangle$  and the bright state

$$|B\rangle = \frac{1}{\Omega}(\Omega_P|1\rangle + \Omega_C|2\rangle). \quad (1.13)$$

Up to this point we have not considered the spontaneous emission from  $|0\rangle$  into the ground states. This incoherent process populates both the bright and the dark state. Note however, that the population pumped in this way into  $|D\rangle$  cannot abandon the dark state, since it is uncoupled from  $|0\rangle$ . This phenomenon receives the name of population trapping and it is crucial for ideas like optical pumping and VSCPT cooling. The latter allows overcoming the recoil temperature limit of laser cooling [AAK<sup>+</sup>88].

#### 1.2.4 Trapping of neutral atoms

Trapping neutral atoms is of course crucial for the controlled study of cold gases. Trapping may be induced by “conservative” traps based on the Zeeman effect for low-field seeking states (using quadrupolar magnetic fields [MPP<sup>+</sup>85, BEM87] or Ioffe-Pritchard configurations [Pri83]) or by means of optical dipole traps, based on the above mentioned dipole force [CBAC86, RPC<sup>+</sup>87,

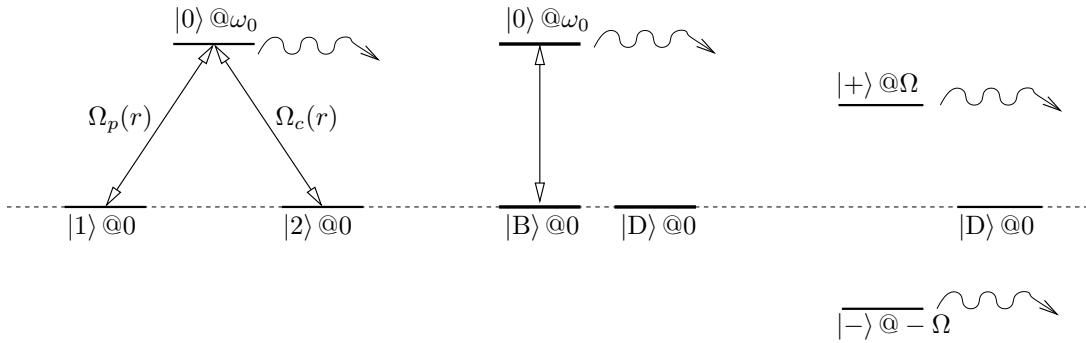


Fig. 1.6: Different bases for the  $\Lambda$ -atom. The energies are shifted to  $\omega_1 = \omega_2 = 0$ : bare states with laser couplings (left), space dependent dark-bright state basis (middle) and dressed states basis (right).

GLJP88, MCH93, TK96]. The radiation pressure may also be employed to form a dissipative trap, which combines both the molasses effect and a restoring force. Such traps are called magneto-optical traps (MOT) [RPC<sup>+</sup>87]. In this section we just briefly comment on the MOT as an example of how atoms may be trapped. A more rigorous description of MOTs and other trapping schemes may be found e.g. in [MdS99].

Here we discuss the idea focusing in the 1D case. This scheme can be easily generalized to 3D. We consider atoms with a ground state with angular momentum  $J_g = 0$  and an excited state with  $J_e = 1$ . The atom is affected by two counter-propagating lasers along  $z$ -axis with the same intensity and frequency (red detuned from the atomic transition) but opposite circular polarization (see fig. 1.7). A pair of coils in anti-Helmholtz configuration induce an inhomogeneous magnetic field, which leads to an inhomogeneous linear dependence of the Zeeman energy  $\propto mz$ . If an atom moves to the right for  $z > 0$ , it absorbs preferentially the counter-propagating photon, and will hence be pushed to the left. The contrary is true for an atom at  $z < 0$ . Note that the arrangement is similar to that of Doppler cooling but with the added ingredient of the spatial dependence of the detuning. The result is a force (in the vicinity of  $z = 0$ ) of the form  $-\eta v - \kappa z$ , where  $\eta$  and  $\kappa$  respectively are the friction and restoring coefficients. Therefore the atom is not only cooled but also spatially confined.

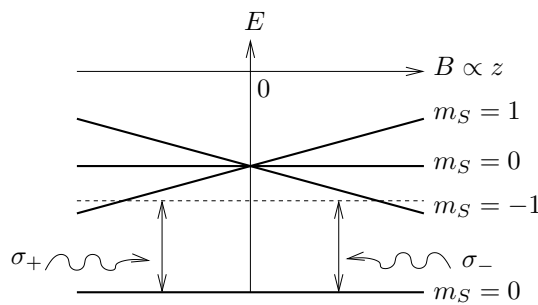


Fig. 1.7: Level scheme of a magneto-optical trap (MOT), for details see text

## 1.3 Atom Optics

### 1.3.1 Thermal de Broglie wavelength

In 1923 Louis de Broglie [dB37] suggested that, similar to the particle-wave duality of radiation, matter should behave also as a wave, with an associated de Broglie wavelength  $\lambda = h/p$ , where  $p$  is the momentum and  $h$  is Planck's constant. The idea of a (quasi-)localized particle is recovered by means of the wavepacket concept, i.e. a superposition of plane waves with different frequencies that yield a localized solution.

Associated with this idea and the concept of temperature, here we encounter the key idea of the thermal de Broglie wavelength. Let us consider a gas of particles in free space in thermal equilibrium. The velocity distribution of the particles obeys the Maxwell-Boltzmann velocity distribution [Hua87]

$$f_0(\mathbf{p}) \propto e^{-(\mathbf{p}-\mathbf{p}_0)^2/2mk_B T}. \quad (1.14)$$

The width of the momentum distribution is directly related to the temperature  $\Delta p = \sqrt{mk_B T} \propto \sqrt{T}$ . This is the reason why cooling is actually achieved by narrowing the velocity distribution. Due to the uncertainty principle the narrower the momentum distribution (i.e. the lower the temperature) the larger the spatial delocalization of the particles, i.e. the more wave-like they are. We can characterize this delocalization by means of the so-called thermal de Broglie wavelength

$$\lambda_T = \sqrt{\frac{2\pi\hbar^2}{mk_B T}}. \quad (1.15)$$

Rubidium atoms at room temperature have  $\lambda_T \approx 1 \cdot 10^{-11}\text{m}$ , which is even smaller than the Bohr radius ( $\simeq 0.5\text{\AA}$ ). This of course explains why quantum mechanical effects are not observable at high temperatures. On the contrary a combination of laser cooling and evaporative cooling allows for temperatures of the order (or even below) 100 nK, for this temperature  $\lambda_T \approx 0.6 \mu\text{m}$ , i.e. about 10000 times the Bohr radius. In that case matter wave phenomena are obviously dominant. Indeed the atoms may enter into the regime of quantum degeneracy as we discuss in following sections. Matter wave behaviour was first observed in electrons [MSS53] and neutrons [GO79]. Atom optics considers the matter wave phenomenology of cold atoms. However, matter wave behaviour is not restricted to single atoms. Diffraction and interference have also been achieved with big molecules such as Fullerenes by Zeilinger's group [ANVA<sup>+</sup>99]. In this section we briefly comment on some topics related to atom optics which are particularly relevant for this thesis. For a good (and much more general) review see ref. [Mey01].

### 1.3.2 Atom Mirror

One of the most basic optical devices is a mirror. Cold atoms may be reflected by a sufficiently strong repulsive potential. From our discussion of the dipole force we know that a blue detuned laser induces a repulsive dipole potential. To use the dipole force efficiently to reflect atoms, Cook and Hill [CH82] suggested an evanescent wave mirror. There, a laser is totally reflected inside a prism and creates an evanescent wave outside the prism, which induces a dipole potential with an exponential profile. The first implementation was accomplished by Balykin and collaborators [BLOS87, BLOS88]. Alternatively, a sheet of alternating currents [RAB<sup>+</sup>95] can produce a magnetic field above its surface, which decreases exponentially with distance from

the surface. An atom with a magnetic moment antiparallel oriented to the mirror experiences a repulsive potential (magnetic mirror).

### 1.3.3 Atom Interferometry

Atom interferometers are devices that coherently split, let evolve, and recombine matter waves. At the recombination an interference pattern may appear that yields precise information about the phase accumulated during the evolution. In this subsection we just review the main ideas very briefly. For more details see e.g. [BMR99, GDSB01] or the book of Berman [Ber97].

In general, one distinguishes two kinds of atom interferometers: the internal state interferometer and the de Broglie interferometer. The internal state was proposed by Bordé in [Bor89]. There, a 2-level-atom in its ground state is split by a laser into a superposition of ground state and excited state. These two states then undergo a different time evolution (the excited state absorbs a photon). A second laser later recombines both states and yields an interference pattern. Experiments can e.g. measure the effects of the geometric phase accumulated in the different paths [MRG<sup>+</sup>92]. The de Broglie interferometers [ROB<sup>+</sup>95] do not explicitly employ the internal states of the atoms but split the atoms spatially without changing the internal state, allowing later a recombination. Using lasers as beam splitters one can also observe Bragg scattering from a standing laser wave [GML95].

The applications for atom interferometers are numerous: Atom clocks, precision measurement (gravitational constant  $G$  and tests of Newton's laws resp. effects of alternative gravitational theories [SMB<sup>+</sup>98] [LCP99], fine-structure constant  $\alpha$ ), gravimetry, general relativity tests etc. Furthermore atom interferometers can be used to measure the rotation of the interferometer itself or that of the Earth (Sagnac effect [ABS94]) [RKWH91, HN93]. For the experiments a variety of atoms are used, e.g. alkali (Li, Na, Rb, Cs), earth-alkaline metastable atoms (Mg<sup>\*</sup>, Ca<sup>\*</sup>), rare gas metastable atoms (He<sup>\*</sup>, Ar<sup>\*</sup>, Ne<sup>\*</sup>), and molecules (I<sub>2</sub>, Na<sub>2</sub>, ...). Other experimentalists are concerned with extending the experiments to bigger objects, like C<sub>60</sub>, organic molecules, and possibly even viruses. Recently, also Bose-Einstein-Condensates (see following sections) have been used for interferometry. They remove some difficulties from atom interferometry because they have a narrower momentum distribution and can permit e.g. a longer interaction time and a higher particle flux [TSK<sup>+</sup>00].

### 1.3.4 Optical Lattices

An interesting possibility for manipulation of cold atoms is provided by the so-called optical lattices. Two counterpropagating lasers induce a stationary wave which leads to a periodic dipole potential (if the lasers are far detuned, we may neglect spontaneous emission and consider the system as conservative)

$$V(z) = V_0 \sin^2(qz) \tag{1.16}$$

where  $q = 2\pi/\lambda$ , with  $\lambda$  the laser wavelength, giving a lattice period of  $\lambda/2$ . Remarkably, the physics of atoms in optical lattices is similar to that of electrons in crystals, linking cold gases physics with fundamental problems of condensed-matter theory. Moreover, optical lattices provide the additional advantage of being free from defects (and of course of phonons). As a consequence, cold atoms in optical lattices have attracted a large interest in recent years. For details see the reviews [LSA<sup>+</sup>07, BDZ08] and also earlier reviews [JD96, GR01, BG05].



As for the case of electrons in solid state physics, the periodicity of the potential results in a band-like structure for the allowed energies of the atoms inside the lattice. The different bands are characterized by a given dispersion law  $E_\nu(\kappa)$  as a function of the quasi-momentum  $\kappa$  inside of the first Brillouin zone, which has an associated group velocity  $v_g = \partial E_\nu / \partial \kappa$ . Forbidden regions (gaps) also appear (see fig. 1.8). The particular dispersion law in the different bands results in striking observable phenomena for cold atoms in optical lattices, as e.g. Bloch oscillations [DPR<sup>+</sup>96, WBM<sup>+</sup>96, MMC<sup>+</sup>01]. The latter are induced when a constant force (e.g. gravity) is applied along the lattice axis. This force drags the wavefunction through the dispersion relation as shown in fig. 1.9. The periodic character (positive and negative) of the group velocity  $v_g$  induces an oscillatory motion of the atom, i.e. the Bloch oscillations.

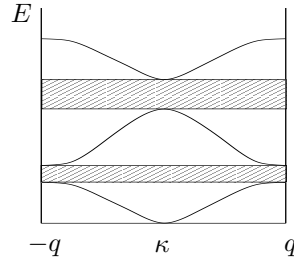


Fig. 1.8: Band structure for the first Brillouin zone for a periodic potential. Allowed energy  $E$  vs. quasi momentum  $\kappa$ , gaps (shaded areas), energy bands are periodic in quasi momentum with period  $2q = 2\frac{2\pi}{\lambda}$

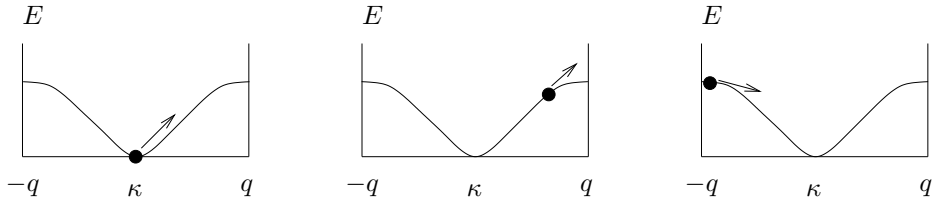


Fig. 1.9: Bloch oscillation in a periodic potential ( $\kappa$ =quasi momentum), shown is a wavepacket prepared in the lowest band (see fig. 1.8), a constant force drags the wavepacket through the band resulting in an oscillatory motion of the atom in  $x$ -space.

Optical lattices have been thoroughly studied during the last years, including the observation of band structure [GBM<sup>+</sup>01, DSH<sup>+</sup>02, FMB<sup>+</sup>02], coherent matter wave interferometry [AK98, MCM<sup>+</sup>02], studies of superfluidity of moving condensates [BCF<sup>+</sup>01], quantum chaos [HHB<sup>+</sup>01], collapse and revival in a matter wave field [GMHB02], etc. Interestingly for sufficiently deep optical lattices, the physics may be reduced to the lowest energy band. The Hamiltonian describing an interacting Bose gas can then be reduced to a Bose-Hubbard Hamiltonian (for more details see e.g. [JZ05])

$$H_{BH} = -J \sum_{\langle i,j \rangle} b_i^\dagger b_j + \frac{U_0}{2} \sum_j b_j^\dagger b_j^\dagger b_j b_j + \sum_j \epsilon_j b_j^\dagger b_j, \quad (1.17)$$

where  $b_i, b_i^\dagger$  are the annihilation and creation operators of particles in the  $i$ -th lattice site,  $J$  is the hopping rate,  $U_0$  is the interaction coupling constant describing the on-site interactions, and  $\epsilon_j$  describes a (possibly inhomogeneous) local on-site energy. The coefficients  $J$  and  $U_0$  are a function of the system parameters. As predicted for this model [FWGF89, JBC<sup>+</sup>98], a superfluid to Mott insulator transition has been observed in a remarkable experiment in 2002 [GME<sup>+</sup>02]. The latter experiment has generated a huge theoretical and experimental interest on optical lattices, which we do not review at this point, since it lies well beyond the scope of this thesis.

## 1.4 Bose-Einstein condensation

Bose-Einstein condensation (BEC) in bosonic gases was predicted by A. Einstein in 1925 [Ein24, Ein25] based on quantum statistic ideas developed by Bose [Bos24]. It took seven decades until it was experimentally achieved [AEM<sup>+</sup>95, DMA<sup>+</sup>95, BSTH95] in a clean way (although the idea of BEC played of course a major role in the theory of superfluid Helium [Lon38]). The experimental realization of BEC was awarded with the Nobel prize 2001 to W. Ketterle [Ket02], E. Cornell and C. E. Wieman [CW02].

Bose-Einstein condensation is a phase transition into a state characterized by the macroscopic occupation of a single quantum state. Remarkably, this transition occurs even in an ideal gas, i.e. in the absence of any interparticle interaction. A careful discussion of BEC in ideal gases may be found in many textbooks [Hua87]. Here we just briefly mention the idea. As discussed in section 1.3, when the temperature decreases the thermal de Broglie wavelength  $\lambda_T \propto \frac{1}{\sqrt{T}}$  increases, see fig. 1.10. For a sufficiently low temperature and sufficiently large particle density  $\lambda_T$  becomes greater than the interparticle distance  $R$ . Below this temperature quantum statistics starts to play an important role. In a homogeneous 3D Bose gas in free space the ground state becomes macroscopically populated when the phase space density  $\rho\lambda_T^3 > 2.612$ . This criterion defines the critical temperature ( $T_C$ ) for the onset of condensation

$$T_C = \frac{2\pi\hbar^2}{mk_B} \left( \frac{n}{2.612} \right)^{2/3}. \quad (1.18)$$

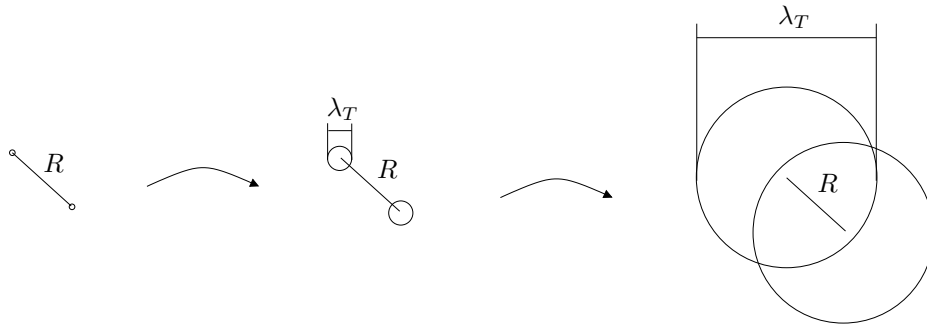


Fig. 1.10: Interparticle distance  $R = \rho^{-1/3}$  versus thermal de Broglie wavelength  $\lambda_T$ , the temperature decreases from left to right

The condensate fraction may then be expressed as:

$$\frac{N_0(T)}{N} = 1 - \left( \frac{T}{T_C} \right)^{3/2}. \quad (1.19)$$

Typically, in experiments on alkali atoms, and due to the very low density of the gas samples, extremely low temperatures (around 100 nK) are necessary to achieve condensation. Normally a combination of laser and evaporative cooling, and of different trapping techniques is required.

### 1.4.1 Interactions in BECs: Introduction into the GPE

The previous discussion dealt with ideal, i.e. non-interacting particles. Interactions, however, play a crucial role in quantum gases, inspite of their extreme diluteness (with typical densities below  $10^{14}$  atoms/cm<sup>3</sup>). In typical experiments, these interactions may be considered as short-range van-der-Waals like interactions, decaying as  $1/r^6$ . In dilute gases we are interested in asymptotic scattering properties. In principle one should perform a full analysis taking into account scattering in different partial waves. However, at the very low temperatures considered here, the centrifugal barrier associated with partial waves with non-zero angular momentum becomes an unsurmountable barrier for such low energetic particles, and consequently only *s*-wave scattering is significant. The *s*-wave scattering is characterized by a single parameter, namely the *s*-wave scattering length *a*. Hence, we just need the value of *a* to fully describe the scattering problem. Therefore, we may substitute the actual interaction potential by an equivalent contact pseudopotential of the form

$$V(\mathbf{r}) = \frac{4\pi a \hbar^2}{m} \delta(\mathbf{r}) \equiv g \delta(\mathbf{r}). \quad (1.20)$$

Let us assume the following ansatz (for foundations see e.g. the review paper of Dalfovo et al. [DGPS99] or the books of Pitaevskii and Stringari [PS04] and Pethick and Smith [PS02]). We can separate the condensate part  $\Psi(r, t)$  from the excitations  $\delta\hat{\Phi}'$  because the condensate part is macroscopic and can be treated as a classical field

$$\hat{\Phi}(r, t) = \Psi(r, t) + \delta\hat{\Phi}'(r, t), \quad (1.21)$$

where  $\Psi(r, t)$  acts as the condensate wavefunction (and also as the order parameter for the BEC transition). The corresponding  $\hat{\Psi}^4$  Hamiltonian leads, under this mean-field approximation, to a non-linear Schrödinger equation (also known as Gross-Pitaevskii equation) for the condensate wavefunction

$$i\hbar \frac{\partial}{\partial t} \Psi(\mathbf{r}, t) = \left( -\frac{\hbar^2 \nabla^2}{2m} + V_{\text{ext}}(\mathbf{r}) + g |\Psi(\mathbf{r}, t)|^2 \right) \Psi(\mathbf{r}, t), \quad (1.22)$$

where  $V_{\text{ext}}$  is the external trapping potential. Because of the cubic nonlinearity  $g\Psi^3$ , BEC physics is hence inherently non-linear. Actually the previous non-linear Schrödinger equation is basically the same as the one found in other nonlinear media (most relevantly in nonlinear optics in Kerr media). Due to this resemblance atom optics of condensates has been called nonlinear atom optics.

### 1.4.2 Solitons

One of the most striking phenomena resulting in various media from nonlinearity is the appearance of solitons, first documented in shallow water channels by Russel in 1834 [Rus44]. A soliton or solitary wave is a wavepacket with a self-preserving shape, as a result of the compensation of the wavepacket spreading by the nonlinearity. One example of a system allowing solitary solutions is the usual, rescaled Gross-Pitaevskii-equation for the order parameter  $\Psi(x, t)$  in one dimension:

$$i\frac{\partial}{\partial t}\Psi(x, t) = \left(-\frac{\partial_x^2}{2} + V_{\text{ext}}(x) + g|\Psi(x, t)|^2\right)\Psi(x, t). \quad (1.23)$$

Let us consider  $\Psi(x, t)$  to be a localized wavepacket. The kinetic energy leads to a spreading of the wavepacket. This can be compensated by a nonlinearity that compresses the wavepacket when  $g < 0$  (attractive interaction). When the wavepacket spreads the density  $|\Psi|^2$  is reduced but  $-|g||\Psi|^2$  increases (i.e. the system gains nonlinear energy). Hence, the attractive nonlinearity works against the kinetic energy term. In a 1D environment (we discuss the issue of dimensionality below) this leads to a stable wavepacket, the so-called bright soliton, see fig. 1.11, which was observed in BEC experiments several years ago [SPTH02, KSF<sup>+</sup>02]. The Gross-Pitaevskii-equation for  $g > 0$  (repulsive interactions) also supports solitonic solutions, the so-called dark solitons, which consist of a density notch (accompanied by a phase slip) propagating without distortion (fig. 1.11). Dark solitons have also been experimentally realized in BECs [BBD<sup>+</sup>99, DSF<sup>+</sup>00].

Although solitons are stable in 1D, they are not stable in higher dimensions. This point is rather easy to understand for bright solitons by means of a simple Gaussian ansatz. Let's consider a  $d$ -dimensional Gaussian with width  $\sigma$ . The energy of the system results from the combination of kinetic energy, trap energy and interaction energy  $E = E_{\text{kin}} + E_{\text{trap}} + E_{\text{int}}$ . Inserting the Gaussian ansatz, we may easily obtain the scaling  $E_{\text{kin}} \propto \sigma^{-2}$ ,  $E_{\text{trap}} \propto \sigma^2$  and  $E_{\text{int}} \propto -\sigma^{-d}$ . Clearly  $E$  possesses a minimum for a given  $\sigma$  only in 1D, and hence stable solitonic solutions are only possible in 1D environments.

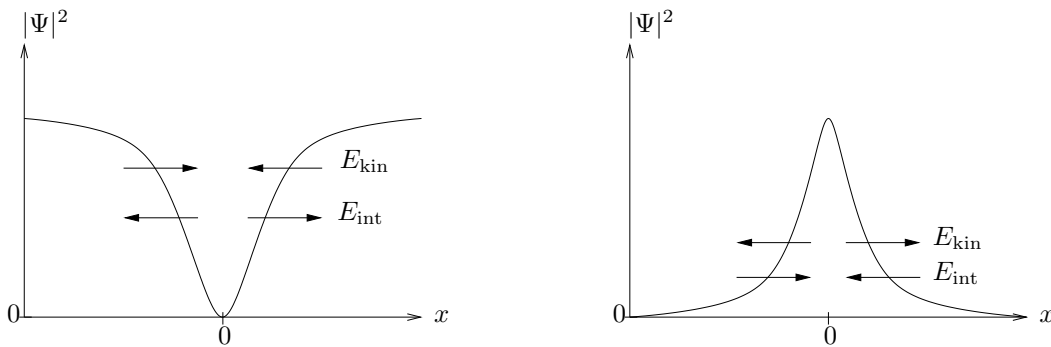


Fig. 1.11: Density profile of a dark soliton with positive mass and repulsive interaction ( $g > 0$ , left) and bright soliton with positive mass and attractive interaction ( $g < 0$ , right)

# Chapter 2

## Artificial Electromagnetism

In this chapter we discuss the idea of artificial electromagnetism induced in neutral atoms. We shall review different possibilities to achieve this goal, with a special emphasis on the generation of artificial electromagnetism using electromagnetically-induced transparency techniques and the possibility of generating non-Abelian electromagnetism. In the last part of this chapter we shall comment on the realization of different non-Abelian gauge fields.

### 2.1 Introduction

Before discussing artificial electromagnetism we recall in this section some basics of standard electromagnetism, which, as it is well-known, is given by the four coupled Maxwell-equations [Max65], which in vacuum are of the form

$$\nabla \cdot \mathbf{E} = \frac{1}{\epsilon_0} \rho \quad \nabla \cdot \mathbf{B} = 0 \quad \nabla \times \mathbf{B} = \mu_0 \mathbf{J} + \mu_0 \epsilon_0 \frac{\partial \mathbf{E}}{\partial t} \quad \nabla \times \mathbf{E} = -\frac{\partial \mathbf{B}}{\partial t}, \quad (2.1)$$

where  $\mathbf{E}$  is the electric field and  $\mathbf{B}$  is the magnetic field. The homogeneous Maxwell equations (second and fourth above when reading from left to right) are immediately satisfied with the introduction of a vector potential  $\mathbf{A}$  and a scalar potential  $\phi$ :

$$\mathbf{B} = \nabla \times \mathbf{A} \quad \mathbf{E} = -\nabla \phi - \frac{\partial \mathbf{A}}{\partial t}. \quad (2.2)$$

Both  $\mathbf{A}$  and  $\phi$  are not uniquely defined, since a gauge transformation

$$\mathbf{A}' = \mathbf{A} + \nabla \Lambda \quad \phi' = \phi - \frac{\partial \Lambda}{\partial t} \quad (2.3)$$

preserves the same fields  $\mathbf{B}$  and  $\mathbf{E}$ . Because of this indefiniteness in  $\mathbf{A}$  and  $\phi$ , they must be specified for the calculations, i.e. we have to choose a gauge. Special types of gauge are the Coulomb gauge ( $\nabla \cdot \mathbf{A} = 0$ ), which is of special interest in magnetostatics, and the Lorenz gauge ( $\frac{1}{c^2} \frac{\partial \phi}{\partial t} + \nabla \cdot \mathbf{A} = 0$ ), which is particularly useful in the treatment of electromagnetic waves.

In quantum mechanics the vector potential  $\mathbf{A}$  and the scalar potential  $\phi$  are used to introduce the electromagnetic fields into the Hamiltonian operator. This is accomplished via the so-called minimal coupling. The Schrödinger equation for an electric charge  $q$  in the presence of an electromagnetic field reads

$$i\hbar \frac{\partial \Psi}{\partial t} = \left( -\frac{\hbar^2}{2m} \left( \nabla - i\frac{q}{c} \mathbf{A} \right)^2 + q\phi \right) \Psi, \quad (2.4)$$

where we have introduced the minimal coupling transformation

$$\frac{\partial}{\partial t} \rightarrow \frac{\partial}{\partial t} + i\frac{q}{\hbar}\phi \quad \nabla \rightarrow \nabla - i\frac{q}{c}\mathbf{A}. \quad (2.5)$$

Artificial electromagnetism is the creation of Hamiltonians that effectively resemble the structure of eq. (2.4), but without any real electromagnetic fields in the system and not even a charge involved. At first, the idea of having electromagnetism in neutral atoms seems certainly surprising. In principle one would not expect any electromagnetism in neutral atoms, especially if we do not take into account the internal structure of the atoms.

Obtaining an artificial electric field is easier than creating an artificial magnetic field, since it only requires an additional scalar potential. An artificial electric field can be created e.g. by using the gravitational field as an equivalent electric field [AK98]. However, obtaining a magnetic field demands the artificial creation of a vector potential. As we show in the following sections of this chapter, this may be done by rotating a quantum gas (see section 2.2), by properly tailoring the hopping rate in optical lattices (section 2.3), or in a continuous implementation by dark-state techniques in  $\Lambda$ - and tripod-configurations (section 2.4). The latter (also the lattice implementation) allows for the creation of non-Abelian gauge fields. We study in detail this possibility in section 2.5 where we discuss general conditions for a non-Abelian vector potential in a tripod configuration. We conclude this chapter in section 2.6.

## 2.2 Rotation

Experiments on cold quantum gases have reached an unprecedented degree of control, offering thus extraordinary possibilities for the analysis of the effects of gauge fields on atomic systems. A simple way of generating a gauge field in ultracold gases is to rotate Bose-Einstein condensates with an angular frequency  $\Omega$ . This is relatively easy to understand as follows [PS04]. Let us start with a non-rotating BEC in a 2D pancake-trap.

$$H_{\text{lab}} = \frac{1}{2m}\mathbf{p}^2 + \frac{1}{2}m\omega^2 r^2. \quad (2.6)$$

We introduce a rotation with angular frequency  $\Omega = (0, 0, \Omega)$  (fig. 2.1). Moving into the co-rotating frame we get:

$$H_{\text{rot}} = H_{\text{lab}} - \Omega \cdot \mathbf{L} \quad (2.7)$$

$$= \frac{1}{2m}\mathbf{p}^2 + \frac{1}{2}m\omega^2 r^2 - \Omega \cdot (\mathbf{r} \times \mathbf{p}) \quad (2.8)$$

$$= \frac{1}{2m}(\mathbf{p} - m\mathbf{A})^2 + \frac{1}{2}m(\omega^2 - \Omega^2)r^2. \quad (2.9)$$

In the rotating frame the Hamiltonian has an effective gauge field  $\mathbf{A} = \Omega \times \mathbf{r}$ . This leads to a magnetic field  $\mathbf{B} = 2\Omega$ . This  $\mathbf{B}$  is homogeneous and its direction is parallel to the axis of rotation  $\Omega$ . Furthermore, the new trap has a frequency of  $\omega^2 - \Omega^2$ . Thus, a rotating condensate resembles a gas under the influence of a constant magnetic field  $B_0 = m\Omega$ . The field of rotating gases is experimentally well-studied, e.g. BEC experiments by the groups of J. Dalibard [MCWD00], W. Ketterle [ASRVK01] and E. Cornell [MAH<sup>+</sup>99]. These lead to the

observation of many interesting phenomena, including e.g. vortices, vortex-lattices, Landau level physics and Quantum-Hall-like phenomena in rotating quantum gases [KMP00, SCE<sup>+</sup>04, BSSD04, WG00].

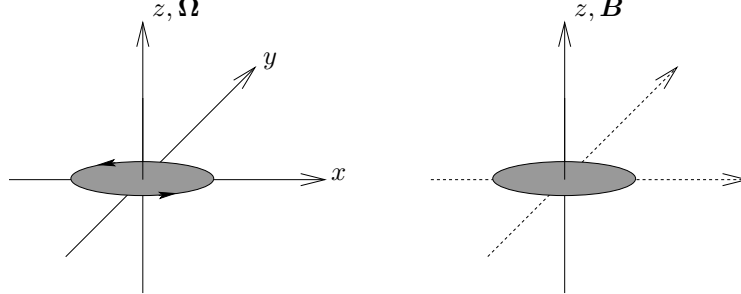


Fig. 2.1: Rotating BEC in a 2D pancake trap in the  $xy$ -plane as seen from the laboratory frame (left, cf. eq. (2.6)). The same BEC in the rotating frame (right, cf. eq. (2.9)) feels an effective magnetic field pointing parallel to the axis of rotation.

## 2.3 Discrete Systems: Lattices

Before discussing the effects of artificial electromagnetism in lattices, we will review briefly the work of D. Hofstadter concerning electrons in a 2D square lattice of lattice size  $a$  under the influence of a magnetic field perpendicular to the lattice [Hof76]. We restrict our analysis to that of a single Bloch band (deep lattice). The Bloch energy function in the tight-binding model acquires the form

$$H(\mathbf{k}) = -2V_0(\cos(k_x a) + \cos(k_y a)). \quad (2.10)$$

In the following we perform the so-called Peierls substitution [Pei33]  $\hbar\mathbf{k} \rightarrow \hat{\mathbf{p}} - e\mathbf{A}/c$ , and thus  $H \rightarrow \hat{H}$ . We then obtain the following eigenvalue equation

$$\epsilon\Psi(x, y) = e^{-i\Delta A_x}\Psi(x + a, y) + e^{i\Delta A_x}\Psi(x - a, y) + e^{-i\Delta A_y}\Psi(x, y + a) + e^{i\Delta A_y}\Psi(x, y - a), \quad (2.11)$$

where  $\Delta = \frac{ea}{\hbar c}$  and  $\epsilon = -\frac{E}{V_0}$ . The corresponding eigenenergies  $\epsilon$  obey a fractal spectrum, the so-called Hofstadter butterfly (see fig. 2.2). This is very different from the case without lattice where equally spaced energy levels are expected, so-called Landau levels [Lan30] discussed in sec. 4.2. Only for small magnetic fields ( $\alpha \ll 1$ , see fig. 2.2) or tending to the the continuum (lattice spacing  $a \rightarrow 0$ ) these Landau levels are regained. It is however difficult to generate high magnetic fields to measure this spectrum, because typical crystal lattice spacings are in the order of 1 Å.

Eq. (2.11) shows that the magnetic field leads to defined phase jumps between different lattice sites. This is a crucial observation, since it is the key for the simulation of magnetic fields in neutral atoms in optical lattices, which was for the first time proposed by Jaksch and Zoller [JZ03]. Now we are going to review how these phase jumps can be created artificially in

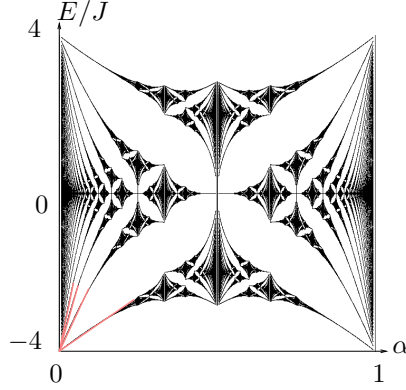


Fig. 2.2: The Hofstadter butterfly is the spectrum of the single-band Hamiltonian in a periodic potential in a magnetic field, e.g. the real magnetic field of the Hofstadter-Hamiltonian (2.12) or the artificial magnetic field of the Jaksch-Zoller-Hamiltonian (2.11).  $\alpha = \frac{a^2 B}{2\pi\hbar c/e}$  is a dimensionless parameter where  $a$  is the lattice spacing,  $\hbar$  is Planck's constant,  $c$  is the speed of light,  $e$  is the electric charge, and  $B$  is the magnetic field. The red lines in the lower left corner are the Landau levels obtained in the continuum limit.

optical lattices using the Jaksch-Zoller scheme (which yields Abelian gauge fields), before we continue with the generalisation of this scheme to non-Abelian gauge fields.

In the original proposal of ref. [JZ03] a 2D optical lattice traps atoms in the lowest band in state  $|g\rangle$  and another 2D lattice that traps atoms in state  $|e\rangle$ . In the total lattice the spacing in  $y$ -direction will be half the spacing in  $x$ -direction, as shown in fig. 2.4. The bands are tilted by e.g. an additional acceleration of the lattice in  $y$ -direction. In  $x$ -direction there is free tunneling and in  $y$ -direction we have laser induced Raman transitions. This system leads to a Hamiltonian

$$H_{JZ} = J \sum_{m,n} (e^{i2\pi\alpha m} a_{n,m}^\dagger a_{n,m+1} + a_{n,m}^\dagger a_{n+1,m}) + \text{H.c.}, \quad (2.12)$$

where  $\alpha$  is a phase determined by the system parameters (in particular the lattice spacing),  $m$  and  $n$  are the lattice sites and  $a$  ( $a^\dagger$ ) are bosonic destruction (creation) operators. Particles moving along a closed path in this lattice acquire a phase factor corresponding to an effective magnetic field. In this setup one can simulate very strong magnetic fields and consequently yield the fractal energy spectrum discussed above. Note that since the origin of these electromagnetic fields is artificial, they do not have to obey Maxwell's equations [Mue04].

The scheme was generalized to Non-Abelian physics by Osterloh et al. [OBS<sup>+</sup>05]. Again controlling the tunneling in a 2D lattice is the key point. The scheme is analogous, but now one has two internal states trapped in each column of the optical lattice. The lattice is accelerated as in the previous setup, see fig. 2.4, but this time we have state-specific Raman transitions in  $x$ - and  $y$ -direction. The exact form of the gauge fields in their paper is then

$$\mathbf{A} = \frac{\hbar c}{ea} \left( \left( \begin{array}{cc} -\frac{\pi}{2} & \frac{\pi}{2} e^{i\phi} \\ \frac{\pi}{2} e^{-i\phi} & -\frac{\pi}{2} \end{array} \right), \left( \begin{array}{cc} 2\pi m \alpha_1 & 0 \\ 0 & 2\pi m \alpha_2 \end{array} \right), 0 \right) = (A_x, A_y(m), 0) \quad (2.13)$$



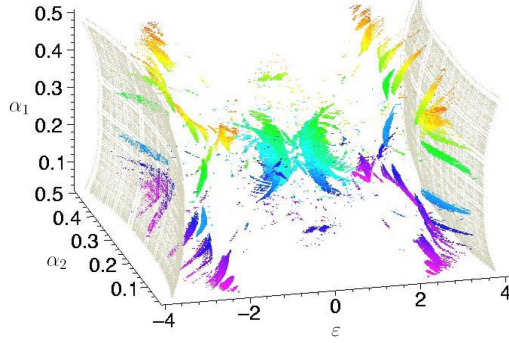


Fig. 2.3: The Osterloh moth is the spectrum of a lattice-Hamiltonian in a non-Abelian gauge field. It is the generalisation of the Abelian spectrum, i.e. the Hofstadter butterfly in fig. 2.2. This is for the sake of completeness and should not be explained in detail. (picture taken from [OBS<sup>+</sup>05])

with

$$\mathbf{B} = \left( 0, 0, \begin{pmatrix} 2\pi\alpha_1 & 0 \\ 0 & 2\pi\alpha_2 \end{pmatrix} \right). \quad (2.14)$$

Note that the vector potential  $\mathbf{A}$  is not a vector with scalar components anymore. The components are now  $2 \times 2$  matrices, and in particular  $[A_x, A_y] \neq 0$  in general, i.e. the gauge field generated is in general non-Abelian. The energy spectrum constitutes a generalisation of the Hofstadter Butterfly [Hof76] from section 1.3.4, although with richer 3D structure, a so-called Osterloh “moth”, as shown in fig. 2.3.

The corresponding Schrödinger equation for this problem is (similar to the Hofstadter butterfly case) of the form:

$$i\hbar\dot{\Psi}_{m,n} = \hat{U}_x\Psi_{m+1,n} + \hat{U}_x^\dagger\Psi_{m-1,n} + \hat{U}_y\Psi_{m,n+1} + \hat{U}_y^\dagger\Psi_{m,n-1}, \quad (2.15)$$

where

$$\hat{U} = \frac{\hbar c}{ea} \left( \begin{pmatrix} 0 & e^{i\phi} \\ e^{-i\phi} & 0 \end{pmatrix}, \begin{pmatrix} e^{-2\pi m\alpha_1 i} & 0 \\ 0 & e^{-2\pi m\alpha_2 i} \end{pmatrix}, 0 \right). \quad (2.16)$$

The dynamics of a wavepacket on the lattice under the non-Abelian gauge may differ significantly from that under an Abelian gauge (see fig. 2.5). Let us consider the expansion dynamics. We start with a Gaussian distribution of e.g.  $\sigma = 2$  on a 2D lattice with  $121 \times 121$  sites, and the following hopping operators:

$$\hat{U}_x = \begin{pmatrix} 0 & 1 \\ 1 & 0 \end{pmatrix} \quad \hat{U}_y^{\text{Non-Abel}} = \begin{pmatrix} 1 & 0 \\ 0 & 0.8 \end{pmatrix} \quad \text{and} \quad \hat{U}_y^{\text{Abel}} = \begin{pmatrix} 1 & 0 \\ 0 & 1 \end{pmatrix}. \quad (2.17)$$

One observes the fringes in the non-Abelian expansion because of constructive and destructive self-interference of the wavefunction. Let us consider the evolution from point A to B, see fig. 2.6: there are several paths a wave function can take to reach point B starting from A. At B all these paths can meet again and together yield the wave function. But if the evolution on different but otherwise symmetric paths gives different phases, we will get interference effects.

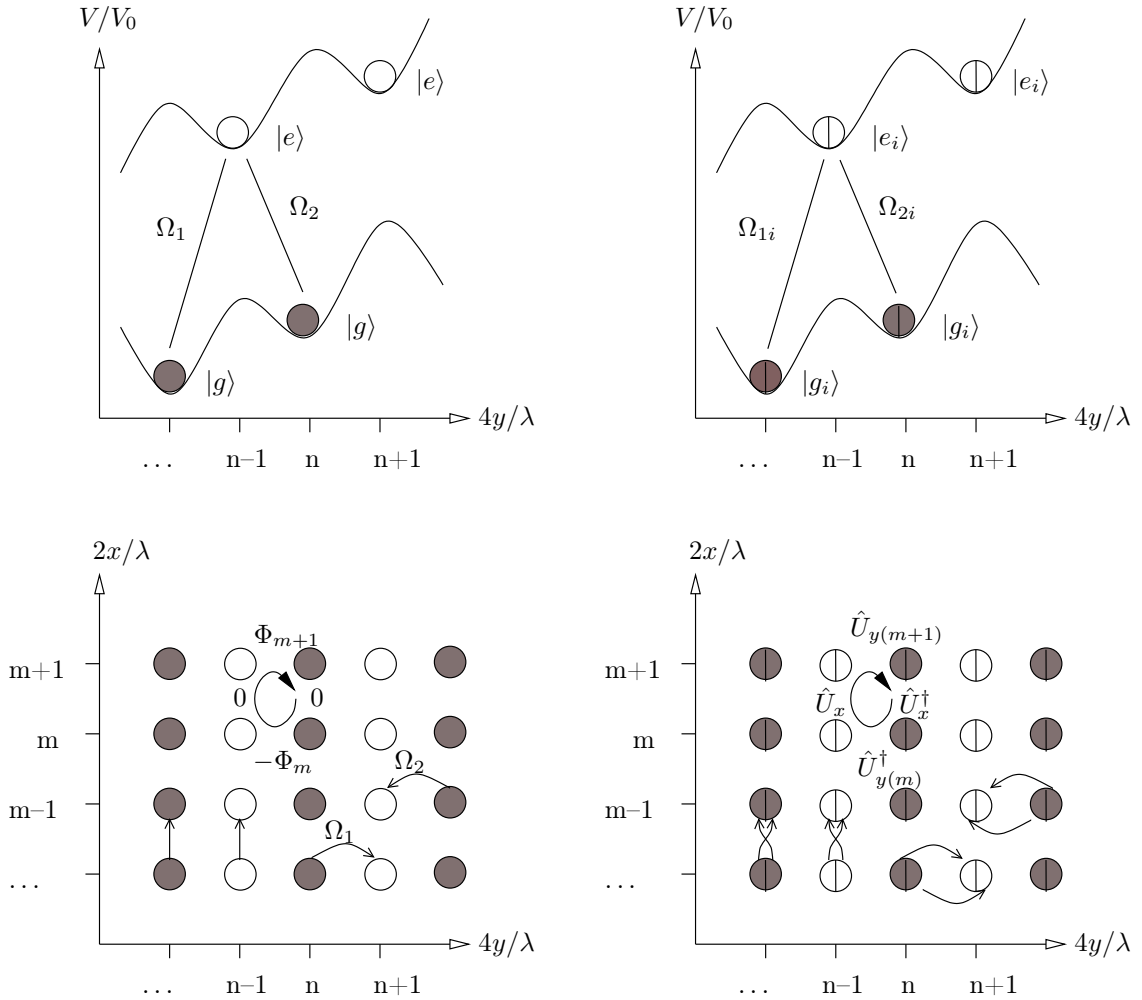


Fig. 2.4: Optical lattices schemes for generating artificial magnetic fields. The Jaksch-Zoller [JZ03] scheme (left column) generates an Abelian gauge field using two lattices trapping the states  $|g\rangle$  and  $|e\rangle$ . The laser assisted tunneling in  $y$ -direction leads to phase factors simulating Abelian gauge fields. The spectrum of this system is the Hofstadter butterfly shown in fig. 2.2. The Osterloh [OBS<sup>+</sup>05] scheme (right column) generates a non-Abelian gauge field using two lattices trapping each two internal states  $|g_i\rangle$  and  $|e_i\rangle$  ( $i=1,2$ ). Laser assisted tunneling in  $x$ - and  $y$ -direction leads to non-Abelian phase factors simulating non-Abelian gauge fields, the spectrum of this system is the Osterloh moth shown in fig. 2.3.

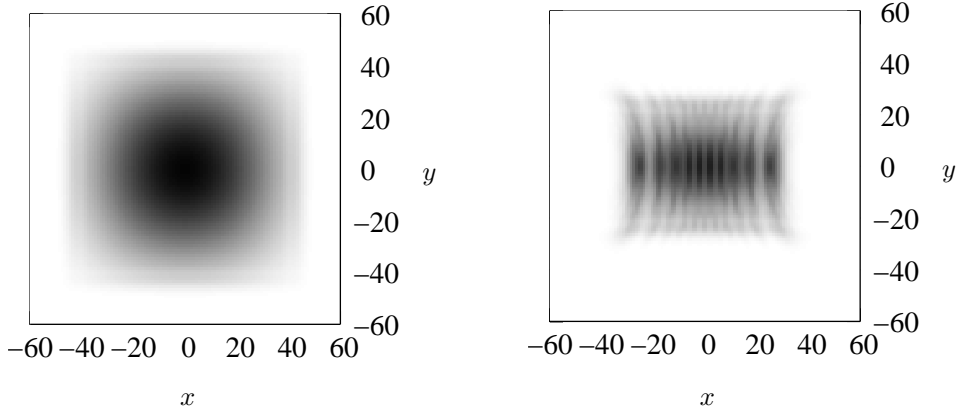


Fig. 2.5: The expansion of a Gaussian wavepacket on a  $121 \times 121$  lattice shows the non-trivial dynamics in non-Abelian gauge field. For the expansion in an Abelian gauge field (left) the shape of the atom cloud seems unchanged, whereas in for the expansion in a non-Abelian gauge field (right) we observe interference fringes, which also oscillate in time. For the simulation we used the hopping operators (2.17).

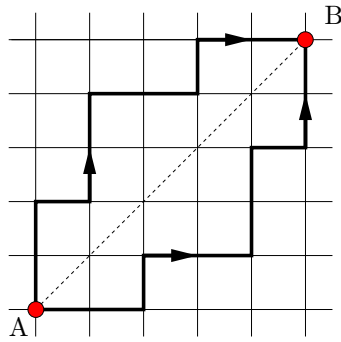


Fig. 2.6: Two out of many possible symmetric paths in expansion from A to B. In the non-Abelian setup these paths collect different phases which explains the non-Abelian expansion dynamics in fig. 2.5.

## 2.4 Continuous Systems: Lambda and Tripod schemes

### 2.4.1 Effective gauge fields for non-degenerate eigenstates

In this section we discuss the creation of an artificial gauge field for an adiabatic motion of a system in a non-degenerate eigenstate. The results of this section will be applied in section 2.4.3 on  $\Lambda$ -atoms. For the derivation we will follow the seminal paper of Berry [Ber84]. We take as a starting point the time-dependent Schrödinger equation where the Hamiltonian depends on a time-dependent parameter  $\mathbf{R}$

$$i\hbar \frac{d}{dt} |\psi(t)\rangle = H(\mathbf{R}(t)) |\psi(t)\rangle. \quad (2.18)$$

The adiabatic theorem [BF28, Kat50, ASY87, AHS90, Mes90] states, that if we start with an eigenstate  $|\psi(0)\rangle = |n(\mathbf{R}(0))\rangle$  and change the system slowly, then we will stay in the same eigenstate  $|n(\mathbf{R}(t))\rangle$  we started with at  $t = 0$ :

$$H(\mathbf{R}(t)) |n(\mathbf{R}(t))\rangle = E_n(\mathbf{R}(t)) |n(\mathbf{R}(t))\rangle. \quad (2.19)$$

At each instant  $t \in \mathbb{R}$ , the eigenstates  $|n(\mathbf{R}(t))\rangle$  of  $H$  form a basis of our Hilbert space and the wave function is a linear combination of them:

$$|\psi(t)\rangle = \sum_n c_n(t) |n(\mathbf{R}(t))\rangle. \quad (2.20)$$

Applying this to the time-dependent Schrödinger equation  $i\hbar \dot{|\psi(t)\rangle} = H(\mathbf{R}(t)) |\psi(t)\rangle$  and using the eigenvalue equation  $H(\mathbf{R}(t)) |n(\mathbf{R}(t))\rangle = E_n(\mathbf{R}(t)) |n(\mathbf{R}(t))\rangle$  yields

$$\sum_n i\hbar \dot{c}_n |n(\mathbf{R}(t))\rangle + \sum_n c_n i\hbar \frac{d}{dt} |n(\mathbf{R}(t))\rangle = \sum_n c_n E_n(\mathbf{R}(t)) |n(\mathbf{R}(t))\rangle. \quad (2.21)$$

With  $\langle m(\mathbf{R}(t))|$  acting from the left, one gets along with the orthogonality condition

$$i\hbar \dot{c}_m + \sum_n c_n \langle m(\mathbf{R}(t)) | i\hbar \frac{d}{dt} |n(\mathbf{R}(t))\rangle = c_m E_m(\mathbf{R}(t)). \quad (2.22)$$

In the adiabatic approximation the off-diagonal elements in the second term on the left side turn out to be zero (because: adiabatic  $\langle m | \frac{d}{dt} |n\rangle = \langle m | \nabla_{\mathbf{R}} |n\rangle \frac{d}{dt} \mathbf{R} \approx 0 \quad \forall m \neq n$  since  $\frac{d}{dt} \mathbf{R} \ll 1$ ). It remains

$$i\hbar \dot{c}_m = E_m(\mathbf{R}(t)) c_m - i\hbar \langle m | \dot{m} \rangle c_m \quad (2.23)$$

with the solution

$$c_m(t) = \exp\left(-\frac{i}{\hbar} \int_0^t E_m(\mathbf{R}(t')) dt' - \int_0^t \langle m | \dot{m} \rangle dt'\right) c_m(0). \quad (2.24)$$

Assume we start with the eigenstate  $|n\rangle$  at  $t = 0$ :  $c_m(t = 0) = \delta_{mn}$

$$|\psi(t)\rangle = \exp\left(-\frac{i}{\hbar} \int_0^t E_n(\mathbf{R}(t')) dt'\right) \exp(i\gamma_n(t)) |n(\mathbf{R}(t))\rangle, \quad (2.25)$$

$$\gamma_n(t) = i \int_0^t \langle n | \dot{n} \rangle dt'. \quad (2.26)$$

Now assume that the system describes a cyclic evolution in the parameter space during the time  $T$ , i.e.  $R(T) = R(0)$  and  $|n(\mathbf{R}(T))\rangle = |n(\mathbf{R}(0))\rangle$ . We denote the cyclic path from  $R(0)$  to  $R(T)$  in parameter space by  $C$  and finally get:

$$|\psi(T)\rangle = \underbrace{\exp\left(-\frac{i}{\hbar} \int_0^T dt' E_n(\mathbf{R}(t'))\right)}_{\text{dynamic phase}} \underbrace{\exp(i\gamma_n(C))}_{\text{geometric phase}} |n(\mathbf{R}(0))\rangle \quad (2.27)$$

$$\gamma_n(C) = i \oint_C \langle n(\mathbf{R}) | \nabla_{\mathbf{R}} n(\mathbf{R}) \rangle \cdot d\mathbf{R} \quad (2.28)$$

$$= \oint_C \mathbf{A}_n(\mathbf{R}) \cdot d\mathbf{R} \quad (2.29)$$

$$\mathbf{A}_n(\mathbf{R}) = i \langle n(\mathbf{R}) | \nabla_{\mathbf{R}} n(\mathbf{R}) \rangle. \quad (2.30)$$

The equations above are the fundamental formulas for the Berry phase in the case of a general adiabatic and cyclic evolution of the parameter  $\mathbf{R}$  in parameter space. Note that  $\gamma$  is real:  $\langle n(\mathbf{R}) | \nabla_{\mathbf{R}} n(\mathbf{R}) \rangle$  is purely imaginary because:  $\langle n(\mathbf{R}) | n(\mathbf{R}) \rangle = 1$ ,  $\nabla_{\mathbf{R}} \langle n(\mathbf{R}) | n(\mathbf{R}) \rangle = 0$ ,  $\langle \nabla n(\mathbf{R}) | n(\mathbf{R}) \rangle + \langle n(\mathbf{R}) | \nabla n(\mathbf{R}) \rangle = 0$ ,  $\langle n(\mathbf{R}) | \nabla | n(\mathbf{R}) \rangle + \langle n(\mathbf{R}) | \nabla^* | n(\mathbf{R}) \rangle = 0$ ,  $2\text{Re} \langle n(\mathbf{R}) | \nabla | n(\mathbf{R}) \rangle = 0$ . The phase  $\gamma$  is actually time-independent in the sense that only its trace in parameter space matters. It does not matter, how fast the path in the parameter space is traced out – as long as it is adiabatic. Therefore it is called geometric phase and sometimes topologic phase.

We can compute  $\gamma$  easily by using the identity:

$$\langle m(t) | \nabla | n(t) \rangle = \frac{\langle m(t) | (\nabla H(t)) | n(t) \rangle}{E_m(t) - E_n(t)}. \quad (2.31)$$

The above equation can be derived by applying the gradient to the stationary Schrödinger equation. If the loop in parameter space comes close to a degeneracy, the terms there will dominate eq. (2.31) and the theory for adiabatic evolution will break down in case of degenerate eigenstates ( $E_m(t) - E_n(t) = 0$ ).

The phase factor  $\gamma_n(C)$  in eq. (2.29) can be written as an integral over the vector field  $\mathbf{V}_n$

$$\gamma_n(C) = \int_S \mathbf{V}_n(\mathbf{R}) \cdot d\mathbf{S}, \quad (2.32)$$

where  $\mathbf{V}_n(\mathbf{R})$  plays the role of a magnetic field for  $\mathbf{A}_n(\mathbf{R})$ . The vector  $\mathbf{A}$  is sometimes referred to as the Berry connection and is related to a curvature (an effective “magnetic” field)  $\mathbf{B}$  as

$$B_i = \frac{1}{2} \epsilon_{ikl} F^{kl}, \quad F_{kl} = \partial_k A_l - \partial_l A_k, \quad (2.33)$$

where  $F$  is the gauge field strength tensor,  $\epsilon_{ikl}$  are the elements of the totally antisymmetric unit tensor. In vector notation we recover the familiar form  $\mathbf{B} = \nabla \times \mathbf{A}$ .

Instead of considering the final result of the evolution as in eq. (2.27) we may consider the Schrödinger equation of the system, which is initially in the eigenstate  $|m\rangle$ ,

$$i\hbar|\dot{m}\rangle = \frac{1}{2m}(-i\hbar\nabla - \mathbf{A}_m)^2|m\rangle. \quad (2.34)$$

Because of the interpretation of the Berry phase in terms of an effective gauge potential, it is useful to look at some generalizations of the standard Berry phase. Many generalizations of the Berry phase have been found by removing the restrictions in the derivation step by step, see e.g. reviews [WS89, BMK<sup>+</sup>03, CJ04]. For example, in the Aharonov-Anandan-phase [AA87] the adiabatic approximation is no longer required. Another generalization is the Samuel-Bhandari-phase [SB88] where the evolution does not even have to be cyclic. Until now we have only considered pure states. The analysis for mixed states was done by Uhlmann [Uhl86, Uhl95] and continued by Sjöqvist et al. [SPE<sup>+</sup>00]. It was later further generalized to cover also degenerated density operators by Singh et al. [STB<sup>+</sup>03]. Complex geometric phases appear in non-Hermitian Hamiltonians resp. dissipative systems [GW88]. Off-diagonal geometric phases [MP00] are used to uncover interference effects when the usual geometric phase is undefined. The most general ansatz is the quantum kinematic approach by Mukunda and Simon [MS93]. An important insight is that the geometric phase can be looked at in a differential geometric framework too [Sim83].

If the adiabatic condition does not apply for eq. (2.22) we would then get off-diagonal terms in the effective vector potential  $\mathbf{A}_{mn} = \langle m|\nabla n\rangle$  (whereas before we considered only diagonal terms  $\mathbf{A}_m = \mathbf{A}_{mm}$ ) during the evolution of our  $N$  non-degenerate eigenstates. This kind of  $(N \times N)$  potential  $\mathbf{A}_{mn}$  is not exactly the non-Abelian gauge potential we will be looking for in the next section. There we consider  $q$  out of  $N$  eigenstates to be degenerate. The adiabatic evolution of these  $q$  eigenstates within their degenerate subspace will give us a non-Abelian vector potential.

## 2.4.2 Effective gauge fields for degenerate eigenstates

The seminal paper of Wilczek and Zee [WZ84] shows that non-Abelian gauge fields can appear during an adiabatic evolution [BF28, Kat50, ASY87, AHS90, Mes90] if there are degenerate eigenstates. In our case we shall employ degenerate dark states in laser coupled atoms, which do not show spontaneous emission. This construction of non-Abelian gauge potentials in the presence of nontrivial light fields coupled to degenerate electronic states of cold atoms was carried out in a recent paper [RJOF05]. These authors considered atoms with  $N$  internal states. For a fixed position  $\mathbf{r}$  the internal Hamiltonian  $\hat{H}_0(\mathbf{r})$  including the space-dependent laser interaction can be diagonalized to give a set of  $N$  dressed states  $|\chi_n(\mathbf{r})\rangle$  with eigenvalues  $\varepsilon_n(\mathbf{r})$ , where  $n = 1, 2, 3 \dots N$ . The full quantum state of the atom describing both internal and motional degrees of freedom can then be expanded in terms of the dressed states according to

$$|\Psi\rangle = \sum_{n=1}^N \Psi_n(r) |\chi_n(r)\rangle. \quad (2.35)$$

Plugging this ansatz into the corresponding time-dependent Schrödinger equation we obtain:

$$i\hbar \frac{\partial}{\partial t} |\Psi\rangle = \left[ \frac{1}{2m} (-i\hbar \nabla)^2 + H_0 + V \right] |\Psi\rangle \quad (2.36)$$

$$= \frac{1}{2m} \sum_n (-i\hbar \nabla)^2 \Psi_n |\chi_n\rangle + \sum_n H_0 \Psi_n |\chi_n\rangle + \sum_n V \Psi_n |\chi_n\rangle \quad (2.37)$$

$$= -\frac{\hbar^2}{2m} \sum_n (\nabla^2 \Psi_n) |\chi_n\rangle - \frac{\hbar^2}{2m} \sum_n 2(\nabla \Psi_n)(\nabla |\chi_n\rangle) - \frac{\hbar^2}{2m} \sum_n \Psi_n \nabla^2 |\chi_n\rangle \\ + \sum_n H_0 \Psi_n |\chi_n\rangle + \sum_n V \Psi_n |\chi_n\rangle \quad (2.38)$$

Applying  $\langle \chi_m |$  from the left at both sides of the equation we obtain

$$i\hbar \frac{\partial}{\partial t} \Psi_m = -\frac{\hbar^2}{2m} \sum_n \delta_{mn} \nabla^2 \Psi_n - \frac{\hbar^2}{2m} \sum_n 2(\nabla \Psi_n) \langle \chi_m | \nabla | \chi_n \rangle - \frac{\hbar^2}{2m} \sum_n \Psi_n \langle \chi_m | \nabla^2 | \chi_n \rangle \\ + \sum_n \varepsilon_n \Psi_n \langle \chi_m | \chi_n \rangle + \sum_n \langle \chi_m | V | \chi_n \rangle \Psi_n \quad (2.39)$$

and using integration by parts we get

$$= \sum_{n,l} \frac{1}{2m} \left( -i\hbar \delta_{ml} \nabla - i\hbar \langle \chi_m | \nabla | \chi_l \rangle \right) \left( -i\hbar \delta_{ln} \nabla - i\hbar \langle \chi_l | \nabla | \chi_n \rangle \right) \Psi_n \\ + \sum_n \left( \varepsilon_n \delta_{mn} + \langle \chi_m | V | \chi_n \rangle \right) \Psi_n \quad (2.40)$$

We may then re-write this without index notation:

$$i\hbar \frac{\partial}{\partial t} \Psi = \left[ \frac{1}{2m} (-i\hbar \nabla - \mathbf{A})^2 + V \right] \Psi, \quad (2.41)$$

where the  $N \times N$  potentials are given by

$$\mathbf{A}_{nm} = i\hbar \langle \chi_n(\mathbf{r}) | \nabla | \chi_m(\mathbf{r}) \rangle \quad (2.42)$$

$$V_{nm} = \varepsilon_n(\mathbf{r}) \delta_{nm} + \langle \chi_n(\mathbf{r}) | V(\mathbf{r}) | \chi_m(\mathbf{r}) \rangle. \quad (2.43)$$

As mentioned in the last section, a non-Abelian situation may be achieved if the off-diagonal elements  $\langle \chi_n(\mathbf{r}) | \nabla | \chi_m(\mathbf{r}) \rangle$  ( $m \neq n$ ) do not vanish (as they vanish in the adiabatic motion case), but this is not the kind of non-Abelian character we are going to explore. There is another way to get the non-Abelian vector potential within adiabatic motion: if two states  $|\chi_m\rangle$  and  $|\chi_n\rangle$  are degenerate they can have transitions between themselves even in the adiabatic case.

If we rewrite the Hamiltonian in eq. (2.41) into an equation for the coefficients of the eigenstates as in eq. (2.24), we will get the following result:

$$c_m(t) = \exp \left( -\frac{i}{\hbar} \int_0^t E_m(\mathbf{R}(t')) dt' \right) \sum_{n=1}^N \mathcal{P} \exp \left( i \oint_C \mathbf{A}_{mn} \cdot d\mathbf{x} \right) c_n(0), \quad (2.44)$$

where  $\mathcal{P}$  is the path-ordering operator, because  $\mathbf{A}_{mn} = \langle m | i\partial_x | n \rangle$  does not commute with itself at different points. Instead of these difficult to evaluate final states  $c_m(t)$ , we will concentrate

on writing the Hamiltonian (2.41) with the explicit form of  $\mathbf{A}$  and use other means of solving the resulting Schrödinger equation, e.g. numerically or using the dispersion relation.

We note that this non-Abelian geometric phase can be used for topological and universal quantum computation [ZR99, PZR00, PC00]. The geometric phase has the advantage of being robust against distortion, similar to the Aharonov-Bohm effect, where the accumulated phase does not depend on the details of the path around the solenoid.

Consider only the subspace of  $q$  degenerate dressed states (which are well separated from the others), and no transitions to other states. We want to obtain an effective Hamiltonian for these degenerate states. To achieve this goal we project out the full  $(N \times N)$ -Hamiltonian onto a  $(q \times q)$ -Hamiltonian. We cannot just truncate  $H$ , as a correction would occur in that case. Only the important term  $A^2$  is shown in intermediate steps of the following calculation:

$$i\hbar \frac{\partial}{\partial t} \begin{pmatrix} \Psi_1 \\ \vdots \\ \Psi_q \\ \Psi_{q+1} \\ \vdots \\ \Psi_N \end{pmatrix} = \left[ \frac{1}{2m} (-\hbar^2 \nabla^2 + A^2 + \text{mixed terms}) + V \right] \begin{pmatrix} \Psi_1 \\ \vdots \\ \Psi_q \\ \Psi_{q+1} \\ \vdots \\ \Psi_N \end{pmatrix} \quad (2.45)$$

apply  $P^q = (\underbrace{1 \dots 1}_q 0 \dots 0)$  from the left

$$= \frac{1}{2m} (\underbrace{1 \dots 1}_q 0 \dots 0)_m \sum_{l=1}^N A_{ml} \cdot A_{ln} \begin{pmatrix} \Psi_1 \\ \vdots \\ \Psi_q \\ \Psi_{q+1} \\ \vdots \\ \Psi_N \end{pmatrix}_n \quad (2.46)$$

$$= \frac{1}{2m} (\underbrace{1 \dots 1}_q 0 \dots 0)_m \sum_{n=1}^N \sum_{l=1}^N A_{ml} \cdot A_{ln} \Psi_n \quad (2.47)$$

$$= \frac{1}{2m} \sum_{m=1}^N P_m \sum_{n=1}^N \sum_{l=1}^N A_{ml} \cdot A_{ln} \Psi_n. \quad (2.48)$$

$m$  and  $n$  are truncated easily when projecting to the  $q$ -dimensional subspace, but the summation over  $l$  is not reduced in the same easy way and remains:

$$i\hbar \frac{\partial}{\partial t} \begin{pmatrix} \Psi_1 \\ \vdots \\ \Psi_q \end{pmatrix}_m = \left[ \frac{1}{2m} (-i\hbar \nabla - A)^2 + V + \underbrace{\frac{1}{2m} \sum_{l=q+1}^N A_{ml} \cdot A_{ln}}_{\Phi_{mn}} \right] \begin{pmatrix} \Psi_1 \\ \vdots \\ \Psi_q \end{pmatrix}_n \quad (2.49)$$

In the truncated  $q \times q$  Hamiltonian the range where  $l > q$  in the above sum is not included, i.e. the whole term  $\Phi_{mn}$  is missing.



Summarizing, we just showed, that if there are  $q$  degenerate dressed states and if the transitions to the other states are negligible, we obtain a coupled  $q$ -level system  $\tilde{\Psi}$  of the form

$$i\hbar\frac{\partial}{\partial t}\tilde{\Psi} = \left[ \frac{1}{2m}(-i\hbar\nabla - \mathbf{A})^2 + V + \Phi \right] \tilde{\Psi}. \quad (2.50)$$

$\Phi_{nm}$  is an additional scalar potential that remains after projecting out the Hamiltonian to the subspace of degenerate dressed states. The potentials in eq. (2.50) are given by

$$\mathbf{A}_{nm} = i\hbar\langle\chi_n(\mathbf{r})|\nabla\chi_m(\mathbf{r})\rangle \quad (2.51)$$

$$V_{nm} = \varepsilon_n(\mathbf{r})\delta_{nm} + \langle\chi_n(\mathbf{r})|V(\mathbf{r})|\chi_m(\mathbf{r})\rangle \quad (2.52)$$

$$\Phi_{nm} = \frac{1}{2m} \sum_{l=q+1}^N A_{nl} \cdot A_{lm} \quad (2.53)$$

$$= \frac{\hbar^2}{2m} \left( \langle\nabla\chi_n|\nabla\chi_m\rangle + \sum_{k=1}^q \langle\chi_n|\nabla\chi_k\rangle\langle\chi_k|\nabla\chi_m\rangle \right). \quad (2.54)$$

Analogous to eq. (2.33), the  $q \times q$  matrix  $\mathbf{A}$  (sometimes referred to as the Berry connection) is related to the curvature (an effective ‘‘magnetic’’ field)  $\mathbf{B}$  as

$$B_i = \frac{1}{2}\varepsilon_{ikl}F^{kl}, \quad F_{kl} = \partial_k A_l - \partial_l A_k - \frac{i}{\hbar}[A_k, A_l]. \quad (2.55)$$

Note that the term  $\frac{1}{2}\varepsilon_{ikl}[A^k, A^l] = (\mathbf{A} \times \mathbf{A})_i$  does not vanish in general, since the vector components of  $\mathbf{A}$  do not necessarily commute. In fact this term reflects the non-Abelian character of the gauge potentials. For only one ‘‘degenerate’’ state our results coincide with these of section 2.4.1.

### 2.4.3 Artificial Abelian fields: Three-level $\Lambda$ -systems

In this subsection we consider atoms with an accessible three-level  $\Lambda$ -system as that introduced in sec. 1.2.3. Recall from that section that we may introduce combinations of the ground state levels which form a dark state  $|\chi_D\rangle$  uncoupled to the lasers. We shall restrict our calculations to the dark state, and calculate (following the reasonings of previous sections) the effective potentials  $\mathbf{A}, \Phi, V$  in the effective Hamiltonian  $H_{\text{eff}} = \frac{1}{2m}(-i\hbar\nabla - \mathbf{A}_{\text{eff}})^2 + V + \Phi$ . Note that the effective gauge fields are Abelian, since the degenerate space consists just of one state.

The Rabi frequencies  $\Omega_P$  and  $\Omega_C$  (we follow the same notation as in sec. 1.2.3) can be parametrized by expressing  $\zeta = \Omega_P/\Omega_C = \tan\theta e^{iS}$ . Thus,

$$\mathbf{A}_{\text{eff}} = i\hbar\langle\chi_D(\mathbf{r})|\nabla\chi_D(\mathbf{r})\rangle = i\hbar\frac{\zeta^*\nabla\zeta - \zeta\nabla\zeta^*}{2(1+|\zeta|^2)} \quad (2.56)$$

$$\mathbf{B}_{\text{eff}} = \nabla \times \mathbf{A}_{\text{eff}} = i\hbar\frac{\nabla\zeta^* \times \nabla\zeta}{2(1+|\zeta|^2)^2} \quad (2.57)$$

$$V = \varepsilon_D(\mathbf{r}) + \langle\chi_D(\mathbf{r})|V(\mathbf{r})|\chi_D(\mathbf{r})\rangle = \frac{V_1(r) + |\zeta|^2 V_2(r)}{1+|\zeta|^2} \quad (2.58)$$

$$\Phi = \frac{\hbar^2}{2m} (\langle\nabla\chi_D|\nabla\chi_D\rangle + \langle\chi_D|\nabla\chi_D\rangle\langle\chi_D|\nabla\chi_D\rangle) = \frac{\hbar^2}{2m} \frac{\nabla\zeta^* \nabla\zeta}{2(1+|\zeta|^2)^2}. \quad (2.59)$$

The effective magnetic field is  $\mathbf{B}_{\text{eff}} = -\hbar \nabla(\sin^2 \theta) \times \nabla S$ . A non-vanishing  $\mathbf{B}_{\text{eff}}$  requires a relative angular momentum of the two light beams. This is e.g. the case for light beams with a vortex (i.e. with optical angular momentum) as in [JO04, JROK05, JRO05, JO05]. It is however also possible to implement it without an optical angular momentum, using shifted spatial beam profiles [JROF06], see fig. 2.7. For recent proposals and experiments in this direction see [GCY<sup>+</sup>09, LCP<sup>+</sup>09, Juz09].

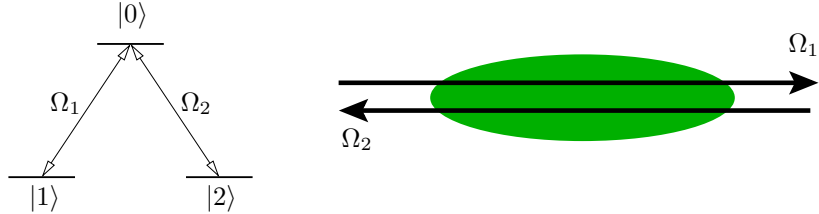


Fig. 2.7: The  $\Lambda$  coupling scheme (of sec. 2.4.3) forms one dark state. The two laser beams  $\Omega_i$  ( $i = 1, 2$ ) are counterpropagating and have shifted spacial beam profiles as suggested in [JROF06]. This leads to an effective Hamiltonian for the dark state with an Abelian gauge field.

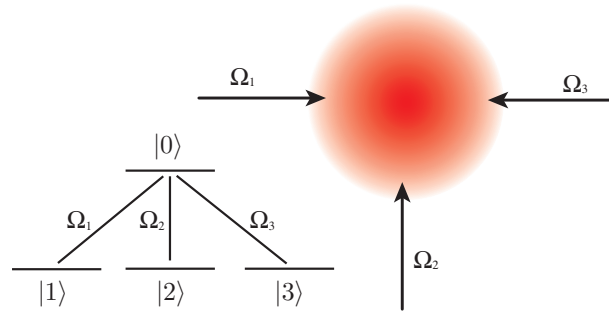


Fig. 2.8: The tripod coupling scheme (of sec. 2.4.4) forms two degenerate dark states with a non-adiabatic coupling. The three laser beams  $\Omega_i$  ( $i = 1, 2, 3$ ) are arranged in the figure as two counter propagating beams ( $\Omega_1$  and  $\Omega_2$ ) and one beam ( $\Omega_3$ ) (of double intensity) in the perpendicular direction. This leads to an effective Hamiltonian for the two dark states with a constant non-Abelian gauge field (see sec. 2.5.1).

#### 2.4.4 Non Abelian electromagnetism: Four-level tripod-systems

To construct a scheme that leads to a  $U(2)$  gauge potential, we need two degenerate (or nearly degenerate) dressed states  $|D_1\rangle$  and  $|D_2\rangle$ . Such a condition is fulfilled in the case of the tripod system shown in fig. 2.8. The beams couple four internal atomic levels in a tripod configuration, in which the atoms are characterized by three lower levels  $|1\rangle$ ,  $|2\rangle$  and  $|3\rangle$  and an excited level  $|0\rangle$ . The  $j$ -th laser induces a transition (with a Rabi frequency  $\Omega_j$ ) between the  $j$ -th lowest level

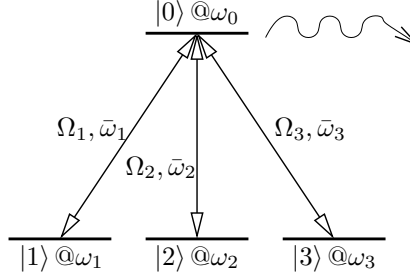


Fig. 2.9: A tripod level atom with laser coupling scheme as described by the Hamiltonian (2.60) (except the spontaneous emission)

and the excited level  $|0\rangle$ . A truly non-Abelian situation emerges if the off-diagonal element  $i\hbar\langle D_1(\mathbf{r})|\nabla D_2(\mathbf{r})\rangle$  is non-zero. The Hamiltonian of the tripod system in fig. 2.9 is according to [RJO05, UFSB98, USB99]

$$H = H_{CM} + \sum_{j=0}^3 \hbar\omega_j|j\rangle\langle j| + \hbar \sum_{j=0}^3 (\Omega_j e^{-i\bar{\omega}_j t}|0\rangle\langle j| + \text{H.c.}), \quad (2.60)$$

where  $H_{CM}$  accounts for the center-of-mass motion and  $|\Psi\rangle = \sum_{j=0}^3 \Psi_j|j\rangle$ . Now, solving the Schrödinger equation  $i\hbar|\dot{\Psi}\rangle = H|\Psi\rangle$  we get for each component (without considering for the moment  $H_{CM}$ )

$$i\hbar\dot{\Psi}_0 = \hbar\omega_0\Psi_0 + \hbar [\Omega_1 e^{-i\bar{\omega}_1 t}\Psi_1 + \Omega_2 e^{-i\bar{\omega}_2 t}\Psi_2 + \Omega_3 e^{-i\bar{\omega}_3 t}\Psi_3] \quad (2.61)$$

$$i\hbar\dot{\Psi}_1 = \hbar\omega_1\Psi_1 + \hbar\Omega_1^* e^{i\bar{\omega}_1 t}\Psi_0 \quad (2.62)$$

$$i\hbar\dot{\Psi}_2 = \hbar\omega_2\Psi_2 + \hbar\Omega_2^* e^{i\bar{\omega}_2 t}\Psi_0 \quad (2.63)$$

$$i\hbar\dot{\Psi}_3 = \hbar\omega_3\Psi_3 + \hbar\Omega_3^* e^{i\bar{\omega}_3 t}\Psi_0. \quad (2.64)$$

These equations can be simplified by transforming the time-dependency away by  $\Psi_0 = \Phi_0 e^{-i(\bar{\omega}_1 + \omega_1)t}$ ,  $\Psi_1 = \Phi_1 e^{-i\omega_1 t}$ ,  $\Psi_2 = \Phi_2 e^{-i(\omega_1 + \bar{\omega}_1 - \bar{\omega}_2)t}$ , and  $\Psi_3 = \Phi_3 e^{-i(\omega_1 + \bar{\omega}_1 - \bar{\omega}_3)t}$ .

$$i\hbar\dot{\Phi}_0 = \hbar [(\omega_0 - \omega_1) - \bar{\omega}_1] \Phi_0 + \hbar(\Omega_1 \Phi_1 + \Omega_2 \Phi_2 + \Omega_3 \Phi_3) \quad (2.65)$$

$$i\hbar\dot{\Phi}_1 = \hbar\Omega_1^* \Phi_0 \quad (2.66)$$

$$i\hbar\dot{\Phi}_2 = \hbar [(\omega_2 - \omega_1) - (\bar{\omega}_1 - \bar{\omega}_2)] \Phi_2 + \hbar\Omega_2^* \Phi_0 \quad (2.67)$$

$$i\hbar\dot{\Phi}_3 = \hbar [(\omega_3 - \omega_1) - (\bar{\omega}_1 - \bar{\omega}_3)] \Phi_3 + \hbar\Omega_3^* \Phi_0. \quad (2.68)$$

For the case of resonance the equations may be further simplified:  $\omega_2 - \omega_1 = \bar{\omega}_1 - \bar{\omega}_2$ ,  $\omega_3 - \omega_1 = \bar{\omega}_1 - \bar{\omega}_3$ . Now we are in the so-called interaction representation where the Hamiltonian looks like

$$\hat{H}_0 = H_{CM} - \hbar \left( \Omega_1 |0\rangle\langle 1| + \Omega_2 |0\rangle\langle 2| + \Omega_3 |0\rangle\langle 3| + \text{H.c.} \right). \quad (2.69)$$

Proceeding as for the case of the  $\Lambda$ -scheme, we find two dark dressed states  $|D_1\rangle = -\frac{\Omega_3}{\Omega_1}|1\rangle + |3\rangle$  and  $|D_2\rangle = -\frac{\Omega_2}{\Omega_1}|1\rangle + |2\rangle$  which are decoupled from the light field. In the dark-bright

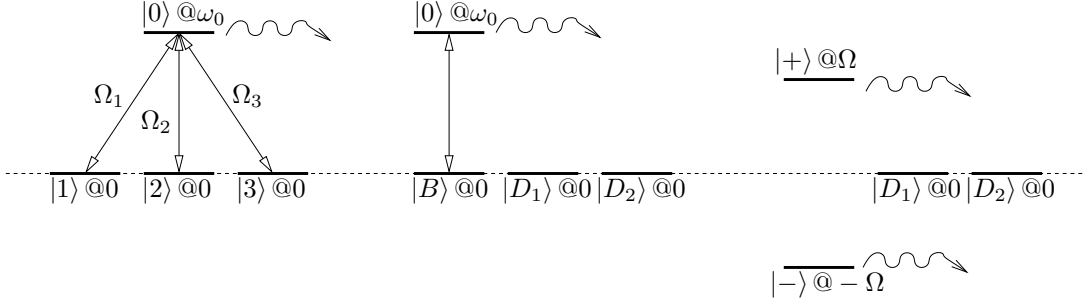


Fig. 2.10: Different bases for the tripod atom (energy shifted to  $\omega_1 = \omega_2 = \omega_3 = 0$ ): bare state bases (left), dark-bright state basis (middle) and complete dressed state basis (right)

basis  $|0\rangle$  is only coupled to the bright state  $|B\rangle = (\Omega_1^*|1\rangle + \Omega_2^*|2\rangle + \Omega_3^*|3\rangle)/\Omega$ , where  $\Omega = (|\Omega_1|^2 + |\Omega_2|^2 + |\Omega_3|^2)^{1/2}$  is the total Rabi frequency. The two states  $|B\rangle$  and  $|0\rangle$  split into a dressed doublet  $|\pm\rangle = (|B\rangle \pm |0\rangle)/\sqrt{2}$  with energies  $\pm\hbar\Omega$ .

We assume that the light fields are sufficiently strong, so that  $\Omega$  is large compared to the two-photon detuning, due to the laser mismatch and/or Doppler shift. The dark states are thus well separated in energies from the doublet  $|\pm\rangle$ , and the internal atomic state evolves within the dark state manifold. The full atomic state-vector  $|\Phi\rangle$  can then be expanded in terms of the dark states,  $|\Phi\rangle = \sum_{j=1}^2 \Phi_{D_j}(\mathbf{r})|D_j(\mathbf{r})\rangle$ , where  $\Psi_j(\mathbf{r})$  is a wave-function for the center of mass motion of an atom in the  $j$ -th dark state. The two-component spinor-like wavefunction  $\{\Phi_{D_1}, \Phi_{D_2}\}^T$  obeys the Schrödinger equation  $i\hbar\partial\Psi/\partial t = H\Psi$ , with the Hamiltonian from section 2.4.2

$$i\hbar\frac{\partial}{\partial t} \begin{pmatrix} \Phi_{D_1} \\ \Phi_{D_2} \end{pmatrix} = \left[ \frac{1}{2m}(-i\hbar\nabla - \mathbf{A})^2 + V + \Phi \right] \begin{pmatrix} \Phi_{D_1} \\ \Phi_{D_2} \end{pmatrix} \quad (2.70)$$

$$\mathbf{A}_{nm} = i\hbar\langle\chi_n(\mathbf{r})|\nabla\chi_m(\mathbf{r})\rangle \quad n, m \in \{1, 2\} \quad (2.71)$$

$$\Phi_{nm} = \frac{1}{2m} \sum_{l \in \{+, -\}} A_{nl} \cdot A_{lm} \quad n, m \in \{1, 2\} \quad (2.72)$$

$$= \frac{\hbar^2}{2m} \left( \langle\nabla\chi_n|\nabla\chi_m\rangle + \sum_{k=1}^2 \langle\chi_n|\nabla\chi_k\rangle\langle\chi_k|\nabla\chi_m\rangle \right) \quad (2.73)$$

$$V_{nm} = \varepsilon_n(\mathbf{r})\delta_{nm} + \langle\chi_n(\mathbf{r})|V(\mathbf{r})|\chi_m(\mathbf{r})\rangle \quad n, m \in \{1, 2\}, \quad (2.74)$$

where  $\mathbf{A}, \Phi, V$  are effective potentials for the case of an adiabatic motion.

For a systematic study of these potentials we parametrize the Rabi frequencies  $\Omega_\mu$  with an

angle (on a sphere) and phase variables ( $e^{iS_j}$ ) according to

$$\begin{aligned}\Omega_1 &= \Omega \sin \theta \cos \phi e^{iS_1} \\ \Omega_2 &= \Omega \sin \theta \sin \phi e^{iS_2} \\ \Omega_3 &= \Omega \cos \theta e^{iS_3},\end{aligned}\tag{2.75}$$

where  $\Omega^2 = |\Omega_1|^2 + |\Omega_2|^2 + |\Omega_3|^2$ . This leads to

$$|D_1\rangle = \frac{\cos \theta e^{iS_{31}}}{\sin \theta \cos \phi} |1\rangle - |3\rangle\tag{2.76}$$

$$|D_2\rangle = \frac{\cos \theta e^{iS_{31}}}{\sin \theta} |1\rangle + |2\rangle\tag{2.77}$$

with  $S_{ij} = S_i - S_j$ . The dressed states basis is not unique, if we change  $\tilde{\Psi} \rightarrow U(r)\tilde{\Psi}$ , so do

$$A \rightarrow U(r)AU^\dagger(r) - i\hbar(\nabla U)U^\dagger(r)\tag{2.78}$$

$$\Phi \rightarrow U(r)\Phi U^\dagger(r)\tag{2.79}$$

$$B \rightarrow U(r)BU^\dagger(r).\tag{2.80}$$

This allows us to obtain a form of the dark states analytically simpler than eqs. (2.76, 2.77). We consider the linear combination

$$|D_1^{\text{new}}\rangle = -\cos \phi e^{iS_{32}}|D_2\rangle,\tag{2.81}$$

$$|D_2^{\text{new}}\rangle = -\sin \theta |D_1\rangle + \cos \theta \sin \phi e^{iS_{32}}|D_2\rangle.\tag{2.82}$$

Dark and bright states are hence now

$$|D_1\rangle = \sin \phi e^{iS_{31}}|1\rangle - \cos \phi e^{iS_{32}}|2\rangle\tag{2.83}$$

$$|D_2\rangle = \cos \theta \cos \phi e^{iS_{31}}|1\rangle + \cos \theta \sin \phi e^{iS_{32}}|2\rangle - \sin \theta |3\rangle\tag{2.84}$$

$$|B\rangle = \sin \theta \cos \phi e^{iS_{31}}|1\rangle + \sin \theta \sin \phi e^{iS_{32}}|2\rangle + \cos \theta |3\rangle.\tag{2.85}$$

Projecting the state of our system  $|\Psi\rangle$  on our new basis states we get

$$\Phi_{D_1} = \langle D_1|\Psi\rangle = \sin \phi e^{-iS_{31}}\Phi_1 - \cos \phi e^{-iS_{32}}\Phi_2\tag{2.86}$$

$$\Phi_{D_2} = \langle D_2|\Psi\rangle = \cos \theta \cos \phi e^{-iS_{31}}\Phi_1 + \cos \theta \sin \phi e^{-iS_{32}}\Phi_2 - \sin \theta \Phi_3\tag{2.87}$$

$$\Phi_B = \langle B|\Psi\rangle = \sin \theta \cos \phi e^{-iS_{31}}\Phi_1 + \sin \theta \sin \phi e^{-iS_{32}}\Phi_2 + \cos \theta \Phi_3,\tag{2.88}$$

which has the inverse transformation

$$\Phi_1 = [\sin \phi \Phi_{D_1} + \cos \theta \cos \phi \Phi_{D_2} + \sin \theta \cos \phi \Phi_B] e^{iS_{31}}\tag{2.89}$$

$$\Phi_2 = [-\cos \phi \Phi_{D_1} + \cos \theta \sin \phi \Phi_{D_2} + \sin \theta \sin \phi \Phi_B] e^{iS_{32}}\tag{2.90}$$

$$\Phi_3 = -\sin \theta \Phi_{D_2} + \cos \theta \Phi_B.\tag{2.91}$$

Now we can rewrite the effective potentials in terms of (experimentally accessible) laser parameters

$$\mathbf{A}_{nm} = i\hbar \langle \chi_n(\mathbf{r}) | \nabla \chi_m(\mathbf{r}) \rangle \quad n, m \in \{1, 2\} \quad (2.92)$$

$$\mathbf{A}_{11} = \hbar (\cos^2 \phi \nabla (S_2 - S_3) + \sin^2 \phi \nabla (S_1 - S_3)) \quad (2.93)$$

$$\mathbf{A}_{12} = \hbar \cos \theta \left( \frac{1}{2} \sin(2\phi) \nabla (S_1 - S_2) - i \nabla \phi \right) \quad (2.94)$$

$$\mathbf{A}_{22} = \hbar \cos^2 \theta (\cos^2 \phi \nabla (S_1 - S_3) + \sin^2 \phi \nabla (S_2 - S_3)). \quad (2.95)$$

This relatively complicated expression for  $\mathbf{A}$  can become non-Abelian under certain conditions, as we shall show below. The effective magnetic and scalar fields are hence:

$$\mathbf{B}_{11} = 0 \quad (2.96)$$

$$\mathbf{B}_{12} = i\hbar \sin \theta e^{-iS} \nabla \theta \times \nabla \phi - \hbar \cos \theta e^{-iS} \nabla S \times \nabla \phi (1 + \cos^2 \theta) \quad (2.97)$$

$$\mathbf{B}_{22} = -2\hbar \cos \theta \sin \theta \nabla \theta \times \nabla S \quad (2.98)$$

$$\Phi_{nm} = \frac{1}{2m} \sum_{l \in \{+, -\}} A_{nl} \cdot A_{lm} \quad n, m \in \{1, 2\} \quad (2.99)$$

$$= \frac{\hbar^2}{2m} \left( \langle \nabla \chi_n | \nabla \chi_m \rangle + \sum_{k=1}^2 \langle \chi_n | \nabla \chi_k \rangle \langle \chi_k | \nabla \chi_m \rangle \right) \quad (2.100)$$

$$\Phi_{11} = \frac{\hbar^2}{2m} \sin^2 \theta \left( \frac{1}{4} \sin^2(2\phi) (\nabla S_{12})^2 + (\nabla \phi)^2 \right) \quad (2.101)$$

$$\Phi_{12} = \frac{\hbar^2}{2m} \sin \theta \left( \frac{1}{2} \sin(2\phi) \nabla S_{12} - i \nabla \phi \right) \left( \frac{1}{2} \sin(2\theta) (\cos^2 \phi \nabla S_{13} + \sin^2 \phi \nabla S_{23}) - i \nabla \theta \right) \quad (2.102)$$

$$\Phi_{22} = \frac{\hbar^2}{2m} \left( \frac{1}{4} \sin^2(2\theta) (\cos^2 \phi \nabla S_{13} + \sin^2 \phi \nabla S_{23})^2 + (\nabla \theta)^2 \right). \quad (2.103)$$

The scalar potential can be represented as  $\Phi_{ij} = \frac{\hbar^2}{2m} \boldsymbol{\kappa}_i^* \cdot \boldsymbol{\kappa}_j$ , where

$$\boldsymbol{\kappa}_1 = \sin \theta \left( \frac{1}{2} \sin(2\phi) \nabla S_{12} + i \nabla \phi \right) \quad (2.104)$$

$$\boldsymbol{\kappa}_2 = \frac{1}{2} \sin(2\theta) (\cos^2 \phi \nabla S_{13} + \sin^2 \phi \nabla S_{23}) - i \nabla \theta. \quad (2.105)$$

Finally the trapping potential is of the form

$$V = V_1(r) |1\rangle \langle 1| + V_2(r) |2\rangle \langle 2| + V_3(r) |3\rangle \langle 3|, \quad (2.106)$$

where  $V_j(\mathbf{r})$  is the trapping potential for an atom in the original internal state  $j = 1, 2, 3$ . Note that the potential  $V_j$  can also accommodate a possible detuning of the  $j$ -th laser from

the resonance of the  $j \rightarrow 0$  transition. Using  $V_{jk} = \langle D_j | V | D_k \rangle$ , we get

$$V_{nm} = \varepsilon_n(\mathbf{r}) \delta_{nm} + \langle \chi_n(\mathbf{r}) | V(\mathbf{r}) | \chi_m(\mathbf{r}) \rangle \quad n, m \in \{1, 2\} \quad (2.107)$$

$$V_{11} = V_2 \cos^2 \phi + V_1 \sin^2 \phi \quad (2.108)$$

$$V_{12} = \frac{1}{2}(V_1 - V_2) \cos \theta \sin(2\phi) \quad (2.109)$$

$$V_{22} = (V_1 \cos^2 \phi + V_2 \sin^2 \phi) \cos^2 \theta + V_3 \sin^2 \theta. \quad (2.110)$$

The previous expression for  $\mathbf{A}$ ,  $\Phi$  and  $V$  provide a remarkable versatility. Recent advances in shaping both the phase and the intensity of light beams, make it possible to choose (almost) any form of the induced gauge potential, provided the corresponding light field obeys Maxwell's equations. This is certainly the case in a two-dimensional geometry, but also in three dimensions light beams can be tailored [MSM<sup>+</sup>03, WC05].

Possible experimental realizations of the above discussed tripod scheme include the transition  $5S_{1/2}$  ( $F = 1$ )  $\leftrightarrow$   $5P_{3/2}$  ( $F = 0$ ) in  $^{87}\text{Rb}$  (see fig. 2.11). Even if there is no suitable ground state available, one can use metastable states as ground states, as for example the transition  $2^3S_1 \leftrightarrow 2^3P_0$  in  $^4\text{He}^*$ , see fig. 2.12.

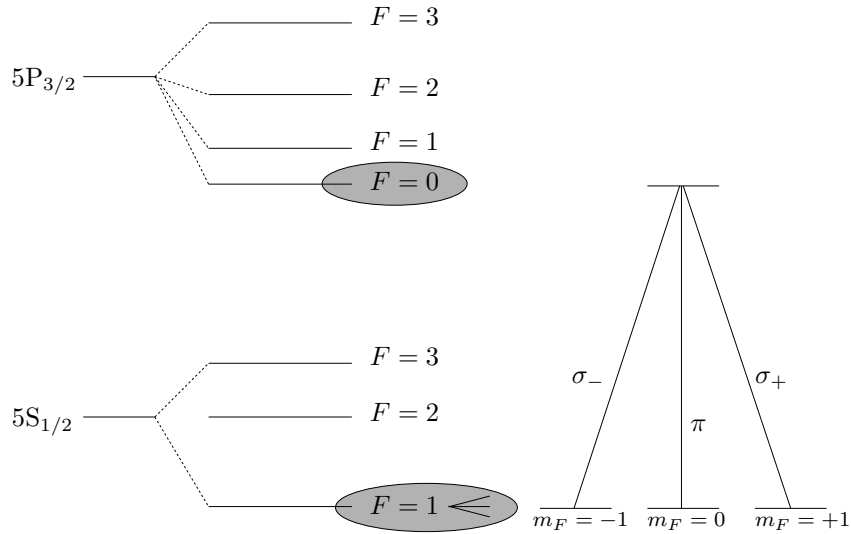


Fig. 2.11: Transition  $5S_{1/2}$  ( $F = 1$ )  $\leftrightarrow$   $5P_{3/2}$  ( $F = 0$ ) in  $^{87}\text{Rb}$ .

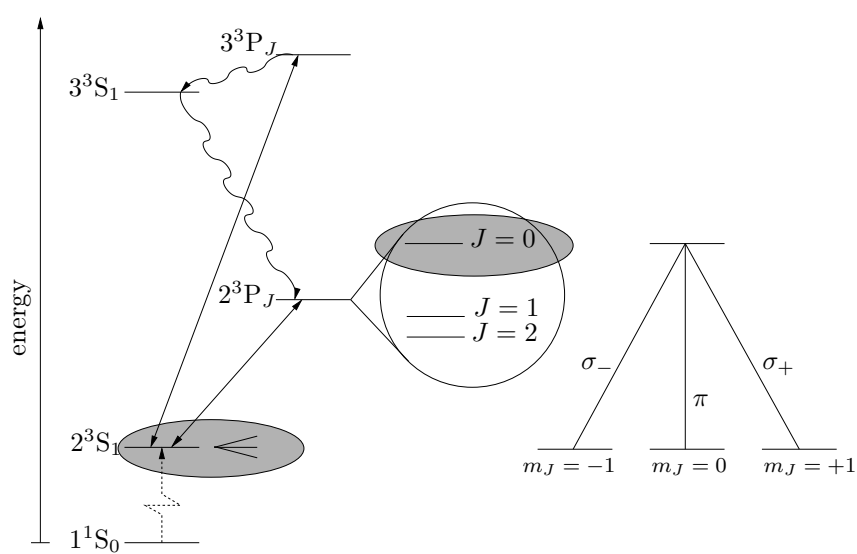


Fig. 2.12: Transition  $2^3S_1 \leftrightarrow 2^3P_0$  in  $^4\text{He}^*$ .



## 2.5 General conditions for non-Abelian gauges

Using the parametrized Rabi frequencies from the last section (eq. (2.75)) we can write a very general expression for the vector potential  $\mathbf{A}$

$$\begin{aligned} \frac{\mathbf{A}}{\hbar} = & \begin{pmatrix} \cos^2 \phi & -\cos \theta \cos \phi \sin \phi \\ -\cos \theta \cos \phi \sin \phi & \cos^2 \theta \sin^2 \phi \end{pmatrix} \nabla S_{23} \\ & + \begin{pmatrix} \sin^2 \phi & \cos \theta \cos \phi \sin \phi \\ \cos \theta \cos \phi \sin \phi & \cos^2 \theta \cos^2 \phi \end{pmatrix} \nabla S_{13} \\ & + \cos \theta \hat{\sigma}_y \nabla \phi. \end{aligned} \quad (2.111)$$

For easier computation we will rewrite  $\mathbf{A}$  as a sum of Pauli sigma matrices:

$$\begin{aligned} \frac{\mathbf{A}}{\hbar} = & \frac{\cos^2 \phi}{2} (\hat{\mathbf{1}} + \hat{\sigma}_z) \nabla S_{23} + \frac{\cos^2 \theta \sin^2 \phi}{2} (\hat{\mathbf{1}} - \hat{\sigma}_z) \nabla S_{23} - \cos \theta \sin \phi \cos \phi \hat{\sigma}_x \nabla S_{23} \\ & + \frac{\sin^2 \phi}{2} (\hat{\mathbf{1}} + \hat{\sigma}_z) \nabla S_{13} + \frac{\cos^2 \theta \cos^2 \phi}{2} (\hat{\mathbf{1}} - \hat{\sigma}_z) \nabla S_{13} + \cos \theta \sin \phi \cos \phi \hat{\sigma}_x \nabla S_{13} + \cos \theta \hat{\sigma}_y \nabla \phi \end{aligned} \quad (2.112)$$

$$\begin{aligned} = & \left[ \frac{1}{2} (\cos^2 \phi + \cos^2 \theta \sin^2 \phi) \nabla S_{23} + \frac{1}{2} (\sin^2 \phi + \cos^2 \theta \cos^2 \phi) \nabla S_{13} \right] \hat{\mathbf{1}} \\ & + \left[ \frac{1}{2} (\cos^2 \phi - \cos^2 \theta \sin^2 \phi) \nabla S_{23} + \frac{1}{2} (\sin^2 \phi - \cos^2 \theta \cos^2 \phi) \nabla S_{13} \right] \hat{\sigma}_z \\ & + \cos \theta \sin \phi \cos \phi \nabla S_{12} \hat{\sigma}_x + \cos \theta \nabla \phi \hat{\sigma}_y \end{aligned} \quad (2.113)$$

In the following we shall assume that the atoms are strongly trapped in the  $z$ -direction, hence they are confined to the  $xy$ -plane. Given two orthogonal vectors  $\boldsymbol{\xi}$  and  $\boldsymbol{\eta}$  in the  $xy$ -plane, we shall be interested in non-Abelian situations, in which  $\hat{A}_\xi \equiv \hat{A} \cdot \boldsymbol{\xi}$  and  $\hat{A}_\eta \equiv \hat{A} \cdot \boldsymbol{\eta}$  fulfill  $[\hat{A}_\xi, \hat{A}_\eta] \neq 0$ .

$$\begin{aligned} [\hat{A}_\xi, \hat{A}_\eta] = & -i \cos \theta [\mathbf{u} \times \nabla \phi]_\lambda \hat{\sigma}_x \\ & + i \cos \theta \sin \theta \cos \phi [\mathbf{u} \times \nabla S_{12}]_\lambda \hat{\sigma}_y \\ & + 2i \cos^2 \theta \sin \phi \cos \phi [\nabla S_{12} \times \nabla \phi]_\lambda \hat{\sigma}_z, \end{aligned} \quad (2.114)$$

where  $\mathbf{u} = (\cos^2 \phi - \cos^2 \theta \sin^2 \theta) \nabla S_{23} + (\sin^2 \phi - \cos^2 \theta \cos^2 \phi) \nabla S_{13}$ . This general condition may be achieved in at least one of the following ways:

- $(\mathbf{u} \times \nabla \phi)_z \neq 0$  (e.g. the constant gauge discussed in section 2.5.1)
- $(\mathbf{u} \times \nabla S_{12})_z \neq 0$  (e.g. the Landau gauge discussed in section 2.5.2)
- $(\nabla S_{12} \times \nabla \phi)_z \neq 0$ , (e.g. the symmetric gauge, discussed in section 2.5.3)

### 2.5.1 Constant non-Abelian gauge

We will consider first homogeneous intensity profiles, i.e. both  $\phi$  and  $\theta$  are now space independent. We choose the particular case with  $\phi = \pi/4$ . Let  $\xi \equiv x$ ,  $\eta \equiv y$ ,  $\lambda \equiv z$ . For constant  $\phi$  the

non-Abelian character demands  $\nabla S_{23} \times \nabla S_{13} \neq 0$ . Let us parametrize the laser parameters as  $S_{j3} = \alpha_j x + \beta_j y$  ( $\nabla S_{j3} = \alpha_j \hat{x} + \beta_j \hat{y}$ ), where  $\alpha_j, \beta_j$  are constants. A simple laser arrangement fulfilling the non-Abelian condition is given by  $\alpha_2 \beta_1 \neq \alpha_1 \beta_2$ :

$$A_x = \frac{1}{4}(1 + \cos^2 \theta)(\alpha_2 + \alpha_1) \hat{\mathbb{1}} + \frac{1}{4}(1 - \cos^2 \theta)(\alpha_2 + \alpha_1) \hat{\sigma}_z + \frac{1}{2} \cos \theta (\alpha_1 - \alpha_2) \hat{\sigma}_x \quad (2.115)$$

$$A_y = \frac{1}{4}(1 + \cos^2 \theta)(\beta_2 + \beta_1) \hat{\mathbb{1}} + \frac{1}{4}(1 - \cos^2 \theta)(\beta_2 + \beta_1) \hat{\sigma}_z + \frac{1}{2} \cos \theta (\beta_1 - \beta_2) \hat{\sigma}_x \quad (2.116)$$

The scalar potential is given by  $\Phi_{ij} = \frac{\hbar^2}{2m} \boldsymbol{\kappa}_i^* \cdot \boldsymbol{\kappa}_j$  with

$$\boldsymbol{\kappa}_1 = \frac{1}{2} \sin \theta (\nabla S_{13} - \nabla S_{23}) = \frac{1}{2} \sin \theta ((\alpha_1 - \alpha_2) \hat{x} + (\beta_1 - \beta_2) \hat{y}) \quad (2.117)$$

$$\boldsymbol{\kappa}_2 = \frac{1}{4} \sin(2\theta) (\nabla S_{13} + \nabla S_{23}) - i \nabla \theta = \frac{1}{4} \sin(2\theta) ((\alpha_1 + \alpha_2) \hat{x} + (\beta_1 + \beta_2) \hat{y}) - i (\partial_x \theta \hat{x} + \partial_y \theta \hat{y}). \quad (2.118)$$

Let us choose for concreteness  $\theta = \pi/4$ . The scalar gauge  $\Phi$  and the scalar potential  $V$  for this particular case are:

$$\Phi = \frac{\hbar^2}{2m} \begin{pmatrix} \frac{1}{8} [(\alpha_1 - \alpha_2)^2 + (\beta_1 - \beta_2)^2] & \frac{1}{8\sqrt{2}} [(\alpha_1^2 - \alpha_2^2) + (\beta_1^2 - \beta_2^2)] \\ \frac{1}{8\sqrt{2}} [(\alpha_1^2 - \alpha_2^2) + (\beta_1^2 - \beta_2^2)] & \frac{1}{16} [(\alpha_1 + \alpha_2)^2 + (\beta_1 + \beta_2)^2] \end{pmatrix} \quad (2.119)$$

$$V = \begin{pmatrix} \frac{V_1 + V_2}{2} & \frac{V_1 - V_2}{2\sqrt{2}} \\ \frac{V_1 - V_2}{2\sqrt{2}} & \frac{V_3}{2} + \frac{V_1 + V_2}{4} \end{pmatrix} = \frac{V_1 + V_2}{2} \hat{\mathbb{1}} + \begin{pmatrix} 0 & \frac{V_1 - V_2}{2\sqrt{2}} \\ \frac{V_1 - V_2}{2\sqrt{2}} & \frac{V_3 - (V_1 + V_2)/2}{2} \end{pmatrix}. \quad (2.120)$$

On the other hand, by choosing  $V_j(\mathbf{r}) = \Delta E_j + U(\mathbf{r})$ , with detunings:

$$\Delta E_1 = -\frac{\hbar^2}{16m} [(\alpha_1^2 - \alpha_2^2) + (\beta_1^2 - \beta_2^2)] \quad (2.121)$$

$$\Delta E_2 = \frac{\hbar^2}{16m} [(\alpha_1^2 - \alpha_2^2) + (\beta_1^2 - \beta_2^2)] \quad (2.122)$$

$$\Delta E_3 = -\frac{\hbar^2}{16m} [(\alpha_1^2 + \alpha_2^2) + (\beta_1^2 + \beta_2^2)] , \quad (2.123)$$

one can prove that (up to an irrelevant constant)  $V + \phi = U(\mathbf{r})$  where  $U(\mathbf{r})$  is a common trapping potential for all components  $V_i$  ( $i = 1, 2, 3$ ). The vector potential is

$$A_x = \frac{3}{8}(\alpha_2 + \alpha_1) \hat{\mathbb{1}} + \frac{1}{8}(\alpha_2 + \alpha_1) \hat{\sigma}_z + \frac{1}{2\sqrt{2}}(\alpha_1 - \alpha_2) \hat{\sigma}_x \quad (2.124)$$

$$A_y = \frac{3}{8}(\beta_2 + \beta_1) \hat{\mathbb{1}} + \frac{1}{8}(\beta_2 + \beta_1) \hat{\sigma}_z + \frac{1}{2\sqrt{2}}(\beta_1 - \beta_2) \hat{\sigma}_x. \quad (2.125)$$

A gauge transformation eliminates the terms proportional to the identity matrix in  $A_x$  and  $A_y$ . Let  $\hbar \kappa_y = (\beta_1 - \beta_2)/2\sqrt{2}$ ,  $\hbar q_y = (\beta_1 + \beta_2)/8$ ,  $\hbar \kappa_x = (\alpha_1 - \alpha_2)/2\sqrt{2}$ ,  $\hbar q_x = (\alpha_1 + \alpha_2)/8$ . A rotation

$$\hat{\sigma}_x \rightarrow \cos \eta \hat{\sigma}_x + \sin \eta \hat{\sigma}_z \quad (2.126)$$

$$\hat{\sigma}_z \rightarrow -\sin \eta \hat{\sigma}_x + \cos \eta \hat{\sigma}_z \quad (2.127)$$

with  $\tan 2\eta = \kappa_y/q_y$ , provides

$$A_x = \hbar\tilde{\kappa}_x\hat{\sigma}_x + \hbar\tilde{q}_x\hat{\sigma}_z, \quad (2.128)$$

$$A_y = \hbar\tilde{q}_y\hat{\sigma}_z \quad (2.129)$$

where  $\tilde{\kappa}_x = \cos(2\phi)\kappa_x - \sin(2\phi)q_x$ ,  $\tilde{q}_x = \cos(2\phi)q_x + \sin(2\phi)\kappa_x$ , and  $\tilde{q}_y = \cos(2\phi)q_y + \sin(2\phi)\kappa_y$ .

The situation discussed above may be easily implemented experimentally. From the parametrization (2.75) we see that  $\phi = \pi/4$  and  $\theta = \pi/4$  means that laser 1 and 2 must have equal intensities, whereas laser 3 has twice that intensity:  $\Omega_1 = \frac{\Omega}{2}e^{iS_1}$ ,  $\Omega_2 = \frac{\Omega}{2}e^{iS_2}$ ,  $\Omega_3 = \frac{\Omega}{\sqrt{2}}e^{iS_3}$ . Assuming  $V_1 = V_2$  the potentials acquire the form:

$$\mathbf{A} = \frac{\hbar}{2} \begin{pmatrix} \nabla(S_{13} + S_{23}) & \frac{1}{\sqrt{2}}\nabla S_{12} \\ \frac{1}{\sqrt{2}}\nabla S_{12} & \frac{1}{2}\nabla(S_{13} + S_{23}) \end{pmatrix} \quad (2.130)$$

$$\Phi = \frac{\hbar^2}{16m} \begin{pmatrix} (\nabla S_{12})^2 & \frac{1}{\sqrt{2}}(\nabla S_{12}) \cdot \nabla(S_{13} + S_{23}) \\ \frac{1}{\sqrt{2}}(\nabla S_{12}) \cdot \nabla(S_{13} + S_{23}) & \frac{1}{2}(\nabla(S_{13} + S_{23}))^2 \end{pmatrix} \quad (2.131)$$

$$V = \begin{pmatrix} V_1 & 0 \\ 0 & (V_1 + V_3)/2 \end{pmatrix}. \quad (2.132)$$

Assuming the phases  $S_j$  as  $z$ -independent, the components of the vector potential are of the form:

$$\begin{aligned} A_x &= \frac{\hbar}{2} \begin{pmatrix} \partial_x(S_{13} + S_{23}) & \frac{1}{\sqrt{2}}\partial_x S_{12} \\ \frac{1}{\sqrt{2}}\partial_x S_{12} & \frac{1}{2}\partial_x(S_{13} + S_{23}) \end{pmatrix} \\ &= \frac{\hbar}{2} \left\{ \partial_x(S_{13} + S_{23}) \left( \frac{3}{4}\hat{1} + \frac{1}{4}\hat{\sigma}_z \right) + \frac{1}{\sqrt{2}}\partial_x S_{12}\hat{\sigma}_x \right\} \end{aligned} \quad (2.133)$$

$$A_y = \frac{\hbar}{2} \left\{ \partial_y(S_{13} + S_{23}) \left( \frac{3}{4}\hat{1} + \frac{1}{4}\hat{\sigma}_z \right) + \frac{1}{\sqrt{2}}\partial_y S_{12}\hat{\sigma}_x \right\}. \quad (2.134)$$

The corresponding commutator is:

$$\begin{aligned} [A_x, A_y] &= \frac{\hbar^2}{4} \left\{ \frac{1}{4\sqrt{2}} [\partial_x(S_{13} + S_{23})\partial_y S_{12}] [\hat{\sigma}_z, \hat{\sigma}_x] + \frac{1}{4\sqrt{2}} [\partial_x S_{12}\partial_y(S_{13} + S_{23})] [\hat{\sigma}_x, \hat{\sigma}_z] \right\} \\ &= \frac{\hbar^2}{16\sqrt{2}} \{ \partial_x S_{12}\partial_y(S_{13} + S_{23}) - \partial_x(S_{13} + S_{23})\partial_y S_{12} \} [\hat{\sigma}_x, \hat{\sigma}_z], \end{aligned} \quad (2.135)$$

and hence the non-Abelian condition requires

$$\partial_x S_{12}\partial_y(S_{13} + S_{23}) - \partial_x(S_{13} + S_{23})\partial_y S_{12} \neq 0. \quad (2.136)$$

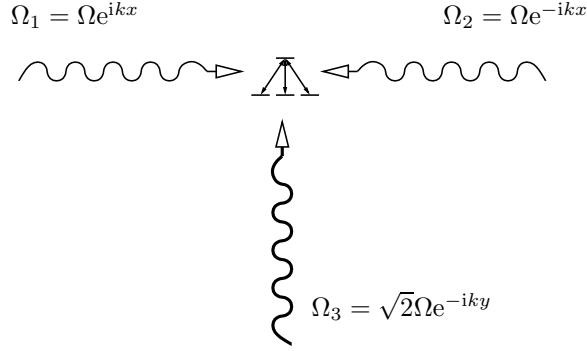


Fig. 2.13: Proposed scheme for generating a constant non-Abelian gauge.

The example (fig. 2.13), where  $S_1 = kx$ ,  $S_2 = -kx$  and  $S_3 = -ky$  results in

$$A_x = \frac{\hbar k}{\sqrt{2}} \hat{\sigma}_x = \frac{\hbar \kappa}{\sqrt{2}} \begin{pmatrix} 0 & 1 \\ 1 & 0 \end{pmatrix} \quad (2.137)$$

$$A_y = \hbar k \left( \frac{3}{4} \hat{\mathbb{1}} + \frac{1}{4} \hat{\sigma}_z \right) = \hbar \kappa \begin{pmatrix} 1 & 0 \\ 0 & \frac{1}{2} \end{pmatrix} \quad (2.138)$$

$$\Phi = \frac{\hbar^2 k^2}{2m} \begin{pmatrix} 1 & 0 \\ 0 & \frac{1}{2} \end{pmatrix} \quad (2.139)$$

Surprisingly, the generation of a non-Abelian gauge field, which as we show in the next chapters already leads to a rather non-trivial physics, does not require any elaborate laser arrangement.

## 2.5.2 Landau Gauge

The classical Landau gauge  $\mathbf{A}(\mathbf{r}) = (0, B_0 x, 0)$  creates a magnetic field in  $z$ -direction. Its most natural non-Abelian generalization would be to transform the vector potential

$$\mathbf{A}(\mathbf{r}) = (\hbar \kappa M_x, B_0 M_y x, 0), \quad (2.140)$$

where  $M_x$  and  $M_y$  are non-commuting matrices and  $\kappa$  is a constant describing the strength of the non-Abelian character. This kind of gauge field will appear if we consider the case  $S_{13} = S_{23} = S$  from the beginning of section 2.5. In that case the non-Abelian character demands  $(\nabla S \times \nabla \phi)_z \neq 0$ . Let  $\xi \equiv x$ ,  $\eta \equiv y$ ,  $\lambda \equiv z$  and use the parametrization  $S = \alpha x + \beta y$  ( $\nabla S = \alpha \hat{x} + \beta \hat{y}$ ) and  $\phi = \gamma x + \delta y$  ( $\nabla \phi = \gamma \hat{x} + \delta \hat{y}$ ) giving the potentials

$$A_x = \alpha(1 + \cos^2 \theta) \hat{\mathbb{1}} + \alpha(1 - \cos^2 \theta) \hat{\sigma}_z + \gamma \cos \theta \hat{\sigma}_x \quad (2.141)$$

$$A_y = \beta(1 + \cos^2 \theta) \hat{\mathbb{1}} + \beta(1 - \cos^2 \theta) \hat{\sigma}_z + \delta \cos \theta \hat{\sigma}_x \quad (2.142)$$

$$\boldsymbol{\kappa}_1 = i \sin \theta (\gamma, \delta, 0) \quad (2.143)$$

$$\boldsymbol{\kappa}_2 = \frac{1}{2} \sin 2\theta (\alpha, \beta, 0) - i \nabla \theta \quad (2.144)$$

The non-Abelian condition (eq. (2.136)) is in this case  $\alpha\delta \neq \gamma\beta$ . We choose the following laser parametrization:  $\cos\theta = \frac{x}{R_c}$ ,  $\sin\theta = \frac{z-z_c}{R_c}$ ,  $R_c^2 = x^2 + (z-z_c)^2$ ,  $z \approx 0$ ,  $z_c \gg |x|$ . Then up to linear order

$$A_x = \alpha(\hat{1} + \hat{\sigma}_z) + \gamma \left( \frac{x}{z_c} \right) \hat{\sigma}_y + O \left( \left( \frac{x}{z_c} \right)^2 \right) \quad (2.145)$$

$$A_y = \beta(\hat{1} + \hat{\sigma}_z) + \delta \left( \frac{x}{z_c} \right) \hat{\sigma}_y + O \left( \left( \frac{x}{z_c} \right)^2 \right). \quad (2.146)$$

For the particular case of  $\gamma = 0$

$$A_x = \alpha(\hat{1} + \hat{\sigma}_z) \quad (2.147)$$

$$A_y = \beta(\hat{1} + \hat{\sigma}_z) + \delta \left( \frac{x}{z_c} \right) \hat{\sigma}_y. \quad (2.148)$$

The scalar potential is given by  $\Phi_{ij} = \frac{\hbar^2}{2m} \boldsymbol{\kappa}_i^* \cdot \boldsymbol{\kappa}_j$ , where

$$\boldsymbol{\kappa}_1 \cong i(0, \delta, 0) \quad (2.149)$$

$$\boldsymbol{\kappa}_2 \cong \frac{x}{z_c}(\alpha, \beta, 0) + \frac{i}{z_c} \left( 1, 0, \frac{x}{z_c} \right). \quad (2.150)$$

Hence:

$$\Phi_{11} \cong \frac{\hbar^2}{2m} \delta^2 \quad (2.151)$$

$$\Phi_{12} \cong -i \frac{\hbar^2}{2m} \beta \delta \left( \frac{x}{z_c} \right) \quad (2.152)$$

$$\Phi_{22} \cong \frac{\hbar^2}{2m z_c^2}. \quad (2.153)$$

Assuming for simplicity  $\beta = 0$ , the scalar potential becomes

$$\Phi = \frac{\hbar^2}{2m} \begin{pmatrix} \delta^2 & 0 \\ 0 & \frac{1}{z_c^2} \end{pmatrix}, \quad (2.154)$$

which may be easily removed by choosing proper detunings such that

$$V_1 = -\frac{\hbar^2}{2m} \delta^2 = V_2 \quad (2.155)$$

$$V_2 = -\frac{\hbar^2}{2m z_c^2}. \quad (2.156)$$

Then, we eliminate the scalar potential, and recover an effective vector potential of the form:

$$A_x = \alpha(\hat{1} + \hat{\sigma}_z) \quad (2.157)$$

$$A_y = \delta \left( \frac{x}{z_c} \right) \hat{\sigma}_y, \quad (2.158)$$

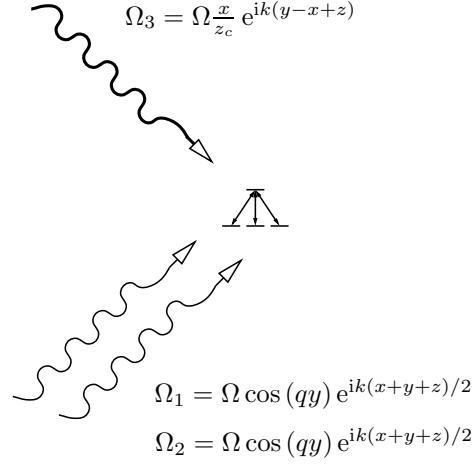


Fig. 2.14: Suggested scheme for generating a non-Abelian Landau-type gauge.

the identity part of  $A_x$  can easily be gauged out

$$A_x = \alpha \hat{\sigma}_z \quad (2.159)$$

$$A_y = B_0 x \hat{\sigma}_y \quad (2.160)$$

where  $B_0 = \delta/z_c$ . Note that  $x/z_c \ll 1$ , but this does not mean that  $\delta$  or  $\alpha$  have to be  $\ll 1$ , i.e.  $B_0$  can be large. In addition, note that  $\alpha$  controls the non-Abelian part.

A possible example of laser arrangement leading to a Landau-gauge field as the one above would be:

$$\Omega_1 = \Omega \cos(\delta y) e^{i\alpha(x+y)/2 + \tilde{\kappa}z} \quad (2.161)$$

$$\Omega_2 = \Omega \sin(\delta y) e^{i\alpha(x+y)/2 + \tilde{\kappa}z} \quad (2.162)$$

$$\Omega_3 = \Omega \frac{x}{z_c} e^{i\alpha(y-x)/2 + \tilde{\kappa}z}. \quad (2.163)$$

### 2.5.3 Symmetric Gauge

We recall that a standard symmetric gauge is of the form  $\mathbf{A} \propto \rho \hat{\phi}$ . Let us choose  $S_{13} = 0$ ,  $S_{23} = -S_{12} = S$ . A symmetric non-Abelian gauge field will appear if we consider the case  $(\nabla S \times \nabla \phi)_\lambda \neq 0$  from the beginning of section 2.5. Let us choose the coordinates  $\xi \equiv \rho$ ,  $\eta \equiv \varphi$ ,  $\lambda \equiv z$  and parametrizations  $S = \alpha \varphi$  ( $\nabla S = \frac{\alpha}{\rho} \hat{\phi}$ ) and  $\phi = \kappa \rho + \phi_0$  ( $\nabla \phi = \kappa \hat{\rho}$ ). In order to avoid divergencies (in  $\mathbf{A}$  and  $\Phi$ ) we need  $\cos \phi \propto \rho$  and  $\cos \theta \propto \rho$  for small  $\rho$ . This is true if

$$\phi = \kappa \rho + \phi_0 \quad \text{with } \phi_0 = -\frac{\pi}{2} \quad (2.164)$$

$$\theta = \tilde{\kappa} \rho + \phi_0 \quad \text{with } \phi_0 = -\frac{\pi}{2}. \quad (2.165)$$

Then:

$$\frac{1}{\hbar}A_\rho = \kappa \sin(\tilde{\kappa}\rho) \hat{\sigma}_y \quad (2.166)$$

$$\begin{aligned} \frac{1}{\hbar}A_\varphi &= \frac{1}{2} [\sin^2(\kappa\rho) + \sin^2(\tilde{\kappa}\rho) \cos^2(\kappa\rho)] \frac{\alpha}{\rho} \hat{\mathbb{1}} + \frac{1}{2} [\sin^2(\kappa\rho) - \sin^2(\tilde{\kappa}\rho) \cos^2(\kappa\rho)] \frac{\alpha}{\rho} \hat{\sigma}_z \\ &\quad + [\sin(\tilde{\kappa}\rho) \cos(\kappa\rho) \sin(\kappa\rho)] \frac{\alpha}{\rho} \hat{\sigma}_x. \end{aligned} \quad (2.167)$$

A gauge transformation  $e^{-i\frac{\kappa}{\tilde{\kappa}} \cos(\tilde{\kappa}\rho) \hat{\sigma}_y} \Psi$  eliminates the  $A_\rho$  part and transforms  $A_\varphi$  into  $C_\varphi$ , where

$$\begin{aligned} \frac{C_\varphi}{\hbar} &= \frac{1}{2} [\sin^2(\kappa\rho) + \sin^2(\tilde{\kappa}\rho) \cos^2(\kappa\rho)] \frac{\alpha}{\rho} \hat{\mathbb{1}} \\ &\quad + \frac{1}{2} [\sin^2(\kappa\rho) - \sin^2(\tilde{\kappa}\rho) \cos^2(\kappa\rho)] \frac{\alpha}{\rho} e^{i\frac{\kappa}{\tilde{\kappa}} \cos(\tilde{\kappa}\rho) \hat{\sigma}_y} \hat{\sigma}_z e^{-i\frac{\kappa}{\tilde{\kappa}} \cos(\tilde{\kappa}\rho) \hat{\sigma}_y} \\ &\quad + [\sin(\tilde{\kappa}\rho) \cos(\kappa\rho)] \frac{\alpha}{\rho} e^{-i\frac{\kappa}{\tilde{\kappa}} \cos(\tilde{\kappa}\rho) \hat{\sigma}_y} \hat{\sigma}_x e^{i\frac{\kappa}{\tilde{\kappa}} \cos(\tilde{\kappa}\rho) \hat{\sigma}_y}. \end{aligned} \quad (2.168)$$

The components of the scalar potential become:

$$\Phi_{11} = \frac{\hbar^2}{2m} \left[ \frac{\alpha^2}{\rho^2} \cos^2(\kappa\rho) \sin^2(\kappa\rho) + \kappa^2 \right] \cos^2(\tilde{\kappa}\rho) \quad (2.169)$$

$$\Phi_{12} = \frac{\hbar^2}{2m} \left[ \sin(\tilde{\kappa}\rho) \cos^2(\tilde{\kappa}\rho) \cos^3(\kappa\rho) \sin(\kappa\rho) \frac{\alpha^2}{\rho^2} + \kappa\tilde{\kappa} \cos(\tilde{\kappa}\rho) \right] \quad (2.170)$$

$$\Phi_{22} = \frac{\hbar^2}{2m} \left[ \sin^2(\tilde{\kappa}\rho) \cos^2(\tilde{\kappa}\rho) \cos^4(\kappa\rho) \frac{\alpha^2}{\rho^2} + \tilde{\kappa}^2 \right] \quad (2.171)$$

Assuming  $\kappa, \tilde{\kappa}$  small, we may expand up to order  $O(\kappa^2, \tilde{\kappa}^2, \kappa\tilde{\kappa})$  to obtain

$$C_\varphi \cong \alpha\rho \left\{ \frac{\kappa^2 + \tilde{\kappa}^2}{2} \hat{\mathbb{1}} + \frac{\kappa^2 - \tilde{\kappa}^2}{2} e^{i\frac{\kappa}{\tilde{\kappa}} \hat{\sigma}_y} \hat{\sigma}_z e^{-i\frac{\kappa}{\tilde{\kappa}} \hat{\sigma}_y} + \kappa\tilde{\kappa} e^{-i\frac{\kappa}{\tilde{\kappa}} \hat{\sigma}_y} \hat{\sigma}_x e^{i\frac{\kappa}{\tilde{\kappa}} \hat{\sigma}_y} \right\} = \alpha\hat{M}\rho \quad (2.172)$$

$$\Phi \cong \frac{\hbar^2}{2m} (\alpha^2 + 1) \hat{M}. \quad (2.173)$$

Hence, the Hamiltonian becomes of the form

$$\hat{H}\Psi = \left[ \frac{\hbar^2}{2m} \left[ -i\nabla + \alpha\hat{M}\rho\hat{\varphi} \right]^2 + \frac{\hbar^2}{2m} (\alpha^2 + 1) \hat{M} + U(\mathbf{r}) \right] \Psi. \quad (2.174)$$

Note that, contrary to the construction of the gauge fields in the previous section, this construction leads by definition to small fields. In addition, it is always accompanied by a non-removable scalar potential.

## 2.6 Summary

Summarizing, in this chapter we have discussed different possible alternatives for generating artificial electromagnetism in cold neutral gases. We have made particular emphasis in the

generation of artificial gauge fields using dark-state arrangements. In particular a four-level tripod-scheme may allow for the generation of non-Abelian electromagnetism. We have discussed the general condition for achieving non-Abelian fields. We then have analyzed three different arrangements: a simple arrangement which leads to a spatially constant field (which we will employ in following chapters), and the non-Abelian equivalent of the Landau-gauge and the symmetric gauge (which we shall also employ in a following chapter).



# Chapter 3

## Non-Abelian Atom Optics

### 3.1 Introduction

In this chapter we investigate the wavepacket dynamics of a cloud of ultracold atoms in the presence of a non-Abelian gauge potential. In sec. 3.2 we discuss how this undoubtedly rather exotic scenario can be envisaged in a sample of cold atoms where the internal electronic energy levels are addressed by laser fields with a nontrivial spatial phase and intensity distribution. This setup opens up a number of new scenarios for ultracold gases, allowing for the study of *non-Abelian atom optics*, which naturally ties together optical and magnetic effects. Remarkably, as shown in the next section, even very simple laser arrangements may induce non-trivial cold-atom dynamics. As a first example of this non-trivial dynamics, we discuss in sec. 3.3 a possible optical tweezer experiment including a non-Abelian flux, for which the population transfer between internal states crucially depends on the path taken. This is the non-Abelian generalization of the Aharonov-Bohm effect [AB59]. This effect resembles indeed what one would expect from scattering protons onto a non-Abelian flux line where the proton can be transferred into a neutron [Hor86]. The tweezer experiment discussed in sec. 3.3 just involves the internal-state dynamics, without exploring the rich dynamics resulting from the interplay between external and internal degrees of freedom in non-Abelian gauge fields. Sec. 3.4 is devoted to the analysis of this interplay. In particular, we show that the dynamics of cold-atom wavepackets can be significantly affected by intrinsically non-Abelian effects, which are crucially dependent on the initial momentum distribution of the wavepacket. We consider in particular the relevant examples of wavepacket propagation and wavepacket reflection at an atomic mirror. Finally, we conclude in sec. 3.5.

### 3.2 Laser-induced non-Abelian gauge fields

In section 2.5.1 we showed that non-Abelian gauge potentials can be constructed in the presence of nontrivial light fields coupled to degenerate electronic states of cold atoms. For this we considered atoms with multiple internal states, see fig. 2.8. For a fixed position  $\mathbf{r}$  the internal Hamiltonian  $\hat{H}_0(\mathbf{r})$  including the laser interaction can be diagonalized to give a set of 4 dressed states  $|\chi_n(\mathbf{r})\rangle$  with eigenvalues  $\varepsilon_n(\mathbf{r})$ , where  $n = 1, 2, 3, 4$ . The full quantum state of the atom describing both internal and motional degrees of freedom can then be expanded in terms of the dressed states according to  $|\Phi\rangle = \sum_{n=1}^4 \Psi_n(\mathbf{r}) |\chi_n(\mathbf{r})\rangle$ . If there are two degenerate dressed states and we can neglect the transitions to the other states we obtain a coupled two level

system of the form

$$i\hbar\frac{\partial}{\partial t}\tilde{\Psi} = \left[ \frac{1}{2m}(-i\hbar\nabla - \mathbf{A})^2 + V + \Phi \right] \tilde{\Psi}, \quad (3.1)$$

where the  $2 \times 2$  potentials are given by

$$V_{n,m} = \varepsilon_n(\mathbf{r}) \delta_{n,m} + \langle \chi_n(\mathbf{r}) | V(\mathbf{r}) | \chi_m(\mathbf{r}) \rangle, \quad (3.2)$$

$$\mathbf{A}_{n,m} = i\hbar \langle \chi_n(\mathbf{r}) | \nabla \chi_m(\mathbf{r}) \rangle. \quad (3.3)$$

$$\Phi_{n,m} = \frac{\hbar^2}{2m} \left( \langle \nabla \chi_n | \nabla \chi_m \rangle + \sum_{k=1}^2 \langle \chi_n | \nabla \chi_k \rangle \langle \chi_k | \nabla \chi_m \rangle \right). \quad (3.4)$$

Surprisingly, the generation of a non-Abelian gauge field does not require any elaborate shaping of the three laser beams employed as we showed in section 2.5.1. Two lasers of equal intensity are counter-propagating in the  $x$ -direction with wave vector  $\kappa$  while the third one (of double intensity) propagates in the  $y$ -direction also with a wave vector  $\kappa$ . The resulting vector potential is of the form:

$$\mathbf{A} = \hbar\kappa \begin{pmatrix} -\mathbf{e}_y & \mathbf{e}_x/\sqrt{2} \\ \mathbf{e}_x/\sqrt{2} & -\mathbf{e}_y/2 \end{pmatrix}, \quad (3.5)$$

whereas

$$V + \Phi = \begin{pmatrix} V_1 + \frac{\hbar^2\kappa^2}{4m} & 0 \\ 0 & (V_1 + V_3)/2 + \frac{\hbar^2\kappa^2}{8m} \end{pmatrix}. \quad (3.6)$$

By choosing the laser detuning such that  $V_3 - V_1 = \hbar^2\kappa^2/4m$  we obtain a scalar potential proportional to the unit matrix,  $V + \Phi = V_1 \mathbb{1}$ . Therefore the scalar potential can be safely neglected as far as the wavepacket dynamics is concerned.

### 3.3 Non-Abelian Aharonov-Bohm effect

In ref. [OBS<sup>+</sup>05] it was proposed that non-Abelian gauge fields created in lattices can be employed to construct non-Abelian atom interferometers. However, the read-out of any non-Abelian atom interferometer may be crucially handicapped by the non-trivial interplay between external and internal degrees of freedom in the wavepacket dynamics of atoms in non-Abelian gauge fields (see sec. 3.4). This coupling between external and internal dynamics may be prevented by considering atoms trapped in mobile optical tweezers. If the tweezer potential is strong enough, the system may be investigated in the so-called single-mode approximation, in which both components share exactly the same center-of-mass wavepacket. As a consequence, the non-Abelian gauge field will just affect the internal dynamics of the atoms. In the following we envisage an experiment in which a cloud of ultra cold atoms is trapped by an optical tweezer under the conditions discussed above. When moving in the  $xy$ -plane the atoms experience the gauge potential given by eq. (3.5). We consider the case where the atoms are moved in the  $x$  and  $y$  direction (fig. 3.1) along two different paths: (clock-wise,  $L$ ) from  $(0, 0)$  to  $(0, s)$  and then from  $(0, s)$  to  $(s, s)$ ; (anti clock-wise,  $R$ ) from  $(0, 0)$  to  $(s, 0)$  and then from  $(s, 0)$  to  $(s, s)$ . The initial state of the atom is assumed to be a linear superposition of both dark states:

$$|\Psi(0)\rangle = \cos(\eta)|D_1\rangle + e^{i\varphi} \sin(\eta)|D_2\rangle, \quad (3.7)$$

where  $\eta$  is the mixing angle, and  $\varphi$  is a relative phase. The dynamics of the two level system obviously depends on the initial state, but more importantly, the final populations of the two dark states depend on which path is taken. After performing the clock-wise path the atoms are in the state

$$|\Psi_L\rangle = e^{i\hat{A}_x s/\hbar} e^{i\hat{A}_y s/\hbar} |\Psi(0)\rangle = c_1^L |D_1\rangle + c_2^L |D_2\rangle, \quad (3.8)$$

whereas after performing the anti clock-wise path we have:

$$|\Psi_R\rangle = e^{i\hat{A}_y s/\hbar} e^{i\hat{A}_x s/\hbar} |\Psi(0)\rangle = c_1^R |D_1\rangle + c_2^R |D_2\rangle. \quad (3.9)$$

Using the vector potential given by eq. (3.5) a straight forward calculation yields

$$c_1^L = e^{-i\kappa s} \cos\left(\frac{\kappa s}{\sqrt{2}}\right) \cos(\eta) + ie^{i(\varphi-\kappa s/2)} \sin\left(\frac{\kappa s}{\sqrt{2}}\right) \sin(\eta) \quad (3.10)$$

$$c_2^L = ie^{-i\kappa s} \sin\left(\frac{\kappa s}{\sqrt{2}}\right) \cos(\eta) + e^{i(\varphi-\kappa s/2)} \cos\left(\frac{\kappa s}{\sqrt{2}}\right) \sin(\eta) \quad (3.11)$$

$$c_1^R = e^{-i\kappa s} \cos\left(\frac{\kappa s}{\sqrt{2}}\right) \cos(\eta) + ie^{i(\varphi-\kappa s)} \sin\left(\frac{\kappa s}{\sqrt{2}}\right) \sin(\eta) \quad (3.12)$$

$$c_2^R = ie^{-i\kappa s/2} \sin\left(\frac{\kappa s}{\sqrt{2}}\right) \cos(\eta) + e^{i(\varphi-\kappa s/2)} \cos\left(\frac{\kappa s}{\sqrt{2}}\right) \sin(\eta). \quad (3.13)$$

Fig. 3.2 shows the final population difference between the two dark states for both paths as a function of the path length  $\kappa s$ . It becomes clear that the outcome of choosing the  $L$  or  $R$  path can be very different. We stress that this effect is not directly linked to the appearance of off-diagonal terms in the corresponding matrices of the vector potential, but rather it is inherently due to the non-Abelian character of the matrices  $\hat{A}_x$  and  $\hat{A}_y$ . This effect is remarkably similar to the scattering of protons onto a non-Abelian flux line, where a conversion of the proton into a neutron is anticipated [Hor86]. A more complete picture is obtained by defining the pseudo spin  $\mathbf{S}(c_1^{L,R}, c_2^{L,R})$  as

$$S_x = \frac{1}{2i}(c_1 c_2^* - c_1^* c_2) \quad (3.14)$$

$$S_y = \frac{1}{2}(c_1 c_2^* + c_1^* c_2) \quad (3.15)$$

$$S_z = \frac{1}{2}(|c_1|^2 - |c_2|^2). \quad (3.16)$$

With the pseudo spin representation we can follow the rotation of the spin vector as a function of position along the different paths. This is shown in fig. 3.3 where the spin vector is seen to follow circular paths whose orientation changes when the direction of the atoms in real space changes. The role of the initial state is now immediately clear. Only a superposition between  $|D_1\rangle$  and  $|D_2\rangle$  will result in a different final state of  $\mathbf{S}$  as a function of taking either the  $L$  or  $R$  path. Note that, in contrast to the previously considered laser-driven population transfer for tripod atoms [UFSB98, USB99], here the non-Abelian dynamics is due to the time-dependence of the phases of light fields “seen” by moving atoms rather than due to the time-dependence of the intensities of laser pulses.

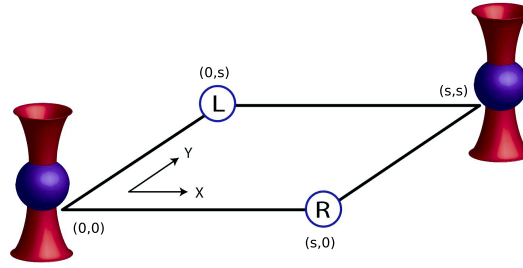


Fig. 3.1: The envisaged experiment. An optical tweezer moves the cloud of atoms along the left (L) path or the right (R) path in the presence of a non-Abelian gauge field. The final dark state population will depend on which path was taken.

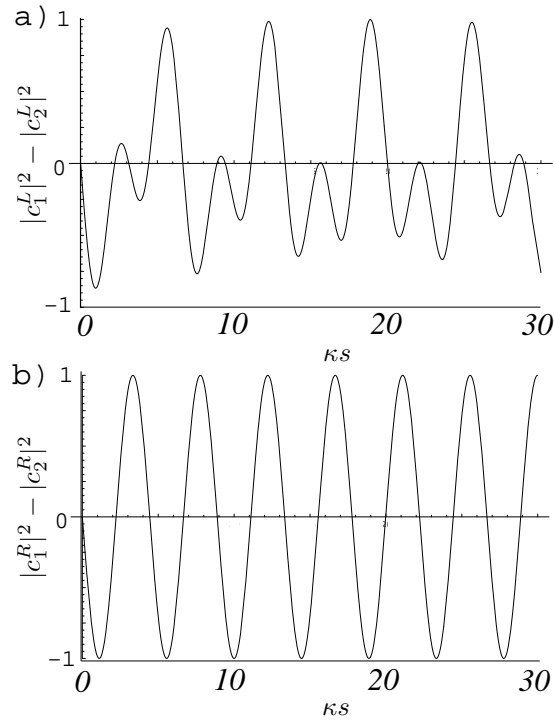


Fig. 3.2: The difference in the populations in the two dark states depends on which path is taken. Fig. (a) shows the total difference  $|c_1^L|^2 - |c_2^L|^2$  as a function of the path length  $\kappa s$ , whereas in fig. (b) we depict  $|c_1^R|^2 - |c_2^R|^2$ . We assume as initial conditions  $\eta = \pi/4$  and  $\varphi = \pi/2$ .

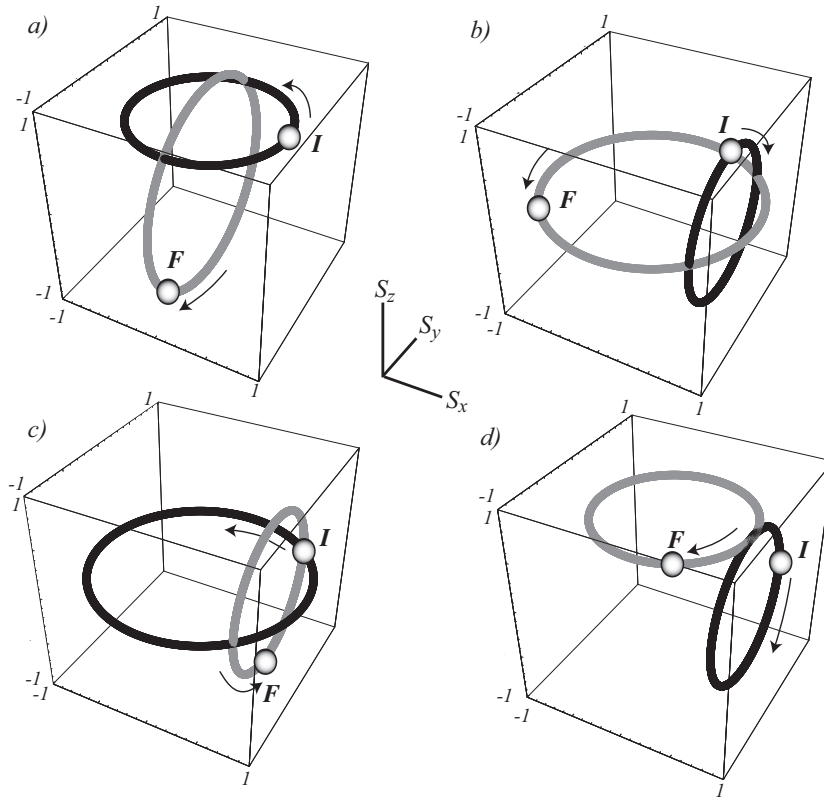


Fig. 3.3: The pseudo spin trajectories depend on the initial state and which path is taken: a) Left path with  $\eta = \pi/8, \varphi = 0$ , b) Right path with  $\eta = \pi/8, \varphi = 0$ , c) Left path with  $\eta = \pi/4, \varphi = \pi/4$ , d) Right path with  $\eta = \pi/4, \varphi = \pi/4$ . The spheres in each figure indicate the initial state (I) and the final state (F). The black circle is always the path first embarked on. In all cases we have chosen  $\kappa s = 34.5$ . This will cause the spin vector to traverse the circular paths several times in each plane.

### 3.4 Wavepackets in free space

The non-Abelian Aharonov-Bohm effect is a striking example where the internal dynamics of a two-level system is highly nontrivial. A question which is not often addressed in the context of non-Abelian systems is the dynamics of a wavepacket. This situation is clearly more complex compared to the previous non-Abelian Aharonov-Bohm scenario where an adiabatic motion with respect to center of mass excitations and shape oscillations was assumed. We now have to take fully into account the coupled internal and external degrees of freedom.

In the following we discuss the evolution of a cold atomic wavepacket in the presence of a non-Abelian gauge field  $\hat{A} = \{\hat{A}_x, \hat{A}_y, 0\}$ . We consider that the atomic gas is sufficiently dilute, and hence in this chapter we neglect the effects of the interatomic interactions. We restrict ourselves to the case in which both matrices  $\hat{A}_x$  and  $\hat{A}_y$  are space-independent. In order to simplify the discussion below, we consider  $\hat{A}_j = \hbar\kappa\hat{M}_j$ , with  $j = x, y$ , where  $\kappa$  has units of wavenumber, and  $\hat{M}_j^2 = \hat{\mathbb{1}}$ . We assume as well that the scalar potential may be considered as a multiple of the identity matrix (as discussed above). Removing unimportant global energy shifts, the Hamiltonian for a free particle becomes

$$\hat{H} = -\frac{\hbar^2}{2m}\nabla^2\hat{\mathbb{1}} - i\frac{\hbar^2\kappa}{m}\left(\hat{M}_x\frac{\partial}{\partial x} + \hat{M}_y\frac{\partial}{\partial y}\right). \quad (3.17)$$

The atomic wavepacket can be represented by a spinorial wavefunction of the form

$$\Psi(\mathbf{r}, t) = \int d\mathbf{p} e^{i\mathbf{p}\cdot\mathbf{r}/\hbar} \Phi(\mathbf{p}, t). \quad (3.18)$$

Thus, we have

$$\hat{H}\Psi(\mathbf{r}, t) = \int d\mathbf{p} \hat{H}_p(\mathbf{p})\Phi(\mathbf{p}, t)e^{i\mathbf{p}\cdot\mathbf{r}/\hbar}, \quad (3.19)$$

where

$$\hat{H}_p(\mathbf{p}) \equiv \frac{p^2}{2m}\hat{\mathbb{1}} + \frac{\hbar\kappa}{m}\left(\hat{M}_x p_x + \hat{M}_y p_y\right). \quad (3.20)$$

Hence for any given momentum  $\mathbf{p}$  the equation of motion  $i\hbar\dot{\Phi}(\mathbf{p}, t) = \hat{H}_p(\mathbf{p})\Phi(\mathbf{p}, t)$  yields

$$\Phi(\mathbf{p}, t) = \exp\left[i\hat{H}_p(\mathbf{p})t/\hbar\right]\Phi(\mathbf{p}, t=0). \quad (3.21)$$

This evolution can be obtained analytically after diagonalizing the matrix  $\hat{H}_p(\mathbf{p})$  for every  $\mathbf{p}$ .

We are interested in comparing the wavepacket evolution in the presence of Abelian and non-Abelian fields. If the fields are Abelian, i.e.  $[\hat{M}_x, \hat{M}_y] = 0$ , then we may find a common eigenbasis for both operators, in which  $\hat{M}_j = \text{diag}\{\lambda_j^+, \lambda_j^-\}$ . As a consequence, the eigenvectors  $\xi_{\pm}$  of  $\hat{H}_p(\mathbf{p})$  are independent of  $\mathbf{p}$ , and the total wavefunction is at any time a linear combination of the form  $\Phi(\mathbf{r}, t) = \Phi_+(\mathbf{r}, t)\xi_+ + \Phi_-(\mathbf{r}, t)\xi_-$ , where

$$\Phi_{\pm}(\mathbf{r}, t) = e^{-i\phi_{\pm}} \int d\mathbf{p} e^{-i\frac{p^2 t}{2m\hbar}} e^{i\mathbf{p}\cdot\mathbf{r}/\hbar} \Psi_{\pm}(\mathbf{p} - \boldsymbol{\eta}^{\pm}, t=0), \quad (3.22)$$

with  $\boldsymbol{\eta}^{\pm} = \hbar\kappa(\lambda_x^{\pm}, \lambda_y^{\pm})$ , and  $\phi_{\pm} = \frac{(\boldsymbol{\eta}^{\pm})^2 t}{2m\hbar} + \boldsymbol{\eta}^{\pm} \cdot \mathbf{r}/\hbar$ . Hence, the wavepacket evolution can be considered as an independent scalar evolution for the wavepackets in each component. In

particular, it may be easily shown that the center of mass position of the wavepacket  $\Phi_{\pm}(\mathbf{r}, t)$  grows linearly in time with a velocity  $(\langle \mathbf{p} \rangle + \boldsymbol{\eta}^{\pm})/m$ . Hence the two wavepackets tend to separate during the time evolution.

The picture changes completely if  $[\hat{M}_x, \hat{M}_y] \neq 0$ . In this case the eigenvectors of  $\hat{H}_p(\mathbf{p})$  do depend on the momentum  $\mathbf{p}$  considered, and hence the time-evolution of the wavepacket depends in a non-trivial way on the momentum distribution of the original wavepacket. We analyze in particular the center of mass (CM) motion of the wavepacket. The  $x$ -coordinate of the CM after a given time  $t$  is better calculated in the momentum representation:  $\langle x \rangle_t = \langle i\hbar\partial/\partial p_x \rangle_t = \langle e^{i\hat{H}t/\hbar} i\hbar\partial/\partial p_x e^{-i\hat{H}t/\hbar} \rangle_0$ , where we have employed the Heisenberg picture. One can then easily obtain that:

$$\langle x \rangle_t = \langle x \rangle_0 + \frac{t}{m} \langle p_x \rangle_0 + \left\langle e^{i\hat{O}t} i\hbar \frac{\partial}{\partial p_x} \left[ e^{-i\hat{O}t} \right] \right\rangle_0, \quad (3.23)$$

where  $\hat{O} = (\kappa t/m)(\hat{M}_x p_x + \hat{M}_y p_y)$ . The last term in the previous equation leads to non-trivial effects, which are easily illustrated by considering the particular example  $\hat{M}_x = \hat{\sigma}_x$ ,  $\hat{M}_y = \hat{\sigma}_z$ :

$$\begin{aligned} \langle x \rangle_t &= \langle x \rangle_0 + \frac{t}{m} \langle p_x \rangle_0 + \frac{\hbar\kappa t}{m} \left\{ \langle c^2 \hat{\sigma}_x + sc \hat{\sigma}_z \rangle_0 \right. \\ &\quad \left. + \left\langle \frac{\sin(2q)}{2q} s^2 \hat{\sigma}_x - \frac{\sin(2q)}{2q} sc \hat{\sigma}_z - \frac{\sin^2 q}{q} s \hat{\sigma}_y \right\rangle_0 \right\}, \end{aligned} \quad (3.24)$$

where  $c = p_x/p$ ,  $s = p_y/p$ ,  $q = \kappa t p/m$ , and  $p^2 = p_x^2 + p_y^2$ . Let us consider an initial Gaussian wavepacket

$$\Psi(\mathbf{r}) = \Psi(\mathbf{r}) \begin{pmatrix} \cos \eta e^{i\varphi/2} \\ \sin \eta e^{-i\varphi/2} \end{pmatrix}, \quad (3.25)$$

where  $\Psi(\mathbf{r})$  is a Gaussian centered in  $x = y = 0$  and with the Fourier-Transform  $\Phi(\mathbf{p}) \sim \exp(-p^2/\Delta p^2)$ . Then:

$$\langle x \rangle_{\tau} = \frac{\hbar}{\sqrt{2}\Delta p} \tau \left[ 1 + \frac{\sqrt{\pi}}{2} \frac{e^{-\tau^2}}{\tau} \operatorname{erfi}(\tau) \right] \sin(2\eta) \cos \varphi, \quad (3.26)$$

where  $\operatorname{erfi}(\tau)$  is the imaginary error function at  $\tau = \frac{\Delta p \kappa}{\sqrt{2}m} t$ . Note, that contrary to the Abelian case, we have two inherently non-Abelian effects. On one hand, the evolution of the center of mass motion is in general a non-trivial non-linear function of time. However, for  $\tau \gg 1$  a linear behavior  $\langle x \rangle_{\tau} \simeq \frac{\hbar}{\sqrt{2}\Delta p} \tau$  is recovered, i.e. there is a characteristic transient stage where an inherently non-Abelian-induced non-linear CM evolution occurs (see fig. 3.4). On the other hand, contrary to the Abelian (or scalar) evolution, the evolution of the CM motion depends on the initial width  $\Delta p$  of the momentum distribution. This effect can be traced back to the dependence of the eigenstates  $\boldsymbol{\xi}_{\pm}$  on  $\mathbf{p}$ .

A third effect can be observed if we consider a Gaussian wavepacket with an initial  $\langle p_y \rangle_0 \neq 0$ . In that case, if  $\langle p_x \rangle_0 = 0$ , one obtains:

$$\langle x \rangle_t = \frac{\hbar\kappa}{t} \left[ 1 - \left\langle \left( \frac{\sin(2q)}{2q} - 1 \right) \frac{p_y^2}{p^2} \right\rangle_0 \right] \sin(2\eta) \cos \varphi. \quad (3.27)$$

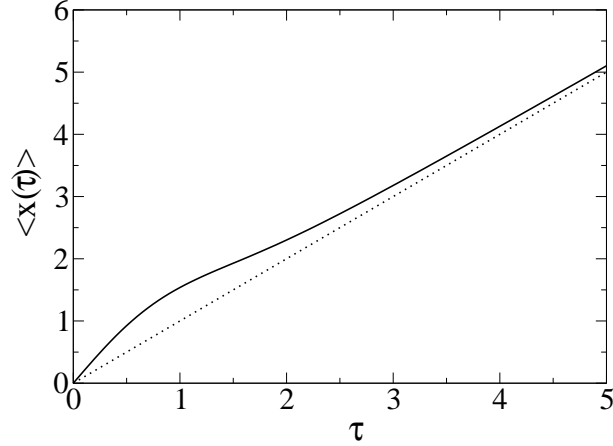


Fig. 3.4: Evolution of the center of mass coordinate  $\langle x \rangle$  in units of  $\sqrt{2}\Delta p/\hbar$ , as a function of  $\tau = \Delta p \kappa t / \sqrt{2}m$ , for  $\hat{A}_x = \hbar\kappa\hat{\sigma}_x$ , and  $\hat{A}_y = \hbar\kappa\hat{\sigma}_z$ ,  $\eta = \pi/4$ ,  $\varphi = 0$ . The dashed line is the function  $f(\tau) = \tau$ . For short times the nonlinear evolution of the center of mass becomes clear.

Hence, the  $x$ -dynamics depends on the momentum distribution in the  $y$ -direction, contrary to the case of Abelian evolution.

Note that the details of the momentum distribution play a very important role in the wavepacket evolution in non-Abelian gauge fields. Obviously, if  $|\langle \mathbf{p} \rangle| \gg \hbar\kappa$  the non-Abelian effects become negligible. But even if  $|\langle \mathbf{p} \rangle| \lesssim \hbar\kappa$ , an Abelian evolution is recovered if  $\Delta p \ll \hbar\kappa$ , i.e. the non-Abelian effects are clearer for wavepackets which at  $t = 0$  are localized in space with uncertainties  $\lesssim 1/\hbar\kappa$ . The latter effect may be explained, because if  $\Delta p \ll \hbar\kappa$  then  $\hat{H}_p$  may be (to a good approximation) simultaneously diagonalized for all relevant values of  $\mathbf{p}$  in the distribution, and hence again two separated wavepackets as those for the Abelian evolution are recovered. In addition, it is important to realize that the particular evolution also depends on the initial spinor configuration of the wavepacket (although this dependence is not inherently non-Abelian since it also occurs in the Abelian evolution).

Fig. 3.5 shows the results of our numerical simulations of the wavepacket evolution for the Gauge field discussed above. Note that contrary to the usual Abelian (or scalar) evolution, there is a stark difference in the evolution of the shape of the wavepacket for different values of the momentum spreading  $\Delta p/\hbar\kappa$ .

The non-Abelian character of the gauge field leads also to interesting effects in the reflection of atomic wavepackets. Ultra cold atomic wavepackets can be reflected at laser or magnetic mirrors [ASB<sup>+</sup>93, BBB<sup>+</sup>99, APSH06]. For typical situations the reflection of the center of mass of the wavepacket can be considered as specular, i.e. the angle of reflection of the wavepacket with the normal vector of the mirror is exactly minus the angle of incidence of the original wavepacket. Mathematically, the reflection can be considered as the superposition (in absence of mirror) of the original wavepacket and an image wavepacket travelling with opposite momentum and with a dephase  $\pi$ . For the case of wavepackets in non-Abelian gauge fields, the effect of the mirror cannot be mimicked by this symmetric picture, since contrary to the scalar



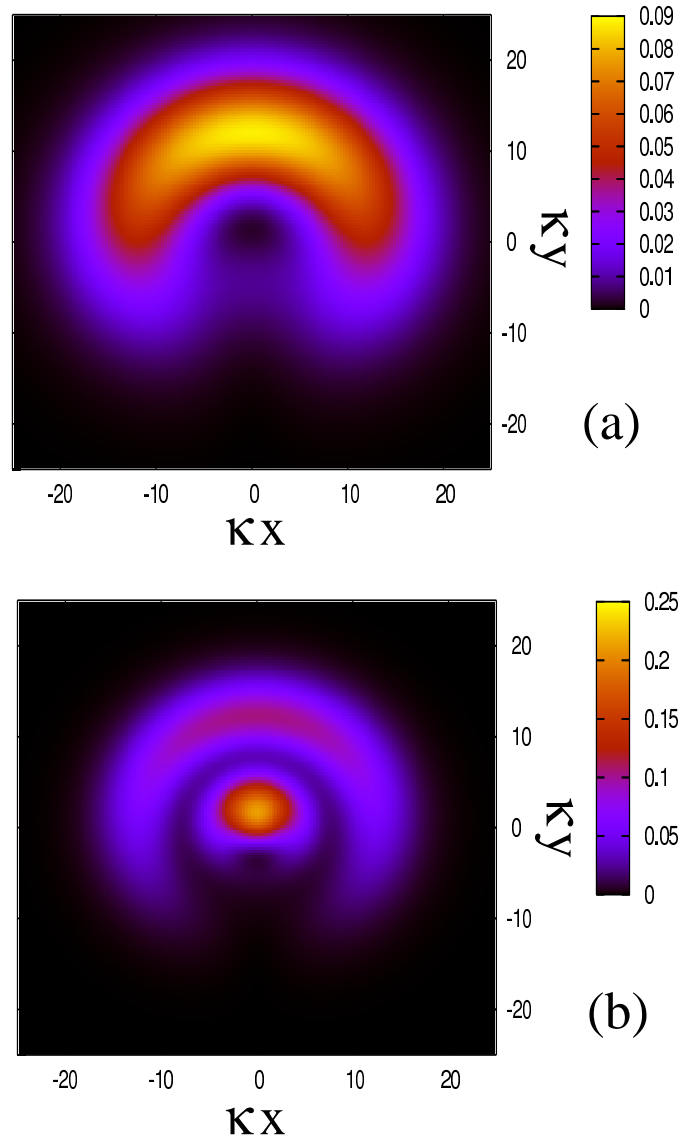


Fig. 3.5: Total density of the wavepacket in the  $xy$ -plane after  $t = 10(2m/\hbar\kappa^2)$ , for (a)  $\Delta p = 0.2\hbar\kappa$  and (b)  $\Delta p = 0.6\hbar\kappa$ . At  $t = 0$ ,  $\eta = 0$ ,  $\varphi = 0$  and  $\langle \mathbf{p} \rangle = 0$ . In the strong non-Abelian case the wavepacket expands asymmetrically. In an Abelian situation with a radially symmetric effective magnetic field the expansion would be symmetric.

case, a sinusoidal solution is not an eigenstate of  $\hat{H}_p$ . As a consequence the intuitive specular-reflection picture must be revised in the case of wavepackets in non-Abelian gauge fields, even for the cases discussed below resp. in figs. 3.6 and 3.7, in which both internal components experience exactly the same mirror potential.

Fig. 3.7 shows the reflection of the wavepacket for  $\Delta p = \hbar\kappa$  (i.e. for momentum spreadings for which, as discussed above, the non-Abelian effects are significant). It is clear from the snapshots in fig. 3.7 that the non-Abelian dynamics after the reflection is certainly not trivial. Remarkably, the center-of-mass position does not show a specular reflection in general. Fig. 3.6 shows the sum of the angle of incidence and that of reflection for different incident angles in the non-Abelian regime. For usual scalar (or Abelian) evolution, this sum equals zero. However, due to inherently non-Abelian effects, this sum is significantly different from zero. Moreover, contrary to the usual scalar (or Abelian) evolution, the angle of reflection crucially depends on the absolute value of the incoming momentum, and on the momentum spreading of the wavepacket. In chapter 6 we discuss even more bizarre effects related with the reflection of atomic wavepackets in the presence of non-Abelian gauge fields.

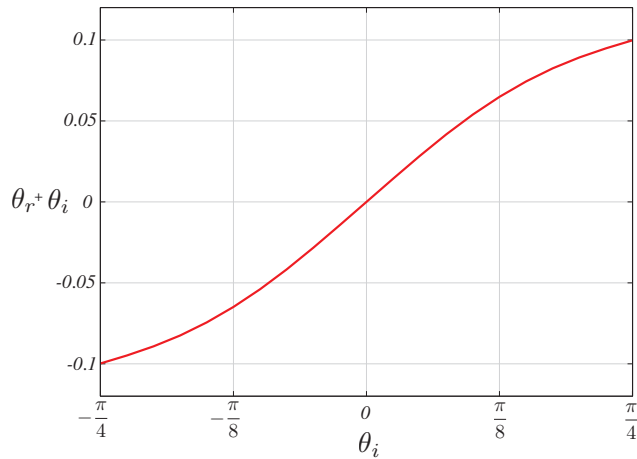


Fig. 3.6: The reflected angle plus the incident angle,  $\theta_r + \theta_i$ , as a function of the incident angle  $\theta_i$ . The deviation from the standard case,  $\theta_r + \theta_i = 0$ , for a non-Abelian system is clearly seen. The parameters were chosen to be  $\kappa = 1$ ,  $\Delta p = 1$  and initial momentum  $|\mathbf{p}_0| = 8$ .

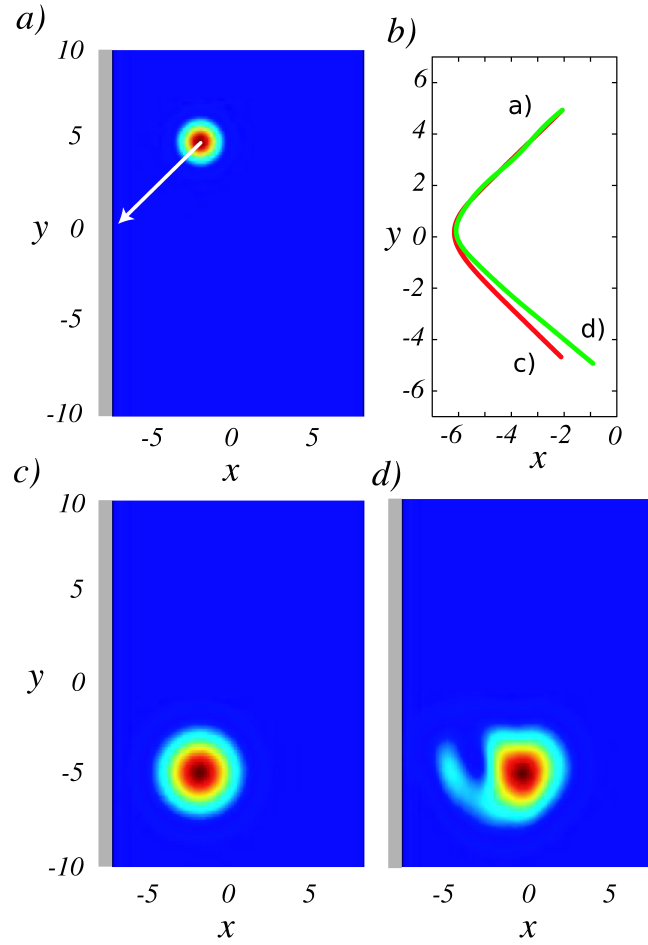


Fig. 3.7: The reflection dynamics of a non-Abelian wavepacket compared to a zero gauge field situation. The reflection takes place at  $x = -7$  where a steep potential is envisaged (gray area). The parameters were chosen to be  $\kappa = 1$ ,  $\Delta p = 1$  and initial momentum  $\mathbf{p}_0 = -\frac{8}{\sqrt{2}}(\hat{\mathbf{x}} + \hat{\mathbf{y}})$ . a) The initial density distribution of the atomic cloud. The initial momentum kick is indicated by the arrow. b) The non-Abelian path of the center of mass, the inner (green) path, for the reflection is clearly different from the standard wavepacket reflection with  $\kappa = 0$  (red outer path). c) A snap shot of the wavepacket at the time corresponding to the mirror image with respect to the  $x$ -axis. For the Abelian case ( $\kappa = 0$ ) the reflected angle is the same as the incident angle. d) A snap shot of the wavepacket at the same time as in c). For the non-Abelian case the reflection dynamics is highly non-trivial where the center of mass path is no longer described by an incident angle equal to the reflected angle.

### 3.5 Summary

Using a very simple laser configuration, spatially homogeneous but non-Abelian vector potentials can be generated. In spite of this spatial homogeneity, the non-Abelian character of the vector potentials can lead to a surprisingly rich physics for the wavepacket dynamics of ultra cold gases. On one hand, the free expansion dynamics of wavepackets crucially differs from what would be expected in scalar (or Abelian) cases. In the latter, the wavepacket center-of-mass follows a linear dependence in time. In the presence of non-Abelian fields, the wavepacket presents a non-linear time dependence during a transient time. In addition, and again contrary to the scalar (or Abelian) case, the center-of-mass dynamics crucially depends on the momentum spreading of the wavepacket. Moreover, in spite of the apparent separability of the corresponding Hamiltonian, the non-Abelian gauge fields introduce a dependence of the dynamics in different spatial directions. The wavepacket reflection off an atomic mirror is also significantly distorted by the non-Abelian gauge field. In particular, the reflection of the center-of-mass ceases in general to be specular, and the angle of reflection depends on the incoming velocity and the initial momentum spreading, which is different from the standard scalar case. The complex interplay between external and internal dynamics should make the read-out of non-Abelian interferometers difficult. However, an experiment performed with optical tweezers, may allow for the analysis of non-Abelian effects in the internal dynamics of the atoms. We have shown that such an arrangement can be employed for the analysis of the equivalent of the non-Abelian Aharanov-Bohm effect, where the final internal state of the atoms crucially depends on the particular path chosen.

# Chapter 4

## Non-Abelian Landau Levels

### 4.1 Introduction

This chapter is devoted to the analysis of non-Abelian effects on the spectral properties of ultracold atomic systems. In particular, we show how purely non-Abelian effects lead to the eventual destruction of the Landau level structure, and may significantly modify the ground state density profile of ideal quantum gases.

In sec. 4.2 and 4.3 we briefly introduce the basic physics of the Landau level and the Fock-Darwin spectrum. In sec. 4.4 we study how to generate different forms of non-Abelian gauge fields, including non-Abelian constant fields, as well as the non-Abelian generalization of the Landau gauge. Sec. 4.5 is devoted to the analysis of constant non-Abelian gauge fields. Sec. 4.6 discusses the non-Abelian Landau gauge, and in particular the destruction of the Landau level structure and the corresponding modified de Haas-van Alphen-effect. In sec. 4.7 we discuss the non-Abelian symmetric gauge. Finally, in sec. 4.8 we conclude and discuss some promising future directions.

### 4.2 Landau Levels

Landau levels [Lan30] are the allowed energy levels of particles in a magnetic field. In electrodynamics a classical particle performs a cyclotron motion in a plane perpendicular to the magnetic field  $\mathbf{B}$ . But in quantum mechanics, due to quantisation, only cyclotron orbits with an energy equal to the eigenenergy of the Hamiltonian  $H = \frac{1}{2m} (-i\hbar\nabla + \mathbf{A})^2$  are allowed. Different choices of  $\mathbf{A}$ , i.e. different gauges, can describe the same magnetic field. Let us consider a constant magnetic field in  $z$ -direction  $\mathbf{B} = (0, 0, B_0)$ . This can be obtained by means of the Landau gauge (see fig. 4.1)

$$\mathbf{A}_{\text{Landau}}(\mathbf{r}) = B_0(0, x, 0) \quad (\text{or } \mathbf{A}_{\text{Landau}}(\mathbf{r}) = B_0(-y, 0, 0)) . \quad (4.1)$$

Another way is employing the so-called symmetric gauge (see fig. 4.2)

$$\mathbf{A}_{\text{symmetric}}(\mathbf{r}) = \frac{1}{2}B_0(-y, x, 0) . \quad (4.2)$$

For calculating the Landau levels for a magnetic field in  $z$ -direction one does not need the Landau gauge, but per definitionem any gauge creating the desired magnetic field gives the same result. Depending on the symmetry of the Hamiltonian and boundary conditions,

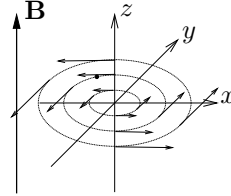
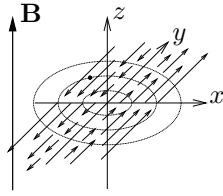


Fig. 4.1: vector potential in Landau gauge    Fig. 4.2: vector potential in symmetric gauge

calculations in a certain gauge are easier. The Landau gauge is suitable if the Hamiltonian is translationally invariant. In this case the eigenfunctions of the translation operator  $\tau_y$  can be used. The symmetric gauge is helpful when dealing with rotational invariant Hamiltonians and the eigenfunctions of  $L_z = xp_y - yp_x$  are useful. The geometry and boundary conditions are also considered in choosing a gauge. For problems on a disc we would prefer the symmetric gauge, whereas for problems defined on a rectangular sample we would opt for the Landau gauge.

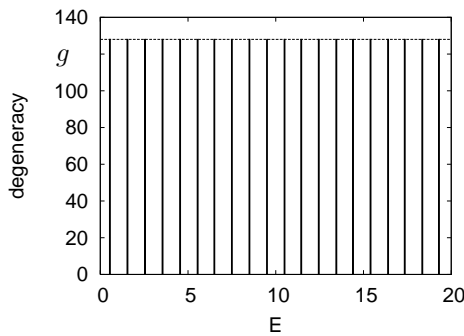
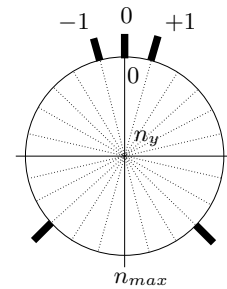
Consider the example of a box with periodic boundary conditions. Let us solve this problem in the Landau gauge:

$$E\Psi = \frac{1}{2m} \left[ p_x^2 + (p_y + B_0x)^2 \right] \Psi. \quad (4.3)$$

Periodic boundary conditions are assumed for simplicity of the discussion. We can use an exponential ansatz for the wave function,  $\Psi = \sum_{n_y} e^{i\frac{2\pi}{L}n_y y} u(n_y, x)$ , to get

$$Eu(q) = \left[ \frac{p_q^2}{2m} + \frac{1}{2}m\omega_c^2 q^2 \right] u(q), \quad (4.4)$$

where  $q = x + \hbar\frac{2\pi n_y}{LB_0}$  and  $\omega_c = B_0/m$ . The Landau levels are the corresponding eigenstates, which hence resemble the energy structure of a harmonic oscillator. All  $n_y$  give the same spectrum and lead to a degeneracy  $g \propto BL^2$  as shown in figs. 4.3 and 4.4.


 Fig. 4.3: Landau level structure. Each possible energy level presents a given maximal degeneracy  $\propto BL^2$  (see text).

 Fig. 4.4: Visualization of the possible values of  $n_y$ . The bars show that they are independent, opposed to the non-Abelian case later-on

### 4.3 Fock-Darwin spectrum

Related to the Landau levels discussed above, we may study the problem of a charged particle in a uniform magnetic field and a 2D harmonic oscillator potential

$$H = \frac{1}{2m} (\mathbf{p} + \mathbf{A})^2 + \frac{1}{2} m \omega^2 \rho^2. \quad (4.5)$$

For small resp. no magnetic field one recovers the harmonic oscillator eigenvalues and their correct degeneracy, see fig. 4.5. For large magnetic fields the trapping term becomes negligible and one recovers the Landau level structure, see fig. 4.6. This is an important toy model e.g. for quantum dots and for trapped Bose-Einstein condensates. Its solution is the so-called Fock-Darwin spectrum [Foc28, Dar30], see fig. 4.7.

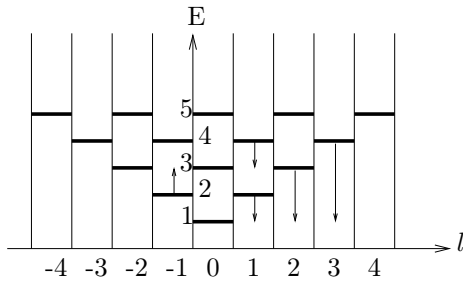


Fig. 4.5: 2D harmonic oscillator energy levels vs. angular momentum  $l$  without a magnetic field, arrows denote maximum shift due to a magnetic field

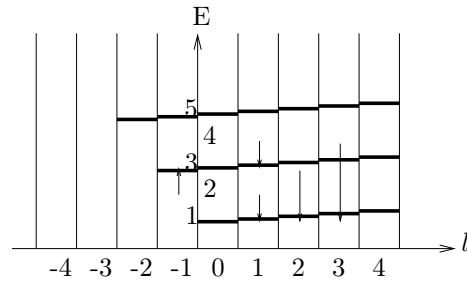


Fig. 4.6: 2D harmonic oscillator energy levels vs. angular momentum  $l$  in a high magnetic field, if the trapping is negligible we regain the Landau levels

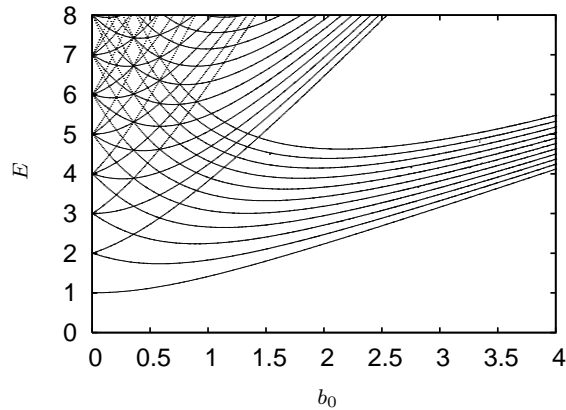


Fig. 4.7: Fock-Darwin spectrum  $E$  in units of  $\hbar\omega\sqrt{1+b_0^2}$  for the Abelian cases as a function of  $b_0 = \omega_c/\omega$ , where  $b_0$  is the ratio between the cyclotron frequency  $\omega_c$  associated with the magnetic field and the trap frequency  $\omega$  of the harmonic confinement.

## 4.4 Laser-induced non-Abelian Gauge fields

In this section we discuss concrete non-Abelian gauge fields following our general discussion in chapter 2.

### 4.4.1 Constant intensities

First, we will consider homogeneous intensity profiles, as in section 2.5.1, i.e. both  $\phi$  and  $\theta$  are now space independent. We choose the case with  $\phi = \theta = \pi/4$ . For constant  $\phi$  the non-Abelian character demands  $\nabla S_{23} \times \nabla S_{13} \neq 0$ . A simple laser arrangement fulfilling this condition is  $S_{j3} = \alpha_j x + \beta_j y$ , where  $\alpha_j, \beta_j$  are constants such that  $\alpha_2 \beta_1 \neq \alpha_1 \beta_2$ . The corresponding  $x$  and  $y$  components of the vector potential are of the form

$$\hat{A}_x = \frac{1}{8}(\alpha_1 + \alpha_2)(3\hat{\mathbb{1}} + \hat{\sigma}_z) + \frac{1}{2\sqrt{2}}(\alpha_1 - \alpha_2)\hat{\sigma}_x, \quad (4.6)$$

$$\hat{A}_y = \frac{1}{8}(\beta_1 + \beta_2)(3\hat{\mathbb{1}} + \hat{\sigma}_z) + \frac{1}{2\sqrt{2}}(\beta_1 - \beta_2)\hat{\sigma}_x. \quad (4.7)$$

On the other hand, by choosing  $V_j(\mathbf{r}) = \Delta E_j + U(\mathbf{r})$ , with  $\Delta E_1 = -(\hbar^2/16m)[(\alpha_1^2 - \alpha_2^2) + (\beta_1^2 - \beta_2^2)] = -\Delta E_2$ , and  $\Delta E_3 = -(\hbar^2/16m)[(\alpha_1^2 + \alpha_2^2) + (\beta_1^2 + \beta_2^2)]$ , one can prove that (up to an irrelevant constant)  $\hat{V} + \hat{\phi} = U(\mathbf{r})$  with  $U(\mathbf{r})$  a common trapping potential for all components.

A gauge transformation eliminates the terms proportional to the identity matrix in  $\hat{A}_x$  and  $\hat{A}_y$ . Let  $\hbar\kappa_y = (\beta_1 - \beta_2)/2\sqrt{2}$ ,  $\hbar q_y = (\beta_1 + \beta_2)/8$ ,  $\hbar\kappa_x = (\alpha_1 - \alpha_2)/2\sqrt{2}$ , and  $\hbar q_x = (\alpha_1 + \alpha_2)/8$ . A rotation  $\hat{\sigma}_x \rightarrow \cos \eta \hat{\sigma}_x + \sin \eta \hat{\sigma}_z$ ,  $\hat{\sigma}_z \rightarrow -\sin \eta \hat{\sigma}_x + \cos \eta \hat{\sigma}_z$ , with  $\tan 2\eta = \kappa_y/q_y$ , provides  $\hat{A}_x = \hbar\tilde{q}_y \hat{\sigma}_z$ , with  $\tilde{q}_y = \cos 2\phi q_y + \sin 2\phi \kappa_y$ , and  $\hat{A}_y = \hbar\tilde{\kappa}_x \hat{\sigma}_x + \hbar\tilde{q}_x \hat{\sigma}_z$ , with  $\tilde{\kappa}_x = (\cos 2\phi \kappa_x - \sin 2\phi q_x)$ , and  $\tilde{q}_x = (\cos 2\phi q_x + \sin 2\phi \kappa_x)$ . We will use this form in sec. 4.5.

### 4.4.2 Landau-like gauge

In this subsection we shall consider the case similar to section 2.5.2,  $S_{13} = S_{23} = S$ . In that case the non-Abelian character demands  $(\nabla S \times \nabla \phi)_z \neq 0$ . We will choose the phase  $S = \kappa x$ , and  $\phi = qy$ , which gives a non-Abelian gauge potential unless  $\kappa = 0$  or  $q = 0$ . In addition, we take  $\cos \theta = x/R_c$ , where  $R_c^2 = x^2 + (z - z_c)^2$ , such that for the relevant  $x$ -range,  $|x| \ll z_c$  is fulfilled. As a consequence, and up to first order in  $(x/z_c)$  we obtain:

$$\hat{A} \simeq \hbar\kappa(\hat{\mathbb{1}} + \hat{\sigma}_z)\hat{x} + B_0 x \hat{\sigma}_y \hat{y}, \quad (4.8)$$

where  $B_0 = q/z_c$ . Note that, although  $x \ll z_c$ ,  $B_0$  can actually have large values. In addition, and again up to first order in  $(x/z_c)$ , we obtain  $\hat{V} + \hat{\phi} = U(\mathbf{r})$ , if  $V_1(\mathbf{r}) = V_2(\mathbf{r}) = \hbar^2 q^2/2m + U(\mathbf{r})$ , and  $V_3(\mathbf{r}) = \hbar^2/2m z_c^2$ . Using a simple gauge transformation  $\Psi \rightarrow \exp(i\kappa x)\Psi$  to eliminate the identity matrix term in  $\hat{A}_x$ , and applying a unitary spin transformation  $U^\dagger \hat{A} U$ , with  $U = (\hat{\sigma}_z + \hat{\sigma}_y)/\sqrt{2}$ , we obtain  $\hat{A} \simeq \hbar\kappa \hat{\sigma}_y \hat{x} + B_0 x \hat{\sigma}_z \hat{y}$ , which we will employ in sec. 4.6. A simple laser arrangement which would lead to this particular gauge is provided by

$$\Omega_1 = \Omega \cos(qy) e^{i\kappa(x+y+z)/2}, \quad (4.9)$$

$$\Omega_2 = \Omega \sin(qy) e^{i\kappa(x+y+z)/2}, \quad (4.10)$$

$$\Omega_3 = \Omega \frac{x}{z_c} e^{i\kappa(x-y+z)/2}, \quad (4.11)$$



where we assume that the illuminated atoms are confined to a region for which  $|x| \ll z_c$  holds.

### 4.4.3 Symmetric gauge

Although we discussed in section 2.5.3 that the tripod scheme is not suitable for the experimental realization of this gauge, due to the appearance of a spurious scalar potential, we include later (section 4.7) the analysis of this gauge field for completeness of our discussion.

## 4.5 Constant non-Abelian gauge

Let us consider a constant matrix gauge of the form  $\hat{A} = (\hat{A}_x, \hat{A}_y, 0)$ . We have already shown that these fields can be generated in a tripod scheme using a simple laser arrangement. Then, the Hamiltonian of the 2D system becomes:

$$\hat{H} = \frac{1}{2m} \left[ (\hat{p}_x + \hat{A}_x)^2 + (\hat{p}_y + \hat{A}_y)^2 \right]. \quad (4.12)$$

In the Abelian case  $[\hat{A}_x, \hat{A}_y] = 0$ . We can therefore choose a common eigenbasis for both matrices:  $\hat{A}_x/\hbar = \text{diag}\{q_{1x}, q_{2x}\}$ ,  $\hat{A}_y/\hbar = \text{diag}\{q_{1y}, q_{2y}\}$ . As a consequence, we recover two independently displaced quadratic spectra  $E_j(\mathbf{k}) = \frac{\hbar^2}{2m} (\mathbf{k} + \mathbf{q})^2$ , where  $\mathbf{q}_j = (q_{jx}, q_{jy})$ .

In the non-Abelian case, on the other hand, we cannot simultaneously diagonalize both matrices, and as a consequence the spectrum becomes distorted. Let us consider a simple, but representative, case, namely  $\hat{A}_x = q_x \hat{\sigma}_x$ ,  $\hat{A}_y = q_y \hat{\sigma}_z$ . Employing the Fourier-like transformation

$$\psi(x, y) = \sum_{k_x, k_y} e^{ik_y y \hat{\sigma}_z} \left( \frac{1 + i\hat{\sigma}_y}{\sqrt{2}} \right) e^{ik_x x \hat{\sigma}_z} \phi(k_x, k_y) \quad (4.13)$$

with  $k_{x,y} = 2\pi n_{x,y}/L$ , we may transform the time-independent Schrödinger equation  $E\psi(x, y) = \hat{H}\psi(x, y)$  into

$$\frac{2mE}{\hbar^2} \phi(k_x, k_y) = [k_x^2 + q_x^2 + (k_y + q_y)^2] \phi(k_x, k_y) + 2q_x k_x \phi(k_x, -k_y). \quad (4.14)$$

Diagonalizing the system of equations for  $\phi(k_x, \pm k_y)$ , we obtain two eigenenergies

$$\frac{2mE_{\pm}}{\hbar^2} = k_x^2 + q_x^2 + k_y^2 + q_y^2 \pm 2\sqrt{k_x^2 q_x^2 + k_y^2 q_y^2}. \quad (4.15)$$

Note that in the Abelian situation  $q_x = 0$  (or  $q_y = 0$ ) and, as expected, there is no coupling between momenta in different directions. However, due to the non-Abelian character, even for a constant gauge there is a non trivial coupling between the different directions.

## 4.6 Landau-like Non-Abelian gauge

### 4.6.1 Periodic boundary conditions

We consider in the following a matrix generalization of the Landau gauge, namely

$$\hat{A} = (\hbar\kappa\hat{M}_x, B_0\hat{M}_y x, 0) \quad (4.16)$$

(the usual Landau gauge is of the form  $\hat{A} = (0, B_0 x, 0)$ ). We will assume that the matrices  $\hat{M}_x$  and  $\hat{M}_y$  are constant. Then the Hamiltonian of the 2D system becomes:

$$\hat{H} = \frac{1}{2m} \left[ (\hat{p}_x + \hbar\kappa\hat{M}_x)^2 + (\hat{p}_y + B_0\hat{M}_y x)^2 \right]. \quad (4.17)$$

We first discuss the typical text book situation, in which the particles are assumed to be confined on a  $xy$ -plane of length  $L$  with periodic boundary conditions (i.e. a toroidal configuration). We are particularly interested in how the non-Abelian character of the fields destroys the usual Landau-level structure of the energy eigenstates. In the following subsection we shall discuss a slightly different scenario closer to actual experimental conditions.

As in sec. 4.5, if  $[\hat{M}_x, \hat{M}_y] = 0$ , one can find a common eigenbasis  $\{\mathbf{e}_1, \mathbf{e}_2\}$ , such that in this basis  $\hat{M}_x = \text{diag}\{\gamma_1, \gamma_2\}$ , and  $\hat{M}_y = \text{diag}\{\lambda_1, \lambda_2\}$ , and hence the Hamiltonian is also diagonal in this basis. Since we assume periodic boundary conditions we can consider wavefunctions of the form

$$\psi_j(\mathbf{r}) = \sum_{n_y} e^{i\frac{2\pi}{L}n_y y + i\kappa\gamma_j q} v_j(n_y, x) \mathbf{e}_j, \quad (4.18)$$

such that

$$E v_j(q) = \left[ \frac{\hat{p}^2}{2m} + \frac{1}{2} m \omega_j^2 q^2 \right] v_j(q). \quad (4.19)$$

where  $q = x + \frac{2\pi\hbar n_y}{LB_0\lambda_j}$ ,  $p = -i\hbar\partial/\partial q$ , and  $\omega_j = B_0|\lambda_j|/m$  is the cyclotron frequency for the state  $j$ . Hence, for the Abelian case we obtain two different sets of Landau levels with energies  $E_j(n) = \hbar\omega_j(n + 1/2)$ , and degeneracies  $g_j = B_0\lambda_j L^2/2\pi\hbar$ . Note that if  $|\lambda_1| = |\lambda_2|$ , as it is the case for  $M_y = \hat{\sigma}_z$ , then the two sets of Landau levels are degenerate.

Let us now discuss what happens if on the contrary  $[\hat{M}_x, \hat{M}_y] \neq 0$ . We work (without lack of generality) in the basis in which  $M_y = \hat{\sigma}_z$ . Note that the Ansatz

$$\psi(\mathbf{r}) = \sum_{n_y} e^{i\frac{2\pi}{L}n_y y \hat{\sigma}_z} \mathbf{u}(n_y, x) \quad (4.20)$$

also fulfills periodic boundary conditions. We insert this Ansatz into the eigenvalue equation to obtain

$$\begin{aligned} E\mathbf{u}(n_y, x) &= \left[ \frac{(p_x + \hbar\kappa M_x)^2}{2m} + \frac{1}{2m} \left( \frac{\hbar 2\pi n_y}{L} + B_0 x \right)^2 \right] \mathbf{u}(n_y, x) \\ &+ \frac{1}{2} \left[ \sigma_z \frac{(p_x + \hbar\kappa M_x)^2}{2m} \sigma_z - \frac{(p_x + \hbar\kappa M_x)^2}{2m} \right] [\mathbf{u}(n_y, x) - \mathbf{u}(-n_y, x)] \end{aligned} \quad (4.21)$$

$$\begin{aligned} E\mathbf{u}(n_y, x) &= \left[ \frac{\hat{\Pi}^2}{2m} + \frac{\hbar^2}{2m} \left( \frac{2\pi n_y}{L} + \frac{B_0}{\hbar} x \right)^2 \right] \mathbf{u}(n_y, x) \\ &+ [\hat{\sigma}_z [\hat{\Pi}^2, \hat{\sigma}_z]] \left[ \frac{\mathbf{u}(n_y, x) - \mathbf{u}(-n_y, x)}{4m} \right], \end{aligned} \quad (4.22)$$

where  $\hat{\Pi} = \hat{p}_x + \hbar\kappa\hat{M}_x$ . For the Abelian case,  $[\hat{M}_x, \hat{\sigma}_z] = 0$ , the last term vanishes, and we get the same equation (eq. (4.19)) as previously. However, for the non-Abelian case, the last

term introduces a coupling between the modes with  $n_y$  and  $-n_y$ , and hence there is an explicit dependence on  $n_y$ . As a consequence of that, the degeneracy of the Landau levels is lifted.

For the particular case of  $\hat{M}_x = \hat{\sigma}_y$ , we get the following set of coupled equations ( $\epsilon = E - \hbar^2 \kappa^2 / 2m$ ):

$$\begin{aligned} \epsilon \mathbf{u}(n_y, x) = & \left[ \frac{\hat{p}_x^2}{2m} + \frac{B_0^2}{2m} \left( x + \frac{2\pi \hbar n_y}{B_0 L} \right)^2 \right] \mathbf{u}(n_y, x) \\ & + \frac{\hbar \kappa}{m} \hat{p}_x \hat{\sigma}_y \mathbf{u}(-n_y, x) \end{aligned} \quad (4.23)$$

$$\begin{aligned} \epsilon \mathbf{u}(-n_y, x) = & \left[ \frac{\hat{p}_x^2}{2m} + \frac{B_0^2}{2m} \left( x - \frac{2\pi \hbar n_y}{B_0 L} \right)^2 \right] \mathbf{u}(-n_y, x) \\ & + \frac{\hbar \kappa}{m} \hat{p}_x \hat{\sigma}_y \mathbf{u}(n_y, x). \end{aligned} \quad (4.24)$$

The coupling prevents the re-absorption of  $n_y$  in the definition of a new  $q$  variable, as it was done in the Abelian case, and hence the spectrum explicitly depends on  $n_y$ . Note that we are imposing periodic boundary conditions, and therefore  $x$  is in a ring of perimeter  $L$ . In this sense,  $\pm L/2$  are the same point, and this must be taken into account when considering the harmonic oscillator potential in each equation. Fig. 4.8 depicts the couplings of the different  $n_y$  in the equations above, compared to the Abelian case of fig. 4.4. Note that the previous equations involve the coupling of harmonic oscillator wavefunctions centered in  $\pm x_c(|n_y|)$ , with  $x_c(|n_y|) = 2\pi \hbar |n_y| / B_0 L$ . Hence, the smaller the overlapping between coupled wavefunctions (see fig. 4.8), i.e. the larger  $x_c$ , the smaller the coupling, and as a consequence only sufficiently small values of  $n_y$  will be affected by the non-Abelian coupling. This point becomes clear after performing first order perturbation theory assuming a small coupling  $\kappa$ . A straightforward calculation shows that the lowest Landau levels, which correspond to the lowest eigenvalues of each harmonic oscillator, experience a maximal energy shift

$$\frac{\Delta E}{\hbar \omega_c} = (\kappa l_c) \frac{n_y}{\Delta n_y} e^{-n_y^2 / \Delta n_y^2}, \quad (4.25)$$

where  $l_c^2 = \hbar / m \omega_c$  is the magnetic length, and  $\Delta n_y = \sqrt{g/2\pi}$ , with  $g$  the degeneracy of the unperturbed Landau levels. Note that for  $n_y = 0$  the first correction should be quadratic in  $\kappa$ , whereas for  $n_y \neq 0$  it should be linear. Clearly, the relative importance of the non-Abelian corrections should decrease as  $g^{-1/2}$ . In particular, the maximal energy shift  $\langle \Delta E \rangle$  averaged over the different  $n_y$  can be approximated as  $\langle \Delta E \rangle / \hbar \omega_c \simeq (\kappa l_c) / \sqrt{2\pi g}$ .

We have solved numerically for the eigenvalues of eqs. (4.23) and (4.24) imposing periodic boundary conditions, for different values of  $g$  which controls the strength of the magnetic field applied, and  $\kappa l_c$  which provides the strength of the non-Abelian corrections. The value of  $L/l_c = \sqrt{2\pi g}$  is chosen in all simulations. Fig. 4.9 shows the behavior of the lowest eigenvalue as a function of  $n_y$  for  $g = 128$  and  $\kappa l_c = 0, 0.2, 0.4, 0.6, 0.8, 1.0$  (from the uppermost to the lowermost curve). The figure follows approximately the perturbative result. For  $n_y = 0$  a higher order contribution appears, but note that a quadratic law for small  $\kappa$  follows, and not a linear one, as in the case for  $n_y \neq 0$ . As expected from the previous calculations only values of  $n_y$  up to the order of  $\sqrt{g}$  contribute significantly to the shift of the lowest Landau level.

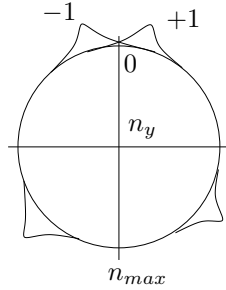


Fig. 4.8: Visualization of the possible values of  $n_y$ . The Gaussians show that the different  $n_y$  are coupled, contrary to the Abelian case in fig. 4.4, and the overlap determines the strength of their coupling.

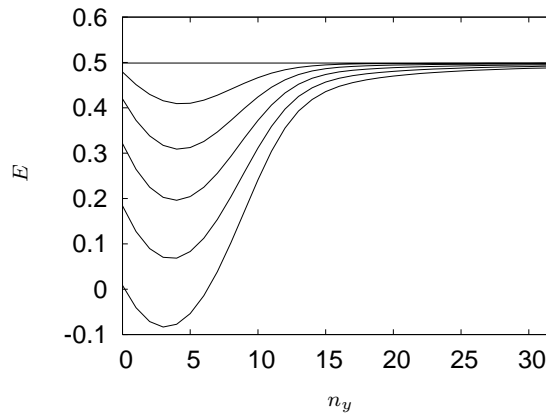


Fig. 4.9: Lowest eigenvalue  $\epsilon_0$  in units of  $\hbar\omega_c$  as a function of  $n_y$ , for  $g = 128$  and  $\kappa l_c = 0, 0.2, 0.4, 0.6, 0.8, 1.0$  (from the uppermost to the lowermost curve).

Fig. 4.10 show the behavior of the Landau levels for  $g = 128$ , and  $\kappa l_c = 0, 0.2, 0.4, 0.6, 0.8, 1.0$ . The figures are presented as histograms in intervals of  $0.05\hbar\omega_c$ , in order to reveal more clearly the destruction of the Landau levels. Note that the gaps (of energy  $\hbar\omega_c$ ) between the Landau levels are filled, and the peaks in the density of states are progressively reduced. For sufficiently large  $\kappa$  the Landau level structure therefore disappears.

#### 4.6.2 Absorbing boundary conditions

In the previous section we discussed how the non-Abelian character of the gauge field significantly modifies the text-book Landau level structure. In the following, we consider a slightly different physical scenario which is closer to the actual experimental conditions discussed in sec. 4.4. The particular procedure devised for the generation of the non-Abelian Landau gauge demands that the  $x$  coordinate cannot be considered as periodic. We take the same box con-

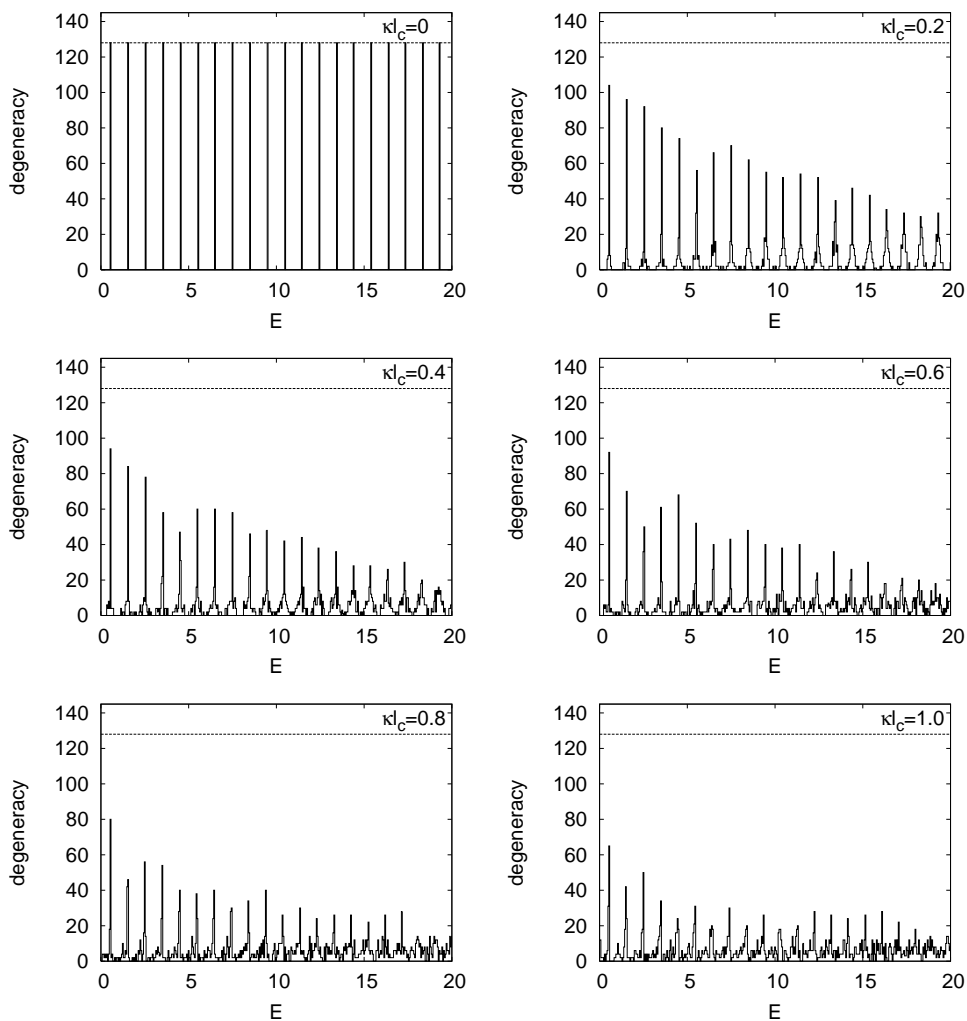


Fig. 4.10: Landau level structure for periodic boundary conditions,  $g = 128$ , and  $\kappa l_c \in \{0, 0.2, 0.4, 0.6, 0.8, 1.0\}$ . We employ (see text)  $\hat{M}_x = \hat{\sigma}_y$  and  $\hat{M}_y = \hat{\sigma}_z$ .

figuration as for the previous subsection, but assume absorbing boundary conditions in the  $x$  direction, while keeping for simplicity periodic boundary conditions in the  $y$ -direction. We consider exactly the same gauge discussed in the previous subsection. The spectrum is provided by eqs. (4.23) and (4.24) but imposing absorbing boundary conditions. Fig. 4.11 shows the lowest Landau levels for the same cases discussed in Fig. 4.10.

Even for the Abelian case the Landau level structure is affected by the absorbing boundary conditions. In the Abelian case, as discussed in the previous section, the problem reduces to two decoupled equations for harmonic oscillators centered at  $\pm x_c(|n_y|)$ . Clearly, when  $x_c$  approaches  $L$  the levels of the resulting potential become largely distorted, leading to a

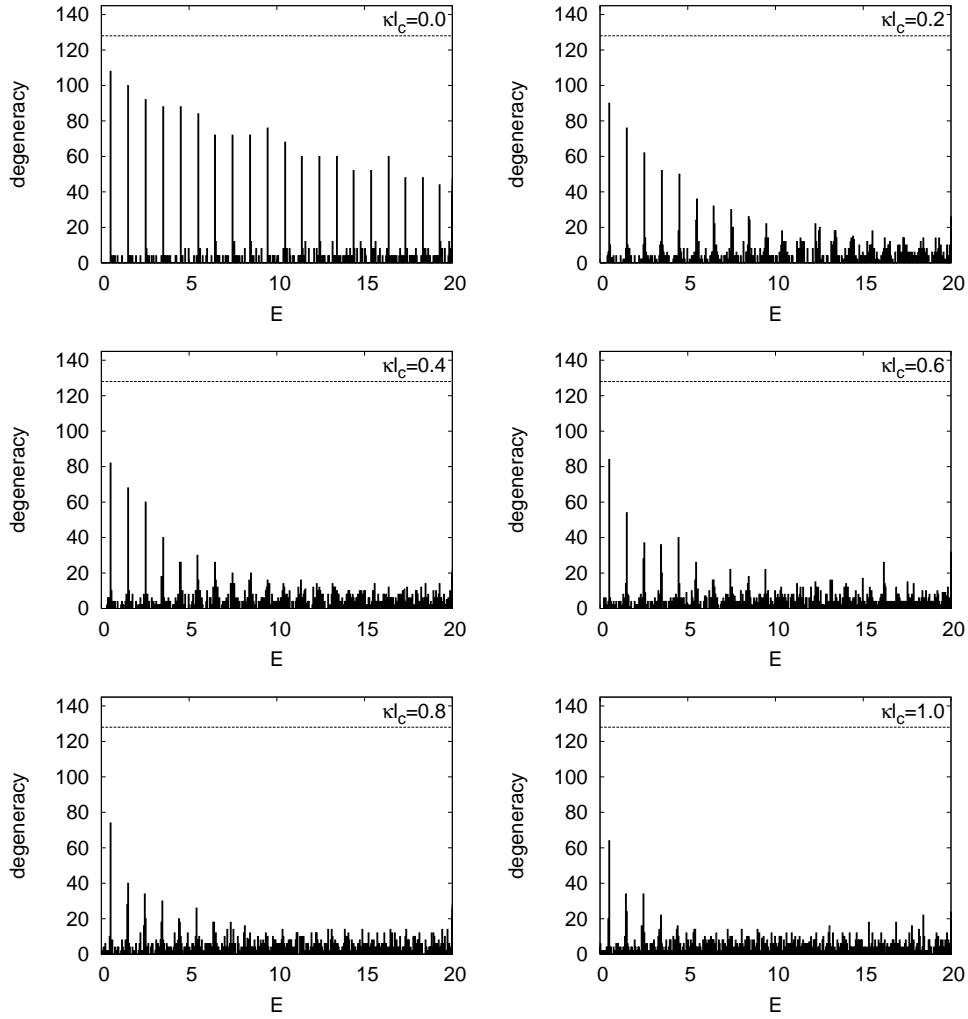


Fig. 4.11: Same cases considered in fig. 4.10 but with absorbing boundary conditions,  $\kappa l_c \in \{0, 0.2, 0.4, 0.6, 0.8, 1.0\}$

significant modification of the Landau level structure when  $n_y$  approaches  $g$ . This reduces the effective degeneracy of the lowest Landau levels to values smaller than  $g$ . The effective degeneracy, as shown in the figures, becomes smaller for higher Landau levels. The non-Abelian effect leads, as in the previous subsection, to the eventual destruction of the Landau level structure.

### 4.6.3 de Haas–van Alphen–Effect

In the last section we predicted the change of Landau levels. In this section we remind the reader how the Landau level structure can be experimentally measured by means of the de Haas–van Alphen–effect [LL02]. The filling of Landau levels (fig. 4.3) using  $N$  non-interacting fermions at low temperatures causes oscillations in physical observables as a function of the magnetic field  $B$ . This is the so-called de Haas–van Alphen–effect.

The degeneracy of the Landau Level is  $g = \frac{BL^2}{2\pi\hbar}$ . At very high magnetic fields  $B$ , if  $g(B) > N$ , all fermions are in the lowest Landau Level (LLL)  $n = 0$ . For decreasing magnetic field one reaches a critical point  $B_c$  for which  $g(B_c) = N$ . In the case of further decrease to  $B < B_c$  the fermions have to hop to the next level  $n = 1$ . If the magnetic field decreases more i.e.  $B < B_c/2$  the fermions will hop to  $n = 2$ . Further decreasing of  $B$  will lead to the occupation of higher and higher Landau Levels,  $\frac{1}{n_0+1} > \frac{B}{B_c} > \frac{1}{n_0+2}$ , meaning the first  $n_0$  Landau levels are fully occupied and level  $n_0 + 1$  is partially occupied. Levels larger than  $n_0 + 1$  are empty. Let us now consider the energy at different magnetic fields  $B$ . For  $B > B_c$  the energy grows linearly with  $B$ . After passing  $B = B_c$  the energy will increase first with decreasing magnetic field, see fig. 4.12. This yields the characteristic oscillations of the energy. Assume that  $N$  non-interacting fermions at low temperatures fill all the states starting from the lowest energy eigenvalue. The ground state energy  $E_0$  is then the sum of the energies  $\epsilon_n$  over the  $N$  lowest 1-particle-states:

$$\begin{aligned} E_0(B) &= g(B) \sum_{n=0}^{n_0} \epsilon_n + \left[ N - \sum_{n=0}^{n_0} g \right] \epsilon_{n_0+1} \\ &= 2\mu_B B \left\{ g(B) \sum_{n=0}^{n_0} \left( n + \frac{1}{2} \right) + [N - (n_0 + 1)g(B)] \left( n_0 + \frac{3}{2} \right) \right\} \\ &= 2\mu_B B N \left\{ \left( n_0 + \frac{3}{2} \right) - \frac{B}{2B_c} (n_0 + 1)(n_0 + 2) \right\}. \end{aligned} \quad (4.26)$$

Using the energy  $E_0$  we calculate the magnetisation  $M = -\frac{1}{V} \frac{\partial E_0}{\partial B}$  and susceptibility  $\chi = -\frac{1}{V} \frac{\partial^2 E_0}{\partial B^2}$ :

$$\frac{E_0(B)}{N} = \begin{cases} \mu_B B & \text{if } B > B_c \\ \mu_B B \left\{ (2n_0 + 3) - \frac{B}{B_c} (n_0 + 1)(n_0 + 2) \right\} & \text{if } \frac{1}{n_0+2} < \frac{B}{B_c} < \frac{1}{n_0+1} \end{cases} \quad (4.27)$$

$$M = \begin{cases} -\frac{1}{V} \mu_B & \text{if } B > B_c \\ -\frac{1}{V} \mu_B \left\{ (2n_0 + 3) - \frac{B}{B_c} (n_0 + 1)(n_0 + 2) \right\} & \text{if } \frac{1}{n_0+2} < \frac{B}{B_c} < \frac{1}{n_0+1} \end{cases} \quad (4.28)$$

$$\chi = \begin{cases} 0 & \text{if } B > B_c \\ \frac{2\mu_B}{B_c V} \left\{ (2n_0 + 3) - \frac{B}{B_c} (n_0 + 1)(n_0 + 2) \right\} & \text{if } \frac{1}{n_0+2} < \frac{B}{B_c} < \frac{1}{n_0+1} \end{cases}, \quad (4.29)$$

where ( $\nu = V/N$ ). Hence the susceptibility  $\chi$  shows plateaus and  $M$  oscillates (fig. 4.12). This is the so-called de Haas–van Alphen–effect.

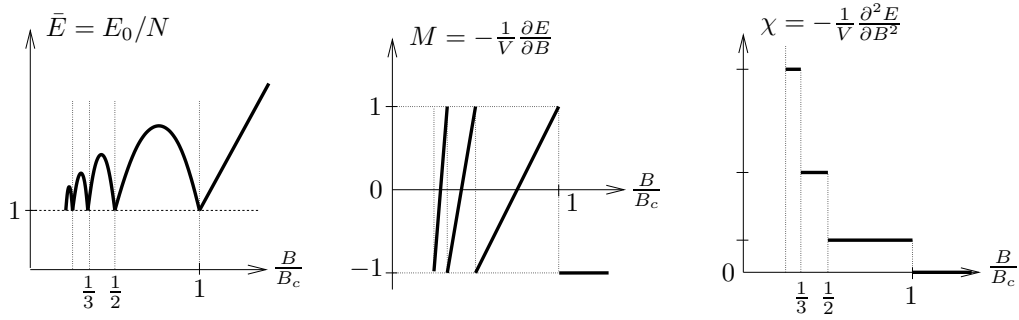


Fig. 4.12: De Haas–van Alphen–effect (theory). The degeneracy of the Landau levels depends on the magnetic field  $B$ . Therefore, the filling of the Landau levels causes oscillatory behaviour in the energy per particle  $\bar{E}$  as a function of  $B$ . Consequently, the magnetisation  $M$  oscillates as well and the susceptibility  $\chi$  shows plateaus.

#### 4.6.4 Modified de Haas–van Alphen–Effect

The destruction of the Landau level structure has experimentally relevant consequences for the behavior of cold atomic gases. As an example we can consider the case of an ideal two-component Fermi gas under the previously mentioned non-Abelian gauge potential (we consider a temperature  $T \ll T_F$ , where  $T_F$  is the Fermi temperature). Equivalently to the well-known de Haas–van Alphen–effect (see last section), we may study the energy per particle,  $\bar{E} = E/N$ , of the Fermi gas, as a function of the applied magnetic field  $B$ , or equivalently of  $g$ . This energy may be monitored by measuring the released energy in time-of-flight experiments. For  $\kappa = 0$  (Abelian case)  $d^2\bar{E}(B)/dB^2$  presents a typical configuration of plateaus, due to the degeneracy of the Landau levels. The destruction of the Landau level structure significantly distorts this picture, rounding-off or eventually destroying this plateaus configuration (see fig. 4.13).



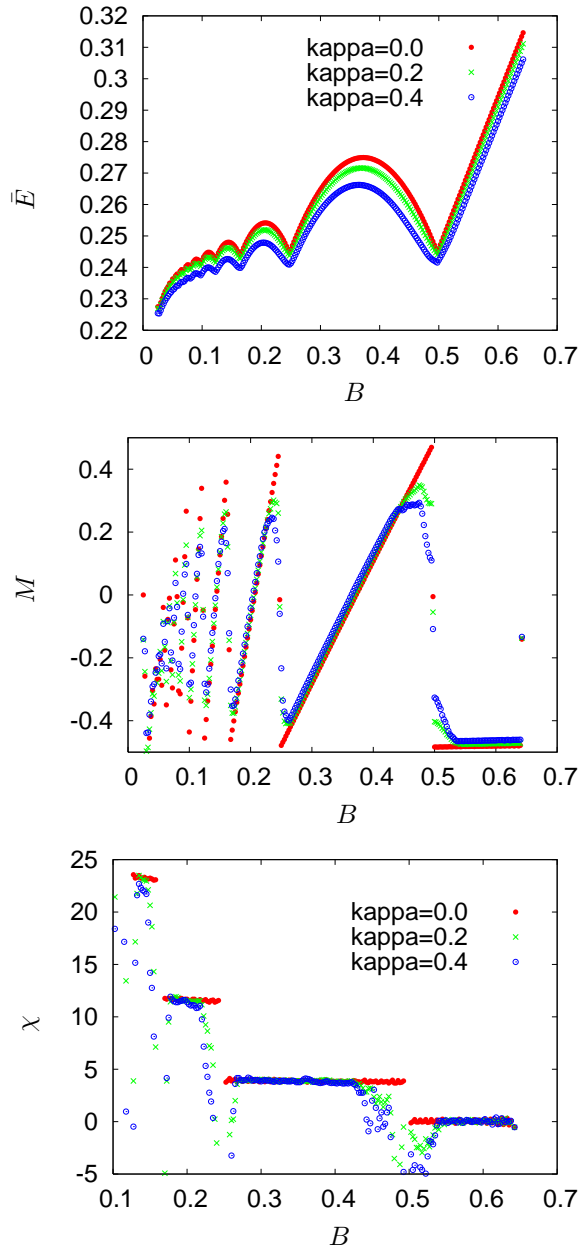


Fig. 4.13: De Haas-van Alphen-effect (simulation): Values of  $\bar{E}$ ,  $M \propto -\partial\bar{E}/\partial B$  and  $\chi \propto -\partial^2\bar{E}/\partial B^2$  as a function of the applied magnetic field  $B$ . These are the same cases as discussed in fig. 4.10 for  $\kappa = 0$  (red filled circles),  $\kappa = 0.2$  (green daggers) and  $\kappa = 0.4$  (blue hollow circles).

## 4.7 Symmetric gauge

In this section we consider an ideal cold atomic sample in an isotropic harmonic trap of frequency  $\omega$ , in the presence of a non-Abelian generalization of the symmetric gauge of the form  $\hat{A} = \hat{A}_\rho \hat{\rho} + \rho \hat{A}_\varphi \hat{\varphi}$ . Although the tripod scheme is not suitable for the experimental realization of this gauge, we include the analysis of this gauge field for completeness of our discussion. Other ways of generating non-Abelian gauge fields, as lattice techniques [OBS<sup>+</sup>05] should be employed in this case. In the following we consider  $A_\rho = \hbar\kappa\hat{U}_\rho$ ,  $A_\varphi = B_0\hat{U}_\varphi$ , where  $\hat{U}_{\rho,\varphi}$  are linear combinations of  $\{\hat{\mathbb{1}}, \hat{\sigma}_x, \hat{\sigma}_y, \hat{\sigma}_z\}$ .

The corresponding time-independent Schrödinger equation is of the form

$$E\psi = \frac{1}{2m} \left[ -i\hbar\nabla + \hat{A} \right]^2 \psi + \frac{m\omega^2}{2} \rho^2 \psi. \quad (4.30)$$

Performing the gauge transformation  $\psi = \exp[-i\hat{A}_\rho\rho/\hbar]\phi$ , the Schrödinger equation transforms into

$$E\psi = \frac{1}{2m} \left[ -i\hbar\nabla + \hat{\varphi}\hat{C}_\varphi(\rho)\rho \right]^2 \psi + \frac{m\omega^2}{2} \rho^2 \psi, \quad (4.31)$$

where

$$\hat{C}_\varphi(\rho) = e^{i\hat{A}_\rho\rho/\hbar} \hat{A}_\varphi e^{-i\hat{A}_\rho\rho/\hbar}. \quad (4.32)$$

Note that  $\hat{C}_\varphi$  becomes  $\rho$ -dependent and different from  $\hat{A}_\varphi$  if  $[\hat{A}_\rho, \hat{A}_\varphi] \neq 0$ .

If we now consider the solutions with angular momentum  $l$ ,  $\phi = \mathbf{R}_l \rho^{|l|} e^{il\varphi}$ , we obtain

$$E\mathbf{R}_l = -\frac{1}{2} \left[ \frac{d^2}{d\rho^2} \mathbf{R}_l + \frac{(2|l|+1)}{\rho} \frac{d}{d\rho} \mathbf{R}_l \right] + \frac{1}{2} \left[ 1 + \hat{C}_\varphi(\rho)^2 \right] \rho^2 \mathbf{R}_l + l\hat{C}_\varphi(\rho)\mathbf{R}_l, \quad (4.33)$$

where we reduce the equations to a dimensionless form by employing oscillator units for the energy ( $\hbar\omega$ ) and for the length ( $l_{\text{ho}} = \sqrt{\hbar/m\omega}$ ). In the previous equation

$$\hat{C}_\varphi(\rho) \equiv (\omega_c/\omega) \exp[i\kappa\hat{U}_\rho\rho] \hat{U}_\varphi \exp[-i\kappa\hat{U}_\rho\rho], \quad (4.34)$$

where  $\omega_c = B_0/m$  is the corresponding cyclotron frequency.

As mentioned above the non-Abelian character of the gauge field induces an additional  $\rho$ -dependent potential. This severely distorts the standard Fock-Darwin spectrum expected for the Landau-level structure in the presence of a symmetric gauge and a harmonic potential (Fig. 4.14). An inspection of the level structure shows that not only the eigenenergies are modified, but also the ordering of the different eigenstates becomes distorted as a consequence of the non-Abelian potential.

Note that for the non-Abelian case

$$\hat{C}_\varphi(\rho) = -b_0 (\cos(2\kappa b_0\rho)\hat{\sigma}_z + \sin(2\kappa b_0\rho)\hat{\sigma}_x) \quad (4.35)$$

and

$$\hat{C}_\varphi^2(\rho) = -b_0^2 \hat{\mathbb{1}}. \quad (4.36)$$

When  $\kappa$  becomes very large  $\hat{C}_\varphi(\rho)$  averages to zero, and we recover a harmonic oscillator with frequency  $\omega\sqrt{1+b_0^2}$ , see fig. 4.15. For  $\kappa > 5$  we then observe no further relevant change in the spectrum.

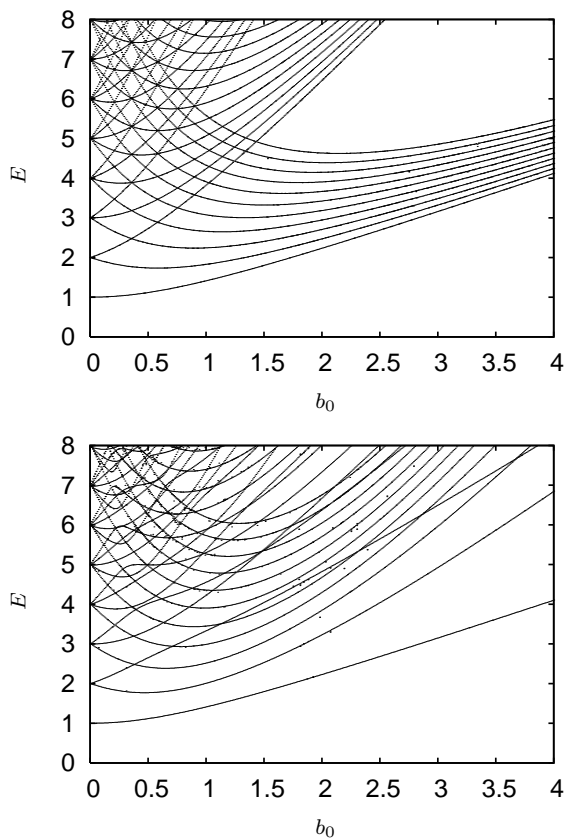
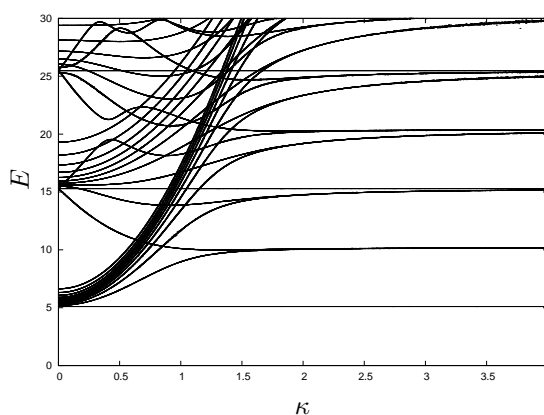


Fig. 4.14: Fock-Darwin spectrum  $E$  in units of  $\hbar\omega\sqrt{1+b_0^2}$  for the Abelian (top) and non-Abelian (bottom) cases discussed in the text as a function of  $b_0 = \omega_c/\omega$ . Here we used for the gauge fields  $\hat{A}_\varphi = b_0\hat{\sigma}_z$ ,  $\hat{A}_\rho^{\text{Abel}} = \kappa b_0\hat{\mathbb{1}}$  resp.  $\hat{A}_\rho^{\text{Non-Abel}} = \kappa b_0\hat{\sigma}_y$ .

Fig. 4.15: Energy  $E$  vs. strength of the non-Abelianity  $\kappa$  for a fixed  $b_0 = 5$ , interesting physics happens if  $\kappa \approx 1$ , i.e. when  $A_\rho$  and  $A_\phi$  have the same order of magnitude. Here we used  $\hat{A}_\varphi = b_0\hat{\sigma}_z$  and  $\hat{A}_\rho = \kappa b_0\hat{\sigma}_x$ .



As a consequence of this extra  $\rho$ -dependent potential in eq. (4.31), the shape of the eigenfunctions change as well, see e.g. fig. 4.16 for the shape of the first four eigenfunctions with angular momentum  $l = 4$ . There one still recognizes the excitation number by counting the notches. Therefore an ideal Fermi gas at zero temperature shows a significantly distorted density profile in the presence of the non-Abelian gauge field, as shown in fig. 4.17, where we summed over the first 56 eigenlevels to obtain a density profile at zero temperature.

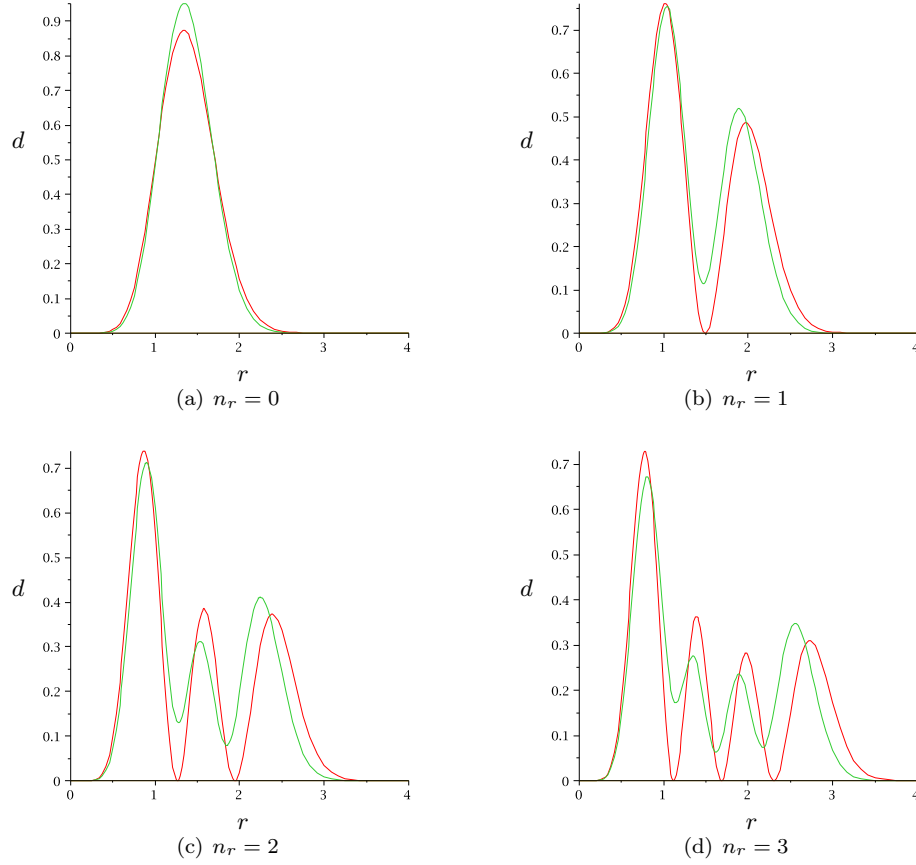


Fig. 4.16: Distortion of the eigenfunctions in the non-Abelian regime, due to the additional  $\rho$ -dependent potential. The panels above show the the density of the first four eigenfunctions ( $n_r = 0 \dots 3$ ) for angular momentum  $l = 4$ ,  $b_0 = 2$ ,  $\kappa = 1$  in the Abelian case (red line,  $\hat{A}_\varphi = b_0 \hat{\sigma}_z$  and  $\hat{A}_\rho = \kappa b_0 \hat{\mathbb{1}}$ ) and non-Abelian case (green line,  $\hat{A}_\rho = \kappa b_0 \hat{\sigma}_x$ ).

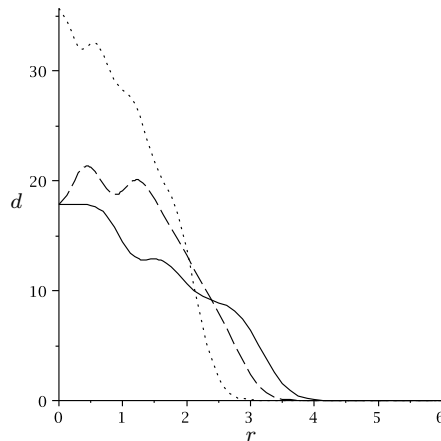


Fig. 4.17: Comparison between the density profile for an ideal Fermi gas occupying up to 56 eigenlevels at zero temperature for the Abelian (solid) and non-Abelian cases discussed in the text with different values of  $\kappa = 1$  (dashed), and  $\kappa = 5$  (dotted).

## 4.8 Summary

In this chapter we have analyzed the physics of ultracold gases in the presence of a non-Abelian gauge field. We have first studied how different types of non-Abelian fields may be created by means of relatively simple laser arrangements with atoms described by an electronic tripod level scheme, including a non-Abelian generalization of the Landau gauge. In a second part we have considered the non-trivial effects that the non-Abelian character has on the eigenlevel structure of the cold atomic system. In particular we have shown that exclusively due to the non-Abelian character of the field, the usual Landau level structure is severely distorted, and even eventually destroyed. We have shown that this effect may be observable in an equivalent experiment to the well-known de Haas–van Alphen–effect. The distortion of the Landau levels leads to a significant modification of the usual plateaux-like susceptibility characteristic for the de Haas–van Alphen–effect. Finally, we have completed our analysis of a non-Abelian version of the symmetric gauge. We have shown that the Fock–Darwin spectrum is significantly distorted in the presence of non-Abelian fields, due to the presence of an extra potential, which is a purely non-Abelian effect.



# Chapter 5

## Quasi-Relativistic Physics with Cold Gases. Veselago Lensing

### 5.1 Introduction

In this chapter we employ the constant non-Abelian gauge potential, proportional to an operator of spin 1/2,  $\mathbf{A} = (\sigma_x, \sigma_y, 0) = \boldsymbol{\sigma}$ , suggested by [JRL<sup>+</sup>08], which is similar to the constant potential we introduced in section 2.5.1:

$$H = \frac{1}{2m} (\mathbf{p} + \kappa \boldsymbol{\sigma})^2 + V. \quad (5.1)$$

Then we demonstrate that this Hamiltonian resembles for small momenta the Hamiltonian of ultra-relativistic two-component Dirac fermions

$$H = \hbar v_F \boldsymbol{\sigma} \cdot \mathbf{k}, \quad (5.2)$$

where  $v_F$  is the Fermi velocity. This is also the Hamiltonian of electrons in graphene [NGM<sup>+</sup>05, MF06, KNG06, GN07, NJZ<sup>+</sup>07, MP07, JP07, Pen07, CFA07] — a two dimensional hexagonal crystal of carbon atoms. Close to the Fermi level the electrons in graphene behave like massless ultra-relativistic two-component Dirac fermions [BLP82] moving with a velocity  $v_F$  as in eq. (5.2). There one expects remarkable effects, such as a half integer quantum Hall effect [NGM<sup>+</sup>05, GN07, NJZ<sup>+</sup>07] and the Klein paradox [KNG06]. It has also been proposed that electrons in graphene [Pen07, CFA07] should undergo negative refraction at a potential barrier, similar to the electromagnetic waves impinging on a barrier where the dielectric permittivity and the magnetic permeability are negative [Ves68, Pen00]. We show in this chapter that cold atoms can experience negative refraction and Veselago-type lensing [Ves68].

The Fermi velocity  $v_F$  in (5.2) is in ultra-relativistic physics the vacuum speed of light  $c \approx 3 \cdot 10^8$  m/s, but it is three orders of magnitude smaller for electrons in graphene, around  $10^5$  m/s. However, in cold atoms the ultra-relativistic effects can even be observed at velocities of  $10^{-2}$  m/s, which is even 10 orders of magnitude smaller than the speed of light. Other proposals to generate quasi-relativistic dynamics of cold atoms use lattices instead, e.g. one-dimensional [RDJ02] or 2D hexagonal (graphene-type) [ZWD07] lattices.

### 5.2 Laser-induced non-Abelian gauge fields

Let us consider the adiabatic motion of tripod atoms with laser couplings as discussed in 2.4.4. To generate our spin 1/2 gauge potential we start with the general parametrization of the lasers

coupling the tripod levels, as in eq. (2.75) of section 2.4.4. We are particularly interested in the case of the first two lasers having the same intensities and counter-propagating in  $x$ -direction while the third laser propagates in the negative  $y$ -direction with the same wave number  $\kappa$

$$\Omega_1 = \Omega \sin \theta e^{-i\kappa x} / \sqrt{2}, \quad (5.3)$$

$$\Omega_2 = \Omega \sin \theta e^{i\kappa x} / \sqrt{2}, \quad (5.4)$$

$$\Omega_3 = \Omega \cos \theta e^{-i\kappa y}, \quad (5.5)$$

where  $\Omega = \sqrt{|\Omega_1|^2 + |\Omega_2|^2 + |\Omega_3|^2}$  is the total Rabi frequency, and  $\theta$  the mixing angle defining the relative intensities.

The electronic Hamiltonian of the tripod atom reads in the interaction representation as in eq. (2.69)

$$\hat{H}_0 = -\hbar \left( \Omega_1 |0\rangle\langle 1| + \Omega_2 |0\rangle\langle 2| + \Omega_3 |0\rangle\langle 3| \right) + \text{H.c.}, \quad (5.6)$$

and the two dark states of this Hamiltonian are

$$|D_1\rangle = \frac{1}{\sqrt{2}} e^{-i\kappa y} \left( e^{i\kappa x} |1\rangle - e^{-i\kappa x} |2\rangle \right) \quad (5.7)$$

$$|D_2\rangle = \frac{1}{\sqrt{2}} e^{-i\kappa y} \cos \theta \left( e^{i\kappa x} |1\rangle + e^{-i\kappa x} |2\rangle \right) - \sin \theta |3\rangle. \quad (5.8)$$

With the Rabi frequencies  $\Omega_j$  being space dependent, the states  $|D_1\rangle$  and  $|D_2\rangle$  are spatially dependent as well. The adiabatic approximation assures that the internal states of the Hamiltonian (5.6) evolve within the dark state manifold. The atomic state-vector  $|\Phi\rangle$  can then be expanded in terms of the dark states according to  $|\Phi\rangle = \sum_{j=1}^2 \Psi_j(\mathbf{r}) |D_j(\mathbf{r})\rangle$ , where  $\Psi_j(\mathbf{r})$  is the wave-function for the center of mass motion of the atom in the  $j$ -th dark state.

Thus the atomic center of mass motion is described by a two-component wave-function  $\Psi = (\Psi_1, \Psi_2)^T$ . The column-matrix  $\Psi$  obeys the Schrödinger equation

$$i\hbar \frac{\partial}{\partial t} \Psi = \left[ \frac{1}{2m} (-i\hbar \nabla - \mathbf{A})^2 + V + \Phi \right] \Psi, \quad (5.9)$$

where  $m$  is the atomic mass, and  $\mathbf{A}$ ,  $\Phi$  and  $V$  are  $2 \times 2$  matrices. The gauge potentials  $\mathbf{A}$  has the elements  $\mathbf{A}_{n,m} = i\hbar \langle D_n(\mathbf{r}) | \nabla | D_m(\mathbf{r}) \rangle$ , the scalar potential is  $V_{n,m} = \langle D_n(\mathbf{r}) | \hat{V} | D_m(\mathbf{r}) \rangle$  with  $\hat{V} = V_1(\mathbf{r}) |1\rangle\langle 1| + V_2(\mathbf{r}) |2\rangle\langle 2| + V_3(\mathbf{r}) |3\rangle\langle 3|$ , where  $V_j(\mathbf{r})$  is the trapping potential for an atom in the internal state  $j = 1, 2, 3$ . Note that the potential  $V_j$  can also accommodate a possible detuning of the  $j$ -th laser from the resonance of the  $j \rightarrow 0$  transition. In chapter 2, the potentials  $\mathbf{A}$ ,  $\Phi$  and  $V$  have been considered for arbitrary light fields. In the present configuration of the light fields, the potentials take the form

$$\mathbf{A} = \hbar \kappa \begin{pmatrix} \mathbf{e}_y & -\mathbf{e}_x \cos \theta \\ -\mathbf{e}_x \cos \theta & \mathbf{e}_y \cos^2 \theta \end{pmatrix}, \quad (5.10)$$

$$\Phi = \begin{pmatrix} \hbar^2 \kappa^2 \sin^2 \theta / 2m & 0 \\ 0 & \hbar^2 \kappa^2 \sin^2(2\theta) / 8m \end{pmatrix}, \quad (5.11)$$

$$V = \begin{pmatrix} V_1 & 0 \\ 0 & V_1 \cos^2 \theta + V_3 \sin^2 \theta \end{pmatrix}, \quad (5.12)$$



where the external trapping potential is assumed to be the same for the first two atomic states,  $V_1 = V_2$ .

To simplify the sum of the scalar potentials  $V + \Phi$  we take  $V_3 - V_1 = \hbar^2 \kappa^2 \sin^2 \theta / 2m$ . This is obtained by detuning the third laser from the two-photon resonance by  $\Delta\omega_3 = \hbar \kappa^2 \sin^2 \theta / 2m$ .

Therefore the overall trapping potential can be made proportional to an identity matrix:  $V + \Phi = V_1 \mathbb{1}$  (up to a constant). Both dark states are affected by the same trapping potential  $V_1 \equiv V_1(\mathbf{r})$ . Furthermore, to represent the gauge potential in a symmetric way in terms of the Pauli matrices  $\sigma_x$  and  $\sigma_z$ , we choose  $\theta = \theta_0$  such that  $\sin^2 \theta_0 = 2 \cos \theta_0$ , giving  $\cos \theta_0 = \sqrt{2} - 1$  and

$$\mathbf{A} = \hbar \kappa' (-\mathbf{e}_x \sigma_x + \mathbf{e}_y \sigma_z) + \hbar \kappa_0 \mathbf{e}_y \mathbb{1}, \quad (5.13)$$

where  $\kappa' = \kappa \cos \theta_0 \approx 0.414\kappa$  and  $\kappa_0 = \kappa(1 - \cos \theta_0)$ .

To obtain the spin 1/2 operator in the  $xy$ -plane one introduces new dark states:

$$|D'_1\rangle = \frac{1}{\sqrt{2}} (|D_1\rangle + i|D_2\rangle) e^{i\kappa_0 y}, \quad (5.14)$$

$$|D'_2\rangle = \frac{i}{\sqrt{2}} (|D_1\rangle - i|D_2\rangle) e^{i\kappa_0 y}. \quad (5.15)$$

The transformation from the old to the new two-component wave function is

$$\Psi' = \exp(-i\kappa_0 y) \exp\left(-i\frac{\pi}{4}\sigma_x\right) \Psi. \quad (5.16)$$

The exponential factor  $\exp(-i\kappa_0 y)$  leads to a shift in the origin of the momentum  $\mathbf{k} \rightarrow \mathbf{k} - \kappa_0 \mathbf{e}_y$ . The Hamiltonian of the new dark states has the vector potential  $\mathbf{A}' = -\hbar \kappa' \boldsymbol{\sigma}_\perp$ , where  $\boldsymbol{\sigma}_\perp = \mathbf{e}_x \sigma_x + \mathbf{e}_y \sigma_y$ . Finally, the equation of the atomic motion is

$$i\hbar \frac{\partial}{\partial t} \Psi' = \left[ \frac{1}{2m} (-i\hbar \nabla + \hbar \kappa' \boldsymbol{\sigma}_\perp)^2 + V_1 \right] \Psi'. \quad (5.17)$$

The vector potential governing the atomic motion is hence proportional to the spin operator  $\boldsymbol{\sigma}_\perp$ .

### 5.3 Dispersion relation

If the trapping potential in eq. (5.17) is constant, we can assume plane-wave solutions

$$\Psi'(\mathbf{r}, t) = \Psi_{\mathbf{k}} e^{i\mathbf{k} \cdot \mathbf{r} - i\omega_{\mathbf{k}} t}, \quad \Psi_{\mathbf{k}} = \begin{pmatrix} \Psi_{1\mathbf{k}} \\ \Psi_{2\mathbf{k}} \end{pmatrix}, \quad (5.18)$$

where  $\omega_{\mathbf{k}}$  is the eigen-frequency in the stationary Schrödinger equation  $H_{\mathbf{k}} \Psi_{\mathbf{k}} = \hbar \omega_{\mathbf{k}} \Psi_{\mathbf{k}}$ . The  $\mathbf{k}$ -dependent Hamiltonian is:

$$H_{\mathbf{k}} = \frac{\hbar^2}{2m} (\mathbf{k} + \kappa' \boldsymbol{\sigma}_\perp)^2 + V_1. \quad (5.19)$$

In the case of small wave-vectors ( $k \ll \kappa'$ ) this Hamiltonian reduces to the Hamiltonian for the 2D relativistic motion of a two-component massless particle of the Dirac type (Weyl equation) [Mag05],

$$H_{\mathbf{k}} = \hbar v_0 \mathbf{k} \cdot \boldsymbol{\sigma}_\perp + V_1 + m v_0^2. \quad (5.20)$$

The velocity  $v_0 = \hbar\kappa'/m$  of such quasi-relativistic particles is given by the recoil velocity corresponding to the wave-vector  $\kappa'$ , which is typically of the order of one centimeter per second.

The 2D chirality operator  $\sigma_{\mathbf{k}} = \mathbf{k} \cdot \boldsymbol{\sigma}_{\perp}/k$ , which commutes with the Hamiltonian  $H_{\mathbf{k}}$ , has the eigenstates

$$\Psi_{\mathbf{k}}^{\pm} = \frac{1}{\sqrt{2}} \begin{pmatrix} 1 \\ \pm \frac{k_x + ik_y}{k} \end{pmatrix}, \quad (5.21)$$

according to  $\sigma_{\mathbf{k}}\Psi_{\mathbf{k}}^{\pm} = \pm\Psi_{\mathbf{k}}^{\pm}$ . The chirality here is associated with the subspace of the dark states given by eqs. (5.14) and (5.15) instead of normal spin states. Note that one can also construct the Poincaré sphere associated with two dark states. The eigenstates (5.21) of the chirality operator are also the eigenstates of the Hamiltonian  $H_{\mathbf{k}}$  with eigenenergies  $\omega_{\mathbf{k}} \equiv \omega_{\mathbf{k}}^{\pm}$ . Assuming the atomic motion is restricted to the  $xy$ -plane, the dispersion relation is given by

$$\hbar\omega_{\mathbf{k}}^{\pm} = \hbar v_0(k^2/2\kappa' \pm k) + V_1 + mv_0^2, \quad (5.22)$$

see fig. 5.1 in which  $V_1 = -mv_0^2/2$ . If the direction  $\mathbf{k}/k$  is fixed, the dynamics in two different dispersion branches is described by different chirality. For small wave-vectors ( $k \ll \kappa'$ ) the dispersion reduces to

$$\hbar\omega_{\mathbf{k}}^{\pm} = \pm\hbar v_0 k + V_1 + mv_0^2, \quad (5.23)$$

where the upper (lower) sign corresponds to a linear cone with a positive (negative) group velocity,  $v_g^{\pm} = \pm v_0$ . Exactly the same dispersion governs the motion of electrons near the Fermi level in graphene [NGM<sup>+</sup>05, MF06, KNG06, GN07, NJZ<sup>+</sup>07].

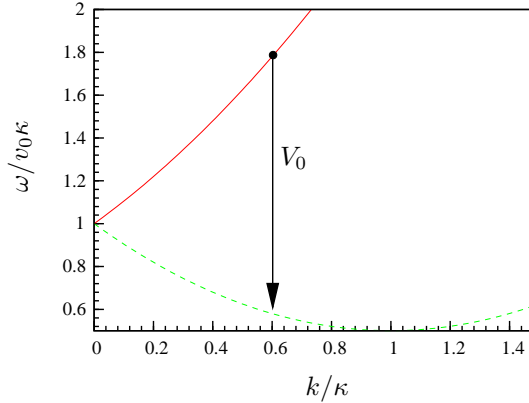


Fig. 5.1: Upper (red solid) and lower (green dashed) dispersion branches for a tripod atom in light fields. The arrow indicates the transition for the Veselago lens simulated in fig. 5.3 with the barrier height  $V_0$  as described in section 5.4.

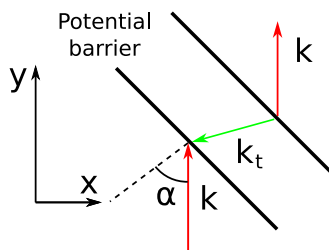


Fig. 5.2: Negative refraction of cold atoms at a potential barrier. The incoming and outgoing atoms are in the upper (red) dispersion branch, whereas the atoms inside the barrier are in the lower (green) one.

## 5.4 Veselago lensing

As a consequence of the constructed Hamiltonian (5.20), the quasi-relativistic atoms can show negative refraction at a potential barrier and thus exhibit focussing by Veselago-type lenses [Ves68, Pen00]. Consider incident atoms that are in the upper dispersion branch (see fig. 5.1) and propagate along the  $y$ -axis with a wave-vector  $\mathbf{k} = k\mathbf{e}_y$ . Let us place a potential barrier of a height  $2\hbar v_0 k$  at an angle of incidence  $\alpha$  (see fig. 5.2). Inside the barrier the atoms are transferred to the lower dispersion branch with  $\mathbf{k}_t = -k[\cos(2\alpha)\mathbf{e}_y + \sin(2\alpha)\mathbf{e}_x]$ . This would lead to the negative refraction of cold atoms at the barrier as shown in fig. 5.2. Thus the potential barrier can act as a flat lens which refocuses the atomic wavepacket.

As another example we demonstrate the simulation of a Veselago lens, see fig. 5.3. The wavepacket is prepared as a squeezed Gaussian, such that it will travel towards the barrier in a way that roughly resembles rays coming from a point source at  $(-70,0)$ . The wavepacket has an initial momentum of  $k = 0.6\kappa$  in the  $x$ -direction. The barrier has a height of  $V_0 = 2k = 1.2\kappa$ , see fig. 5.1. Therefore the main bulk of the wavepacket will experience a vertical transition in the dispersion relation and hence a refraction index of  $n = -1$ . Due to the finite width of the wavepacket in momentum space there is a tail of the wavepacket not matching exactly the vertical transition. This part of the wavepacket experiences transitions that are not exactly vertical in the dispersion relation and refract with an index  $n \neq -1$ .

In the simulation of our example with  $k = 0.6\kappa$  we observe a drastic slowing down of the wavepacket inside the lens. This is due to the reduced group velocity at  $k = 0.6\kappa$  while going from the upper to the lower branch (the ratio is  $\frac{v_+}{v_-} = \frac{k+1}{k-1} = \frac{1.6}{0.4} = 4$ ).

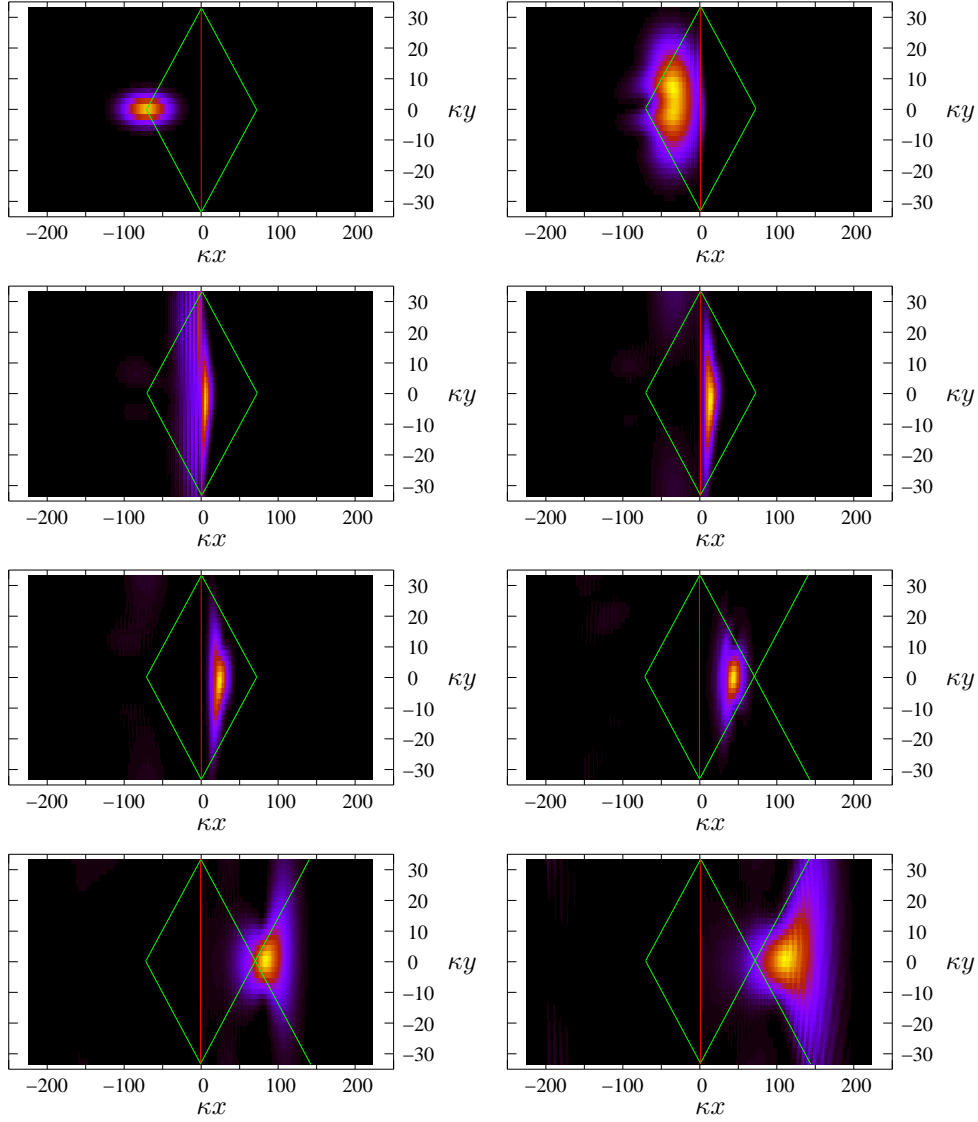


Fig. 5.3: Simulation of a Veselago lens. A gaussian atomic cloud initially centered at  $(-70,0)$  with a width  $\sigma_x = 25$ ,  $\sigma_y = 3.75$  and an initial momentum  $k = 0.6\kappa$  in the x-direction. For  $x > 0$  the potential barrier has a height of  $V_0 = 1.2\kappa$ . The plots are at  $t = 0, 1, 2, 3, 4, 6, 11$  and  $15$ .

## 5.5 Summary

In this chapter we have shown how the atomic motion can be equivalent to the dynamics of ultra-relativistic (massless) two-component Dirac fermions. As a result the ultracold atoms can experience negative refraction and focusing by Veselago-type lenses.



# Chapter 6

## Negative Reflection under Non-Abelian Gauge Fields

### 6.1 Introduction

Atomic mirrors, created by optical or magnetic potential barriers, play a crucial role in atom optics, i.e. in the manipulation of matter waves [Mey01]. Wave reflection at a mirror is typically specular, where the reflection angle equals the incidence one. However, richer reflection scenarios are also possible. For optical waves a double reflection appears in optically active media, such as in chiral liquids characterized by different refractive indices for left and right polarized light [Bar04]. This manifests itself as a tiny splitting of the reflected wave into two parts [GF06]. An additional striking example is Andreev reflection [And64, Bee06] in which an electron incident at the interface between a normal metal and a superconductor is reflected to a positively charged hole propagating backwards, where the missing charge of  $2e$  enters the superconductor as a Cooper pair.

In this chapter we analyze atom reflection in the presence of a non-Abelian vector potential proportional to a spin-1/2 operator produced by a relatively simple laser arrangement for tripod-scheme atoms. We show that the appearance of two different dispersion branches with positive or negative chirality leads to a double reflection at the mirror, an ordinary specular reflection, and an additional non-specular one. Remarkably, the latter can exhibit a negative reflection, resembling the Andreev reflection [And64, Bee06]. The negatively reflected wave becomes evanescent if the angle of incidence exceeds a critical value. These reflection properties could become crucial for the design of future non-Abelian atom optics devices, as e.g. non-Abelian atom interferometers.

### 6.2 Laser arrangement

In the following we consider an atom with a tripod electronic level scheme  $\{|0\rangle, |1\rangle, |2\rangle, |3\rangle\}$  (see chapter 2) under the influence of three stationary laser beams. Although elaborate laser configurations may allow for a wealth of possible gauge potentials in the tripod scheme, as shown in chapter 2, here we concentrate on a relatively simple laser setup providing non-Abelian potentials. The first two laser beams are assumed to counterpropagate with the same intensity along the  $x$ -axis,  $\Omega_1 = \Omega \sin \theta e^{-i\kappa_0 x}/\sqrt{2}$  and  $\Omega_2 = \Omega \sin \theta e^{i\kappa_0 x}/\sqrt{2}$ , and the third one propagating in the  $z$ -direction,  $\Omega_3 = \Omega \cos \theta e^{i\kappa_0 z}$  [JRL<sup>+</sup>08]. Here  $\kappa_0$  is the wave-number, and the mixing angle  $\theta$  characterizes the relative intensity of the third laser. A set of two dark

states is then given by

$$|D_1\rangle = \frac{1}{\sqrt{2}} (|\tilde{1}\rangle - |\tilde{2}\rangle) e^{-i\kappa'z}, \quad (6.1)$$

$$|D_2\rangle = \left[ \frac{1}{\sqrt{2}} \cos\theta (|\tilde{1}\rangle + |\tilde{2}\rangle) - \sin\theta |3\rangle \right] e^{-i\kappa'z}, \quad (6.2)$$

with  $\kappa' = \kappa_0(1 - \cos\theta)$ , where the modified atomic state-vectors  $|\tilde{1}\rangle = |1\rangle \exp[i\kappa_0(x+z)]$  and  $|\tilde{2}\rangle = |2\rangle \exp[-i\kappa_0(x-z)]$  accommodate the phases of the laser fields. An additional phase factor  $\exp(i\kappa'z)$  introduces a shift in the origin of the momentum  $\mathbf{k} \rightarrow \mathbf{k} + \kappa'\mathbf{e}_z$ . By imposing  $\cos\theta = \sqrt{2} - 1$ , the vector potential becomes  $\mathbf{A} = -\hbar\kappa\boldsymbol{\sigma}_\perp$ , where  $\boldsymbol{\sigma}_\perp = \mathbf{e}_x\sigma_x + \mathbf{e}_z\sigma_z$  is the operator of spin 1/2 in the  $xz$ -plane, and  $\kappa = \kappa_0 \cos\theta \approx 0.414\kappa_0$ . The Cartesian components  $A_x$  and  $A_z$  are proportional to the Pauli matrices  $\sigma_x$  and  $\sigma_z$  which do not commute, so the vector potential  $\mathbf{A}$  is non-Abelian.

Furthermore we take the trapping potentials  $V_1 = V_2$  and  $V_3 - V_1 = \hbar^2\kappa_0^2 \sin^2\theta/2M$ . This can be achieved by detuning properly the third laser from the two-photon resonance. Hence the overall trapping potential  $V + \Phi$  becomes proportional to the unit matrix, both dark states being affected by the same potential  $V_1 \equiv V_1(\mathbf{r})$ , giving

$$H = \frac{1}{2M} (-i\hbar\nabla + \hbar\kappa\boldsymbol{\sigma}_\perp)^2 + V_1(\mathbf{r}). \quad (6.3)$$

### 6.3 Dispersion law

We shall consider a two dimensional case where the atomic motion is confined to the  $xz$ -plane. If the trapping potential  $V_1$  is constant, the eigenfunctions of the Hamiltonian (6.3) are the plane waves

$$\Psi_{\mathbf{k}}^\pm(\mathbf{r}) = g_{\mathbf{k}}^\pm e^{i\mathbf{k}\cdot\mathbf{r}}, \quad g_{\mathbf{k}}^\pm = \frac{1}{2} \begin{pmatrix} 1 \mp ie^{i\varphi_{\mathbf{k}}} \\ -i \pm e^{i\varphi_{\mathbf{k}}} \end{pmatrix}, \quad (6.4)$$

where  $\varphi_{\mathbf{k}}$  is the angle between the atomic wave-vector  $\mathbf{k}$  and the  $x$ -axis. The two-component spinors  $g_{\mathbf{k}}^\pm$  are eigenfunctions of the chirality operator  $\sigma_{\mathbf{k}} = \boldsymbol{\sigma} \cdot \mathbf{k}/k$  representing a spin along the atomic motion,  $\sigma_{\mathbf{k}} g_{\mathbf{k}}^\pm = \pm g_{\mathbf{k}}^\pm$ . It should be emphasized that the chirality is here associated with the subspace of two dark states rather than with the spin in the usual sense.

The corresponding eigenenergies of the Hamiltonian (6.3) are isotropic,  $\hbar\omega_{\mathbf{k}}^\pm \equiv \hbar\omega_k^\pm$ , with

$$\hbar\omega_k^\pm = \frac{\hbar^2}{2M} (k \pm \kappa)^2 + \hbar\omega_0 + V_1, \quad (6.5)$$

where  $\omega_0 = \hbar\kappa^2/2M$  is the recoil frequency. The relative dispersion  $\omega_k^\pm/\omega_0$  is plotted in fig. 6.1 for  $V_1 = -\hbar\omega_0$ . The upper (lower) dispersion branch is characterized by a positive (negative) chirality. For small wave-numbers  $k \ll \kappa$  the dispersion is linear,  $\omega_k^\pm \sim \pm k$ , so the atoms behave like ultra-relativistic Dirac fermions [JRL<sup>+</sup>08] similar to electrons in graphene [GN07, NGM<sup>+</sup>05]. For larger wave-numbers each  $k = k_1 < 2\kappa$  has a counterpart,  $k_2 = 2\kappa - k$ , characterized by the same eigen-frequency  $\hbar\omega_{k_2}^- = \hbar\omega_{k_1}^-$  and opposite slope in the lower dispersion branch (a similar kind of dispersion appears for optical waves in a medium with a single chiral resonance considered by [Pen04], as one can see comparing our figure 6.1 with the figure 2c by Pendry [Pen04]). As shown in the following sections, this leads to unusual reflection properties.



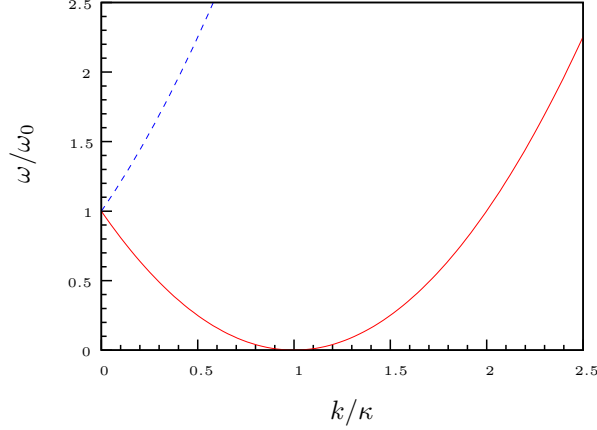


Fig. 6.1: Upper (blue dashed) and lower (red solid) dispersion branch for tripod atoms in our light fields.

## 6.4 Double and negative reflection of atoms

The incident atoms are assumed to be in the lower dispersion branch with a wave-vector  $\mathbf{k} = k\mathbf{e}_z$ . This can be achieved using the following procedure. Initially all three lasers are off. The atom is in the internal state  $|3\rangle$  and its center of mass motion is characterized by a wave-vector  $\mathbf{k}_{\text{in}} = \mathbf{k} - \kappa'\mathbf{e}_z$ , i.e.  $|\Phi\rangle = |3\rangle \exp(i\mathbf{k}_{\text{in}} \cdot \mathbf{r})$  (the cold atoms can be set in motion using various techniques, e.g. by means of a two-photon scattering which induces a recoil momentum  $\hbar\mathbf{k}_{\text{in}} = \hbar\mathbf{k}_{2\text{phot}}$  to the atoms, where  $\mathbf{k}_{2\text{phot}}$  is the wave-vector of the two-photon mismatch, see e.g. [DHW<sup>+</sup>99]). Subsequently the lasers 1 and 2 are switched on first followed by the laser 3, so that initially the atomic internal state coincides with the second dark state,  $|3\rangle = |D_2\rangle \exp(i\kappa'z)$ . If the lasers are switched on sufficiently slowly, the atom remains in the dark state  $|D_2\rangle$ , and the lasers prepare the atom in the state  $|\Phi\rangle = i|D_2\rangle \exp(i\mathbf{k} \cdot \mathbf{r})$ . By taking  $\mathbf{k} = k\mathbf{e}_z$ , the corresponding multi-component wave-function  $\Psi_{\mathbf{k}}^-(\mathbf{r})$  is in the lower dispersion branch with a negative chirality as required. The atoms prepared in this way will propagate along the  $z$  axis for  $k > \kappa$  or opposite to it for  $k < \kappa$ . Note that the duration of the switching-on should be short enough to avoid any atomic motion at this stage.

The atoms are impinging on an infinitely high potential barrier at an angle of incidence  $\alpha$ . We shall take  $k < 2\kappa$ , so that both reflected waves  $\Psi_{\mathbf{k}_1}^-$  and  $\Psi_{\mathbf{k}_2}^-$  remain in the lower dispersion branch with wave-numbers  $k_1 = k$  and  $k_2 = 2\kappa - k$ . Fig. 6.3 show the case of an incident wave with  $\kappa < k < 2\kappa$ . Here the group velocity  $v_k^- = \partial\omega_k^-/\partial k$  is positive, so the wave-vectors of the incident and second reflected waves point inwards to the surface, whereas the wave-vector of the first reflected wave points outwards from the surface. Since  $v_k^- = v_{k_1}^- = -v_{k_2}^-$ , the forward propagation of the incident wave and backward propagation of the reflected ones are ensured. Fig. 6.2 illustrates a situation where  $0 < k < \kappa$ . Here the group velocity  $v_k^-$  is negative and hence the wave-vectors are reversed.

We will first discuss the case where  $0 < k < \kappa$ . In front of the barrier the solution to the stationary Schrödinger equation  $(H - \hbar\omega_k^-)\Psi = 0$  is a linear superposition of the incident wave

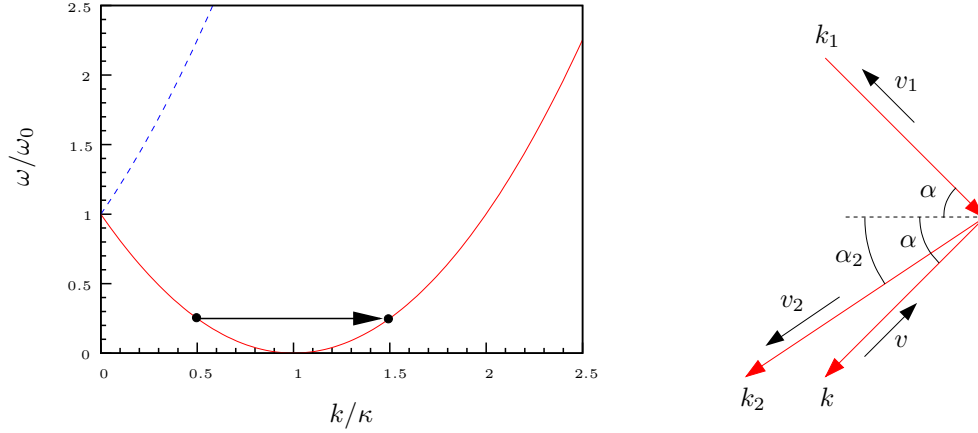


Fig. 6.2: Reflection of atoms with negative chirality for  $0 < k < \kappa$ . The incoming wavepacket is located on the left side of the lower dispersion branch (e.g. at  $k/\kappa = 0.5$ ). At the mirror the wavepacket is split. A part of it stays at  $k_1 = k$ , the other part is transferred to the right side of the lower dispersion branch to  $k_2 = 2\kappa - k$  (e.g. to  $k/\kappa = 1.5$ ).

and two reflected waves:

$$\Psi = \Psi_{\mathbf{k}}^- + r_1 \Psi_{\mathbf{k}_1}^- + r_2 \Psi_{\mathbf{k}_2}^- . \quad (6.6)$$

The wave-vector is conserved along the reflection plane,  $k_{\parallel} = k_{1\parallel} = k_{2\parallel}$ , so the first wave exhibits an ordinary reflection with the reflection angle equal to the angle of incidence,  $\alpha_1 = \alpha$ . The second wave is characterized by the opposite group velocity  $v_{k_2}^- = -v_{\mathbf{k}}^- = -v_{k_1}^-$ , and hence it experiences a *negative reflection* at an angle

$$\alpha_2 = \arcsin \left( \frac{k}{k_2} \sin \alpha \right) . \quad (6.7)$$

The reflection coefficients  $r_1$  and  $r_2$  are determined using Eqs. (6.4) and (6.6) together with the boundary condition at the potential barrier  $\Psi|_{\text{barrier}} = 0$ , giving

$$r_1 = \frac{e^{i\alpha} - e^{i\alpha_2}}{e^{-i\alpha} + e^{i\alpha_2}} , \quad r_2 = -1 - r_1 . \quad (6.8)$$

The corresponding reflection probabilities are

$$P_1 = |r_1|^2 , \quad P_2 = \frac{\cos \alpha_2}{\cos \alpha} |r_2|^2 , \quad (6.9)$$

with  $P_1 + P_2 = 1$ , where the weight factor  $\cos \alpha_2 / \cos \alpha$  appears when calculating the flow of atoms in and out of the surface for the incident and reflected waves. The probabilities  $P_1$  and  $P_2$  plotted in Figure 6.4 depend both on the angle of incidence  $\alpha$  and also on the wave-number  $k$ . For small angles,  $\alpha \ll 1$ , there is predominantly a negative reflection to the second branch,  $|P_1| \ll 1$  and  $|P_2| \approx 1$ . For large angles of incidence ( $\alpha \rightarrow \pi/2$ ) and  $0 < k < \kappa$  we have mostly a specular reflection to the first branch,  $|P_2| \ll 1$  and  $|P_1| \approx 1$ .

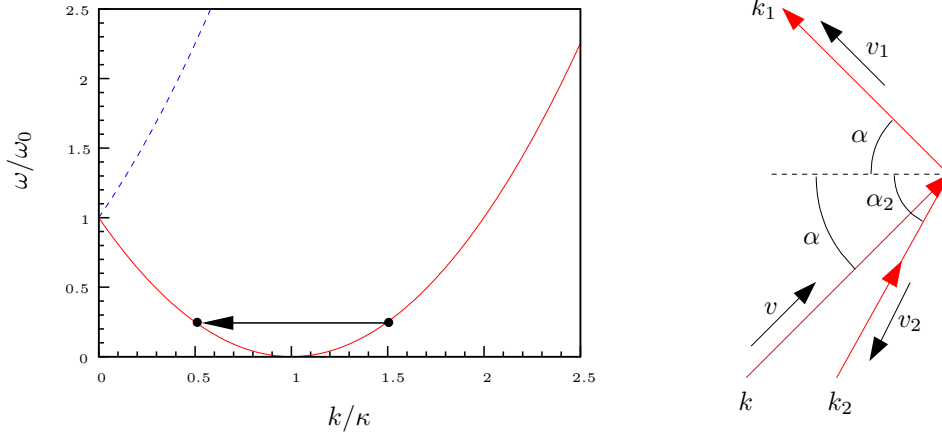


Fig. 6.3: Reflection of atoms with negative chirality for  $\kappa < k < 2\kappa$ . The incoming wavepacket is located on the right side of the lower dispersion branch (e.g. at  $k/\kappa = 1.5$ ). At the mirror the wavepacket is split. A part of it stays at  $k_1 = k$ , the other part is transferred to the left side of the lower dispersion branch to  $k_2 = 2\kappa - k$  (e.g. to  $k/\kappa = 0.5$ ).

If  $\kappa < k < 2\kappa$ , the situation is more complex. In this case the second reflected wave becomes evanescent when the angle of incidence  $\alpha$  exceeds a critical value given by  $\sin \alpha_{\text{crit}} = k_2/k$ , i.e. for  $k_{\parallel} = k_{2\parallel} > k_2$ . Consequently the out-of-plane projection of the wave-vector  $\mathbf{k}_2$  becomes imaginary,  $k_{2\perp} = -iq$ , with  $q = \sqrt{k_{\parallel}^2 - k_2^2}$ . In the region where  $x < 0$  we can once again use eq. (6.6) in which  $\Psi_{\mathbf{k}_2}^-$  is now an evanescent wave. The boundary condition at the potential barrier gives the reflection coefficient

$$r_1 = \frac{e^{i\alpha} \sqrt{k_{\parallel} + q} - i\sqrt{k_{\parallel} - q}}{e^{-i\alpha} \sqrt{k_{\parallel} + q} + i\sqrt{k_{\parallel} - q}}, \quad (6.10)$$

with  $|r_1| = 1$ . Thus, there is a total reflection to the first mode at an angle  $\alpha_1 = \alpha$  accompanied by a phase shift, with the second reflected wave being evanescent. The phenomenon resembles the total internal reflection of optical waves at an interface with an optically thinner medium. In our situation, however, the evanescent wave is the reflected wave rather than the refracted one.

Our plane-wave analysis may be easily extended to the case of wavepacket reflection. Similar results may be found if the momentum width of the wavepacket  $\Delta k$  is sufficiently small with respect to  $\kappa$ . Fig. 6.5 displays the double and negative reflection of atomic wavepackets from an atomic mirror, for an incident wavepacket  $\Psi(\mathbf{r}) = g_{\mathbf{k}}^- e^{i\mathbf{k}\cdot\mathbf{r}} f(r)$ , with  $f(r)$  a Gaussian, and  $\bar{\mathbf{k}}$  the central wavenumber. The propagation direction and population of each of the reflected wavepackets are in good agreement with the analytical plane-wave results (6.7)-(6.9). Similar results are also found for more realistic Gaussian or evanescent atomic mirrors, as long as the potential barrier is sufficiently high compared to the incident kinetic energy.

Let us now consider finitely high potentials and smooth barriers. For small barriers, where the potential height is small compared to the energy of the wavepacket considered, we expect

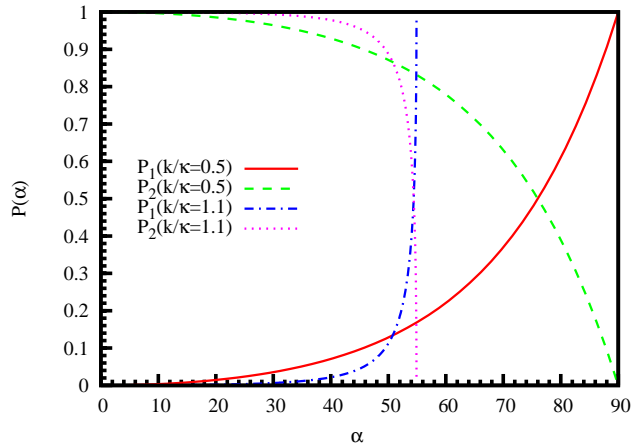


Fig. 6.4: Reflection probabilities  $P_1$  and  $P_2$  for  $k/\kappa = 0.5$  and  $k/\kappa = 1.1$  versus angle of incidence  $\alpha$  (in degrees).

transmission and tunneling. Let us have a look at the intermediate case, where the maximum height of the barrier is bigger than the energy of the wavepacket. We consider a smooth barrier around position  $x_p = 50$ , with maximum barrier height  $V_0 = 0.8$  (around twice the energy of the wavepacket prepared at  $k = 0.5\kappa$  and  $k = 1.5\kappa$ , see fig. 6.6), i.e.

$$V(x) = \frac{V_0}{2} (\tanh(s(x - x_p)) + 1), \quad (6.11)$$

where  $s$  determines the smoothness of the barrier, the smaller  $s$  the wider the transition region, see fig. 6.7 for examples.

For the numerical simulations we assume again that the wavefunction in momentum space is initially a Gaussian around  $(k_x^0, k_y^0)$  with  $k = 1.5\kappa$  (or  $0.5\kappa$ ) and with width  $\sigma_x = 10$ . For an infinitely high barrier a part of the wavefunction will transfer directly to  $k = 0.5\kappa$  (or  $1.5\kappa$ ), as described before. Also for the smooth barrier in fig. 6.7 ( $s = 3$ ) the wavepacket still undergoes double reflection without change. But for the very smooth barrier (having a transition region of the order of the wavepacket size  $\sigma_x = 10$ ) in fig. 6.7 ( $s = 0.03$ ) the wavepacket will undergo only negative reflection, see fig. 6.8. In momentum space one can observe that the wavepacket will move continuously from  $k = 1.5\kappa$  to  $k = 0.5\kappa$ . This can be explained in the following way: the wavepacket sees (theoretically infinitesimally small, infinitely many) small potential steps. At these small steps it will gain potential energy. Due to energy conservation it will lose kinetic energy and the kinetic energy will hence follow the dispersion relation continuously.

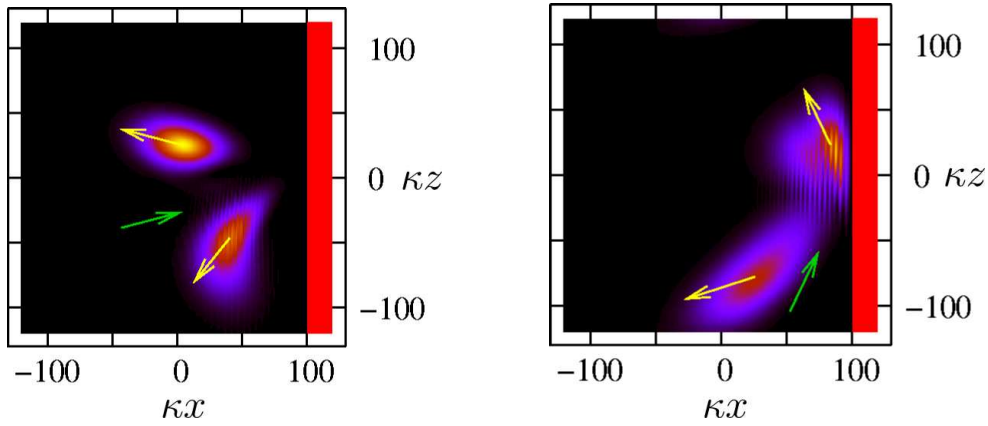


Fig. 6.5: Reflection of an atomic wavepacket with a negative chirality for  $\alpha = 15^\circ$ ,  $k = 1.5\kappa$  (left) and  $\alpha = 65^\circ$ ,  $k = 0.5\kappa$  (right). The incident wavepacket is taken to be Gaussian with momentum width  $\Delta k = 0.1\kappa$ . An additional green arrow indicates the incident direction.

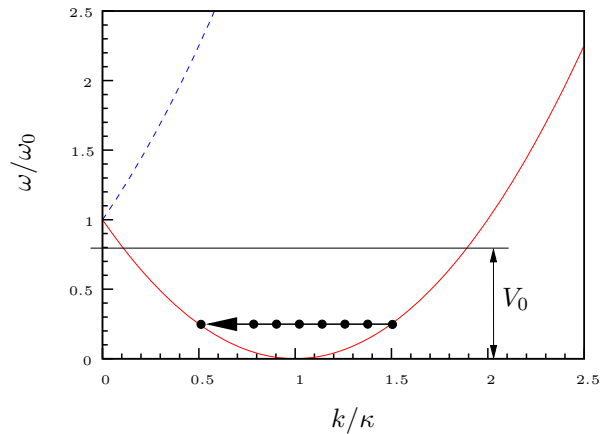


Fig. 6.6: Smooth and sharp barriers imply different reflection behaviour which can be outlined in the dispersion relation. Assume we start with a wavepacket on the right side of the lower branch at  $k/\kappa = 1.5$  and choose the height of the potential barrier  $V_0 = 0.8$  more than twice as high. For an infinitely sharp barrier a part of the wavefunction will directly transfer to the left side, i.e. to  $k/\kappa = 0.5$ , giving the negative dispersion branch. For a smooth barrier the kinetic energy of the wavepacket has to move along the lower dispersion relation and all population is transferred continuously to the negative reflection branch.

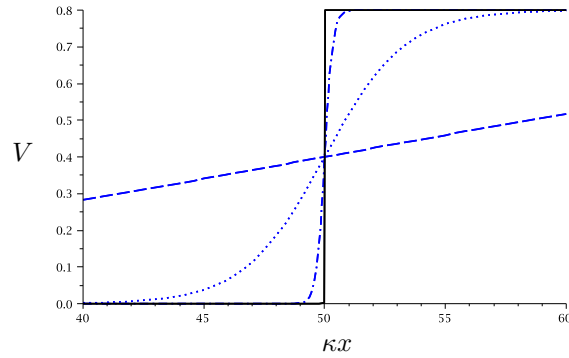


Fig. 6.7: Tanh-barrier  $V(x) = V_0 (\tanh(s(x - x_p)) + 1)/2$ . If the transition region of the reflection potential is relatively narrow ( $s = 3$ , dashed-dotted line) compared to the wavepacket width  $\sigma_x = 10$  we obtain the usual double reflection. The smoother barrier ( $s = 0.3$ , dotted line) leads to mainly negative reflection, whereas for the very smooth barrier ( $s = 0.03$ , dashed line) only negative reflection is observed, as shown in fig. 6.8.

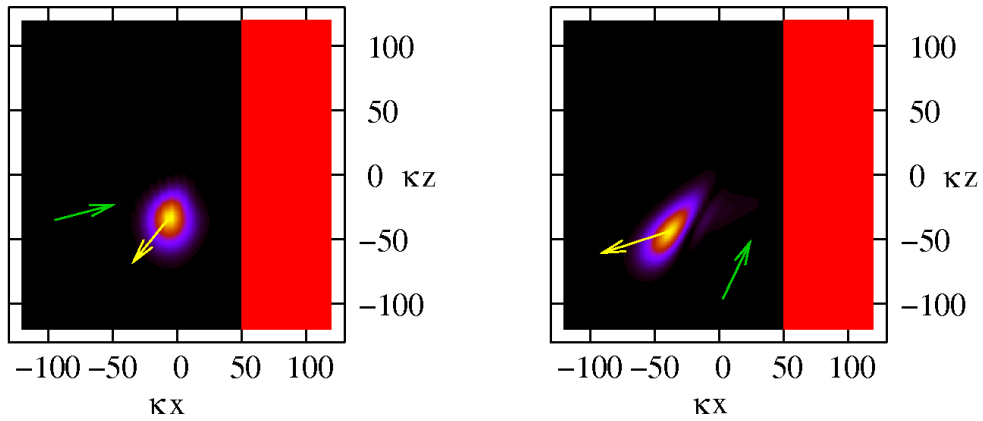


Fig. 6.8: Reflection of an atomic wavepacket with a negative chirality on a smooth barrier for  $\alpha = 15^\circ$ ,  $k = 1.5\kappa$  (left) and  $\alpha = 65^\circ$ ,  $k = 0.5\kappa$  (right). The incident wavepacket is taken to be Gaussian with momentum width  $\Delta k = 0.1\kappa$ . An additional green arrow indicates the incident direction.

## 6.5 Summary

Summarizing, the reflection of atoms under a non-Abelian gauge potential presents unusual features. In particular, one can have a double reflection comprising a specular and a non-specular one. Remarkably, the latter wave shows negative reflection due to the special properties of the dispersion law, and becomes evanescent for sufficiently large incident angles. Atom mirrors are a key tool in atom optics. Hence, the anomalous reflection properties may be of crucial importance for the design of non-Abelian atom optics elements, e.g. atom interferometers which exploit the non-Abelian Aharonov-Bohm effect.





# Chapter 7

## Trapped and Interacting Bose Gases in Non-Abelian Gauge Fields

In the previous chapters we have mainly considered the case of a non-interacting untrapped cold atomic cloud under the influence of non-Abelian gauge fields. In the prior discussion we have considered neither the effects of trapping nor the phenomenon of Bose-Einstein condensation, and we have neglected interactions. This final chapter is devoted to these issues and constitutes mainly an outlook at interesting future directions.

### 7.1 Trapped gas in the presence of a “simple” non-Abelian gauge: Single branch case

In chapter 5 we have first introduced the simple non-Abelian gauge  $A = \hbar\kappa\hat{\sigma}_\perp$ , with  $\sigma_\perp = (\sigma_x, \sigma_y)$ . In this section we would like to discuss in some detail the scenario in which a 2D atomic cloud in the presence of this non-Abelian gauge is confined in an optical trap. All components of the ground-manifold of the tripod scheme are assumed to experience the same harmonic trapping potential, which for simplicity of the discussion is considered as isotropic (with frequency  $\omega$ ). The Hamiltonian is then of the form:

$$\hat{H} = \frac{1}{2M}(\hat{\mathbf{p}} - \hbar\kappa\hat{\sigma}_\perp)^2 + \frac{1}{2}M\omega^2 r^2. \quad (7.1)$$

We may express this Hamiltonian more conveniently in the momentum representation:

$$\hat{H} = -\frac{\hbar^2}{2}M\omega^2\nabla_p^2 + \frac{1}{2M}(\hat{\mathbf{p}} - \hbar\kappa\hat{\sigma}_\perp)^2. \quad (7.2)$$

As we already know, the eigenenergies (in absence of a trap) present the dispersion branches  $E_\pm(p) = (|p| \pm \hbar\kappa)^2/2M$ . The eigenvectors are of the form  $\xi_\pm^T = (\exp(-i\phi/2), \pm \exp(i\phi/2))/\sqrt{2}$ . In the following we consider the situation in which only momenta close to the dispersion minimum of the  $E_-$  branch are relevant. Assuming that no other energy is high enough to enable population transfer from the  $E_-$  to the  $E_+$  branch, we can restrict our discussion to the lowest branch. The case in which this approximation is violated will be treated in the next section.

Adiabatically eliminating the upper branch, we obtain the effective Hamiltonian for the lowest branch:

$$\hat{H}_- = -\frac{\hbar^2}{2}M\omega^2\left(\nabla_p^2 + \frac{1}{4p^2}\right) + \frac{1}{2M}(p - \hbar\kappa)^2. \quad (7.3)$$

Note that the single-branch approximation must be taken with some care. In particular, the extra factor  $1/4p^2$  in eq. (7.3) results from the angular dependence of the eigenvectors. Let  $\boldsymbol{\rho} = \mathbf{p}/(\hbar l_{\text{HO}})$ ,  $\rho_0 = \kappa l_{\text{HO}}$ , with  $l_{\text{HO}} = \sqrt{\hbar/(m\omega)}$ , and  $\hat{H} \equiv \hat{H}_-/\hbar\omega$ . Hence, we obtain the dimensionless Hamiltonian

$$\hat{H} = -\frac{1}{2}\nabla^2 + \frac{1}{2}(\rho - \rho_0)^2 + \frac{1}{8\rho^2}. \quad (7.4)$$

This is actually the Hamiltonian for a particle moving in a *Mexican-hat* potential centered at  $\rho = \rho_0$  (with an additional repulsive potential  $1/8\rho^2$ ). We shall assume that  $\rho_0 \gg 1$ , i.e.  $\kappa l_{\text{HO}} \gg 1$ , which in turn implies that  $\hbar^2\kappa^2/2M \gg \hbar\omega$  (fully consistent with our assumption that only the lowest branch is to be considered). The eigenstate of  $\hat{H}$  are of the form

$$\Psi_m(\mathbf{r}) \propto e^{im\phi} \frac{\varphi_m(\rho)}{\sqrt{\rho}}, \quad (7.5)$$

such that

$$E_m\varphi_m = -\frac{1}{2}\frac{d^2}{d\rho^2}\varphi_m + \left[\frac{1}{2}(\rho - \rho_0)^2 + \frac{m^2}{2\rho^2}\right]\varphi_m. \quad (7.6)$$

Since  $\rho_0 \gg 1$ , we may use for  $m^2 \ll \rho_0^2$  the approximation

$$\left[E_m - \frac{m^2}{2\rho_0^2}\right]\varphi_m = -\frac{1}{2}\frac{d^2}{d\rho^2}\varphi_m + \frac{1}{2}(\rho - \rho_0)^2\varphi_m. \quad (7.7)$$

The rhs of the previous equation is a 1D harmonic oscillator centered at  $\rho_0$ , and hence the problem may be easily solved in terms of the harmonic oscillator levels and eigenfunctions. Restoring the original units we obtain then the eigenenergies:

$$\frac{E_{n,m}}{\hbar\omega} = n + \frac{1}{2} + \frac{m^2}{(2\kappa l_{\text{HO}})^2} \quad (7.8)$$

and the corresponding (unnormalized) eigen-spinor

$$\boldsymbol{\Psi}_{n,m}(\mathbf{k}) = e^{im\phi} \frac{1}{\sqrt{\kappa l_{\text{HO}}}} e^{-(k-\kappa)^2 l_{\text{HO}}^2/2} H_n((k-\kappa)l_{\text{HO}}) \boldsymbol{\xi}_-(\phi). \quad (7.9)$$

We recall that these expressions are just valid for momenta  $\kappa l_{\text{HO}} \gg 1$ . Note that due to the  $\phi$ -dependence of the spinors, the wavefunctions are uniquely determined only if  $m \pm 1/2 = \tilde{m}$  is an integer. Hence  $m = \tilde{m} \mp 1/2$ .

We may already notice a rather important fact at this stage: Let us consider an ideal gas of  $N$  bosons under the above mentioned conditions. Note that in the thermodynamic limit  $N \rightarrow \infty$ ,  $\omega \rightarrow 0$ , but  $N\omega^2$  remains finite. It is clear that in the thermodynamic limit  $l_{\text{HO}} \rightarrow \infty$ , and hence  $E_{n,m}/\hbar\omega \rightarrow n + 1/2$ . The spectrum hence reduces to an  $m$ -fold degenerate 1D harmonic oscillator. Obviously, strict condensation into the lowest eigenstate  $(n, m) = (0, \pm 1/2)$  is then precluded due to the divergence in the occupation of the  $(n, \pm 1/2) \neq (0, 0)$  states in the thermodynamic limit. The absence of condensation has been discussed recently by Stanescu and collaborators [SAG08].

In a finite-size trap the situation is different, and at least quasi-condensation may be achieved. The lowest eigenstate is in principle a linear combination of  $\boldsymbol{\Psi}_{n,1/2}(\mathbf{k})$  and  $\boldsymbol{\Psi}_{0,-1/2}(\mathbf{k})$ , and

hence the system shows an  $SU(2)$  symmetry in addition to the usual  $U(1)$  symmetry of scalar BECs. The  $SU(2)$  symmetry is the result of the degeneracy of the dark states and is either spontaneously broken or broken by slight deviations from degeneracy. In the following we consider that the system at zero temperature condenses into the (unnormalized) spinor

$$\Psi_{0,1/2}(\mathbf{k})^T = \frac{1}{\sqrt{k}} e^{-(k-\kappa)^2/2} (1, -e^{i\phi}) \equiv \psi(k) (1, -e^{i\phi}), \quad (7.10)$$

where we have introduced again the oscillator units. We may then Fourier transform to obtain the condensate wavefunction in real space in both components  $D1$  and  $D2$

$$\psi_{D1}(\mathbf{r}) = \int d^2k \psi(k) e^{i\mathbf{k}\cdot\mathbf{r}} \propto \int_0^\infty dk \sqrt{k} J_0(kr) e^{-(k-\kappa)^2/2}, \quad (7.11)$$

and similarly

$$\psi_{D2}(\mathbf{r}) = e^{i\alpha} \int_0^\infty dk \sqrt{k} J_1(kr) e^{-(k-\kappa)^2/2}, \quad (7.12)$$

where  $\alpha$  is the polar angle in real space. In fig. 7.1 we depict the corresponding density profile for  $\kappa = 6$ . Remarkably, an ideal 2D BEC in an isotropic trap with a dispersion law provided by the lowest branch  $E_-$  shows a density profile characterized by the appearance of concentric rings for  $D1$  and  $D2$ . Note that  $D1$  and  $D2$  show a different dependence, since  $D2$  shows a zero at the trap center  $(x, y) = (0, 0)$  (due to the  $J_1$  dependence above), whereas  $D1$  shows a maximum in the center. Furthermore, if the  $SU(2)$  symmetry mentioned above is spontaneously broken the imaging of the densities of  $D1$  and  $D2$  may give in general a large fluctuation from shot to shot, since the general situation would randomly interpolate between the profiles shown in the figure. In the next section we shall show that a full calculation taking into account all branches converges nicely to this result for large  $\kappa$ .

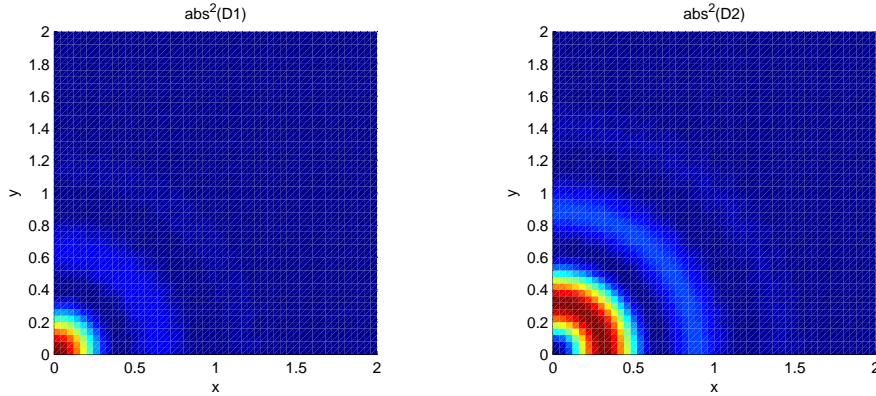


Fig. 7.1: Density of the condensate wavefunction in real space for  $\kappa = 6$ .  $D1$  (left, cf. eq. (7.11)) shows a maximum at the trap center and  $D2$  (right, cf. eq. (7.12)) is zero at the center of the trap.

## 7.2 Trapped gas in the presence of a “simple” non-Abelian gauge: Two branch case

In the previous section we considered the case in which the additional gauge potential was sufficient to reduce the discussion to the lowest branch  $E_-$ . However, this is generally not the case. In this section we discuss the situation in which both branches must be considered, i.e. full spinor character of the wavefunctions must be taken into account. We consider as in the previous section a two-dimensional system with the simple constant non-Abelian gauge  $\hbar^2\kappa\sigma_\perp$  and an additional isotropic harmonic trapping:

$$\hat{H} = \frac{1}{2m} [-i\hbar\nabla - \hbar\kappa\hat{\sigma}_\perp]^2 + \frac{1}{2}m\omega^2\rho^2. \quad (7.13)$$

In sec. 7.1 we reduced  $\hat{H}$  to the lowest dispersion branch, and hence the problem could be reduced to an equivalent Hamiltonian in momentum space. If this cannot be done, in particular because the gauge potential is not strong enough with respect to the trapping potential, we must proceed in a different way. Except for a constant energy  $\hbar\kappa^2/2M$  we may write the Hamiltonian in the form

$$\hat{H} = \hat{H}_{\text{HO}} + \frac{i\hbar^2}{M}\kappa\hat{\sigma}_\perp \cdot \nabla, \quad (7.14)$$

where  $\sigma_\perp = (\sigma_x, \sigma_y)$ , and  $\hat{H}_{\text{HO}}$  is the Hamiltonian of the 2D harmonic oscillator. We may then employ the basis of eigenstates of the Harmonic oscillator  $|\mathbf{n}, \alpha\rangle$ , where  $\mathbf{n} = \{n_x, n_y\}$  denotes the eigenstates of the harmonic oscillator, and  $\alpha = 1, 2$  denotes the internal spinor state. Using oscillator units  $\hat{H} \equiv \hat{H}/\hbar\omega$ ,  $\kappa \equiv \kappa l_{\text{HO}}$ , and  $x \equiv x/l_{\text{HO}}$ , the matrix elements of the Hamiltonian in the oscillator basis are of the form:

$$\langle \mathbf{n}, \alpha | \hat{H} | \mathbf{n}', \beta \rangle = (n_x + n_y + 1) \delta_{\mathbf{n}, \mathbf{n}'} \delta_{\alpha, \beta} + i\kappa \langle \mathbf{n}, \alpha | \sigma_x \partial_x + \sigma_y \partial_y | \mathbf{n}', \beta \rangle. \quad (7.15)$$

The second term at the rhs of eq. 7.15 is zero if  $\alpha = \beta$ . Employing the well-known relation  $\partial_x = (\hat{a} - \hat{a}^\dagger)/\sqrt{2}l_{\text{HO}}$  (with  $\hat{a}$  the ladder operator of the  $x$ -harmonic oscillator), we may obtain the form of the off-diagonal terms:

$$\begin{aligned} \frac{\langle \mathbf{n}, \{1, 2\} | \hat{H} | \mathbf{n}', \{2, 1\} \rangle}{i\kappa} &= \frac{\delta_{n_y, n'_y}}{\sqrt{2}} \left[ \sqrt{n'_x} \delta_{n_x, n'_x-1} - \sqrt{n'_x+1} \delta_{n_x, n'_x+1} \right] \\ &\mp i \frac{\delta_{n_x, n'_x}}{\sqrt{2}} \left[ \sqrt{n'_y} \delta_{n_y, n'_y-1} - \sqrt{n'_y+1} \delta_{n_y, n'_y+1} \right]. \end{aligned} \quad (7.16)$$

We then obtain the eigenstates of the Hamiltonian after diagonalizing the previous matrix. The results are shown in figs. 7.2 - 7.4 for different values of  $\kappa = 0.2, 1.0$ , and  $6.0$ . The comparison of the figure with  $\kappa = 6$  and that obtained for the same value of  $\kappa$  in the single-branch approximation show an excellent agreement.

## 7.3 Interaction Hamiltonian in the tripod system

Up to this point of the thesis we did not consider the effects of the interparticle interactions. In this section we introduce short-range interactions in the tripod scheme. Since the ground-state

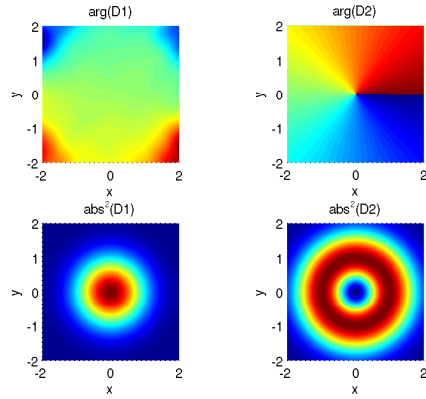


Fig. 7.2: Phase and density for the condensate wavefunction D1 (left) and D2 (right) for  $\kappa = 0.2$

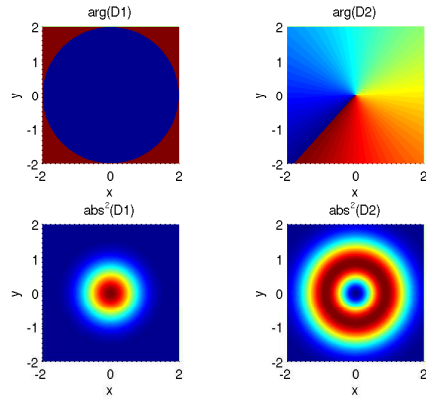


Fig. 7.3: Phase and density for the condensate wavefunction D1 (left) and D2 (right) for  $\kappa = 1$

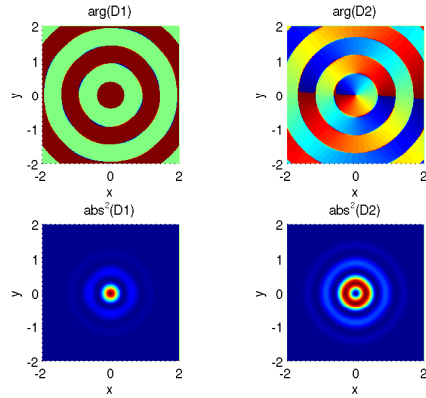


Fig. 7.4: Phase and density for the condensate wavefunction D1 (left) and D2 (right) for  $\kappa = 6$

of the tripod scheme is a spin-1 system, we consider in the following first the general theory for the short-range interactions of a spinor system in the manifold of the three ground states of the tripod system. We shall then project into the dark state basis and assume that the interparticle interactions do not mix the dark states and the bright state. The latter demands of course sufficiently large laser intensities. First we present the general case (with different scattering lengths for the different interaction channels) and then obtain a simplified interaction Hamiltonian for the case of equal scattering lengths in all interaction channels.

In the following we restrict our discussion to the case of bosons with spin-1 (lowest three states of the tripod system). We do not consider interactions with the upper state of the tripod, since, as always, we assume a very low population of the excited state. By symmetry arguments,  $s$ -wave scattering (the only scattering relevant at low energies) is just possible between two identical bosons for colliding pairs with even total angular momentum. For spin-1 bosons this restricts the interactions to a total spin  $S = 0$  and  $S = 2$  (we denote the spin as  $S$  although it must be understood as the composition of the individual hyperfine momenta). The interaction Hamiltonian is then of the form

$$\hat{H}_{SR} = \frac{1}{2} \int d^3r \sum_{S=0,2} g_S P_S(r), \quad (7.17)$$

where  $g_S = 4\pi\hbar^2 a_S/m$  is the interaction strength, with  $a_S$  the  $s$ -wave scattering length in the  $S$  channel, and  $P_S(r)$  is the projection onto the subspace with total spin  $S = 0, 2$ :

$$P_S(r) = \sum_{M=-S}^S A_{SM}^\dagger(r) A_{SM}(r), \quad (7.18)$$

with

$$A_{SM}(r) = \sum_{m_1=-1}^1 \sum_{m_2=-1}^1 \langle S, M | 1, m_1; 1, m_2 \rangle \hat{\Psi}_{m_1}(r) \hat{\Psi}_{m_2}(r). \quad (7.19)$$

In the previous expression we introduced the field operators for particles in the states, and  $\langle S, M | 1, m_1; 1, m_2 \rangle$  are the Clebsch-Gordan coefficients. In the following, and for simplicity of future discussions below, we employ the notation  $m = 1, 2, 3$  instead of  $m = -1, 1, 0$ . Using the tables of Clebsch-Gordan coefficients, we obtain

$$A_{00} = \frac{-1}{\sqrt{3}} \hat{\Psi}_3 \hat{\Psi}_3 + \frac{2}{\sqrt{3}} \hat{\Psi}_2 \hat{\Psi}_1 \quad (7.20)$$

$$A_{20} = \sqrt{\frac{2}{3}} \hat{\Psi}_3 \hat{\Psi}_3 + \sqrt{\frac{2}{3}} \hat{\Psi}_2 \hat{\Psi}_1 \quad (7.21)$$

$$A_{21} = \frac{2}{\sqrt{2}} \hat{\Psi}_2 \hat{\Psi}_3 \quad (7.22)$$

$$A_{2-1} = \frac{2}{\sqrt{2}} \hat{\Psi}_1 \hat{\Psi}_3 \quad (7.23)$$

$$A_{22} = \hat{\Psi}_2 \hat{\Psi}_2 \quad (7.24)$$

$$A_{2-2} = \hat{\Psi}_1 \hat{\Psi}_1. \quad (7.25)$$

In the following we substitute the operators by  $\mathbb{C}$ -numbers. Although, strictly speaking, this may be just performed at the final stage, when considering the Bogoliubov approximation associated to the condensate in the dark states, the final results (for the interactions in the dark state manifold) are not modified and the expressions are then enlightened. The different projectors acquire the form:

$$P_0 = \frac{1}{3} (|\Psi_3|^4 + 4|\Psi_2|^2|\Psi_1|^2 - 2(\Psi_3^*)^2\Psi_2\Psi_1 - 2\Psi_2^*\Psi_1^*\Psi_3^2), \quad (7.26)$$

$$P_2 = \frac{2}{3} (|\Psi_3|^4 + |\Psi_2|^2|\Psi_1|^2 + (\Psi_3^*)^2\Psi_2\Psi_1 + (\Psi_3)^2\Psi_2^*\Psi_1^* + 2|\Psi_2|^2|\Psi_3|^2 + 2|\Psi_1|^2|\Psi_3|^2 + |\Psi_2|^4 + |\Psi_1|^4) \quad (7.27)$$

and hence the final form of the interaction Hamiltonian is

$$H_{SR} = \int d^3r \left\{ \left( \frac{g_0}{6} + \frac{g_2}{3} \right) |\Psi_3|^4 + \left( \frac{g_2}{3} + \frac{2g_0}{3} \right) |\Psi_2|^2|\Psi_1|^2 + g_2|\Psi_2|^2|\Psi_3|^2 + g_2|\Psi_1|^2|\Psi_3|^2 + \frac{g_2}{2}|\Psi_2|^4 + \frac{g_2}{2}|\Psi_1|^4 + \left( \frac{g_2}{3} - \frac{g_0}{3} \right) [(\Psi_3^*)^2\Psi_2\Psi_1 + \Psi_2^*\Psi_1^*\Psi_3^2] \right\}. \quad (7.28)$$

Since we are interested in the dark states of the tripod scheme, we project at this point onto the basis of the two dark states. Using the parametrization of the laser arrangement introduced in section 2.4.4 we may express the dark-state wavefunctions (and equivalently the corresponding field operators) as a function of the original tripod levels

$$\Psi_{D_1} = \sin \phi e^{-iS_{31}} \Psi_1 - \cos \phi e^{-iS_{32}} \Psi_2 \quad (7.29)$$

$$\Psi_{D_2} = \cos \theta \cos \phi e^{-iS_{31}} \Psi_1 + \cos \theta \sin \phi e^{-iS_{32}} \Psi_2 - \sin \theta \Psi_3, \quad (7.30)$$

with the corresponding inverse transformation

$$\Psi_1 = (\sin \phi \Psi_{D_1} + \cos \theta \cos \phi \Psi_{D_2}) e^{iS_{31}} \quad (7.31)$$

$$\Psi_2 = (-\cos \phi \Psi_{D_1} + \cos \theta \sin \phi \Psi_{D_2}) e^{iS_{32}}. \quad (7.32)$$

The corresponding interacting terms in the coupled Gross-Pitaevskii equations for the dark states (we indicate with the notation  $\propto$  that we just consider here the interaction terms) become

hence of the form:

$$\begin{aligned}
 i\hbar\dot{\Psi}_{D_1} &= i\hbar \sin \phi e^{-iS_{31}} \dot{\Psi}_{-1} - i\hbar \cos \phi e^{-iS_{32}} \dot{\Psi}_1 \\
 &\propto \frac{1}{6} (g_0 + 5g_2 + (-g_0 + g_2) \cos 4\phi) |\Psi_{D_1}|^2 \Psi_{D_1} \\
 &\quad - \frac{1}{3} (g_0 - g_2) \cos \theta \cos 2\phi \left( -\sin^2 \theta e^{-i(S_{31}+S_{32})} + \cos^2 \theta \sin 2\phi \right) |\Psi_{D_2}|^2 \Psi_{D_2} \\
 &\quad + \frac{1}{3} (g_0 - g_2) \cos \theta \sin 4\phi |\Psi_{D_1}|^2 \Psi_{D_2} \\
 &\quad + \frac{2}{3} (g_0 - g_2) \cos \phi \sin \phi \left( e^{-i(S_{31}+S_{32})} \sin^2 \theta - \cos^2 \theta \sin 2\phi \right) \Psi_{D_1}^* (\Psi_{D_2})^2 \\
 &\quad + \frac{1}{6} (g_0 - g_2) \cos \theta \sin 4\phi \Psi_{D_2}^* \Psi_{D_1}^2 \\
 &\quad + \frac{1}{6} (g_0 + 5g_2 + (g_0 - g_2)(\cos 2\theta + 2 \cos^2 \theta \cos 4\phi)) |\Psi_{D_2}|^2 \Psi_{D_1}
 \end{aligned} \tag{7.33}$$

$$\begin{aligned}
 i\hbar\dot{\Psi}_{D_2} &= i\hbar \cos \theta \cos \phi e^{-iS_{31}} \dot{\Psi}_{-1} + i\hbar \cos \theta \sin \phi e^{-iS_{32}} \dot{\Psi}_1 - i\hbar \sin \theta \dot{\Psi}_0 \\
 &\propto \frac{1}{6} (g_0 - g_2) \cos \theta \sin 4\phi |\Psi_{D_1}|^2 \Psi_{D_1} \\
 &\quad + \frac{1}{3} (\cos^2 \theta (g_0 + 2g_2 + (g_0 - g_2) \cos 4\phi) + 3g_2 \sin^2 \theta) |\Psi_{D_1}|^2 \Psi_{D_2} \\
 &\quad - \frac{1}{3} (g_0 - g_2) \cos \theta \cos 2\phi \left( -\sin^2 \theta e^{-i(S_{31}+S_{32})} + \cos^2 \theta \sin 2\phi \right) \Psi_{D_1}^* (\Psi_{D_2})^2 \\
 &\quad + \frac{2}{3} (g_0 - g_2) \cos \phi \sin \phi \left( e^{i(S_{31}+S_{32})} \sin^2 \theta - \cos^2 \theta \sin 2\phi \right) \Psi_{D_2}^* \Psi_{D_1}^2 \\
 &\quad + \frac{2}{3} (g_0 - g_2) \cos \theta \cos 2\phi \left( e^{i(S_{31}+S_{31})} \sin^2 \theta - \cos^2 \theta \sin 2\phi \right) |\Psi_{D_2}|^2 \Psi_{D_1} \\
 &\quad + \frac{1}{48} (9g_0 + 39g_2 - (g_0 - g_2)(4 \cos 2\theta - 3 \cos 4\theta \\
 &\quad \quad + 8 \cos^4 \theta \cos 4\phi + 8 \cos S_{31} + S_{32} \sin^2 2\theta \sin 2\phi)) |\Psi_{D_2}|^2 \Psi_{D_2}
 \end{aligned} \tag{7.34}$$

These complicated general expressions simplify enormously for the case  $g_0 = g_2 = g$ . Note that typically  $g_0$  and  $g_2$  are very close to each other, and hence corrections to this approximation may be considered in typical experiments as being of higher order (although spin-changing collisions, which occur when  $g_0 \neq g_2$  may induce interesting physics which may be the topic of future research). Under the previous approximation we obtain a very simple expression for the coupled Gross-Pitaevskii equations

$$\dot{\Psi}_{D_1} \propto g (|\Psi_{D_1}|^2 + |\Psi_{D_2}|^2) \Psi_{D_1} \tag{7.35}$$

$$\dot{\Psi}_{D_2} \propto g (|\Psi_{D_1}|^2 + |\Psi_{D_2}|^2) \Psi_{D_2}. \tag{7.36}$$

Note that the interaction term just depends on the total density, and it is the same for  $\Psi_{D_{1,2}}$  and any combination of them. This, of course, notably simplifies the analysis of the problem.



The effective  $\Psi^4$  Hamiltonian for the dynamics of the interacting spinor system becomes hence of the form

$$\begin{aligned} \hat{H} &= \int d^2r \hat{\Psi}^\dagger(\mathbf{r}) \left[ -\frac{\hbar^2}{2m} (\nabla - \mathbf{A})^2 + V_{\text{ext}}(\mathbf{r}) \right] \hat{\Psi}(\mathbf{r}) \\ &+ \frac{g}{2} \int d^2r \left( \hat{\Psi}^\dagger(\mathbf{r}) \cdot \hat{\Psi}(\mathbf{r}) \right) \left( \hat{\Psi}^\dagger(\mathbf{r}) \cdot \hat{\Psi}(\mathbf{r}) \right). \end{aligned} \quad (7.37)$$

Assuming pseudo-condensation (as we mentioned above strict condensation is precluded in the thermodynamic limit) we may reduce the previous equation to the Gross-Pitaevskii equation for the spinor quasi-BEC under the non-Abelian gauge:

$$\begin{aligned} \hat{H} &= \int d^2r \Psi^*(\mathbf{r}) \left[ -\frac{\hbar^2}{2m} (\nabla - \mathbf{A})^2 + V_{\text{ext}}(\mathbf{r}) \right] \Psi(\mathbf{r}) \\ &+ \frac{g}{2} \int d^2r \left( \Psi^*(\mathbf{r}) \cdot \Psi(\mathbf{r}) \right)^2. \end{aligned} \quad (7.38)$$

## 7.4 Effects of interactions in trapped condensates in the presence of the “simple” gauge: an outlook

In the discussion of secs. 7.1 and 7.2 we have assumed that our Bose gas could be considered as ideal. In the previous section we showed how interactions could be incorporated in the tripod theory. Although a careful analysis of the role of interactions in BECs in non-Abelian gauge potentials is well beyond the scope of this thesis, we would like to point out briefly at this point that due to the relatively small splitting  $(E_{0,m+1} - E_{0,m})/\hbar\omega = (2m+1)/(\kappa l_{\text{HO}})^2$  especially for low  $m$ , the conditions for non-interacting BEC in this particular case is necessarily rather restrictive. The mean interaction energy  $U$  must satisfy  $U \ll \Delta E \equiv \hbar\omega/(\kappa l_{\text{HO}})^2$ . Since we assume  $\kappa l_{\text{HO}} \gg 1$ , we may attain a situation in which  $U \ll \hbar\omega$ , but  $U \gg \Delta E$ . In that case, the interactions should produce a strong mixing between different ideal  $(0, m)$  states, without mixing  $n = 0$  with other  $n \neq 0$ . Note that the interactions are local in real space, and hence completely non-local in momentum space. As a consequence, the system can be discussed as a quasi-1D ring in momentum space with completely nonlocal interactions. This system is in general only tractable by means of many-body (beyond mean-field) approaches. This is a particularly intriguing situation, which certainly deserves a future analysis.

Another interesting future research direction could be the analysis of fluctuations in trapped systems. As already mentioned at several points quasi-condensation is actually a finite-size effect in the discussed systems, due to the absence of strict condensation in the thermodynamic limit. Although the finite trapping may allow for quasi-condensation, fluctuations may play hence a very relevant role, similar as e.g. the case of one-dimensional quasi-BECs in the absence of artificial electromagnetism.

## 7.5 Solitons in 1D systems in the presence of the “simple” non-Abelian gauge

As an illustration of the effects that the artificial non-Abelian gauge may induce in an interacting Bose gas, we would like to discuss in some detail the case of solitons in a one-dimensional configuration. Solitons are indeed one of the most fascinating phenomena in nonlinear physics. As discussed in section 1.4.2, the one-dimensional Gross-Pitaevskii-equation

$$i\hbar\frac{\partial}{\partial t}\Psi(x,t) = \left(-\frac{\hbar^2}{2m}\partial_x^2 + g|\Psi(x,t)|^2\right)\Psi(x,t) \quad (7.39)$$

allows a bright soliton in the case of attractive interactions ( $g < 0$ ). In this section we shall show that solitons with repulsive interactions ( $g > 0$ ) may be attained in the presence of the “simple” non-Abelian gauge  $\hbar\kappa\hat{\sigma}_\perp$ .

In the following we restrict our discussion to the  $x$ -direction. In absence of interactions the Hamiltonian of the system is hence given by

$$\hat{H} = \frac{1}{2m}(p_x - A_x)^2 + V + \Phi, \quad (7.40)$$

where we follow the same notation as in chapter 5. We consider the simple gauge laser arrangement, which provides:

$$A_x = \hbar\kappa \begin{pmatrix} 0 & -\cos\theta \\ -\cos\theta & 0 \end{pmatrix} = \hbar\kappa'\sigma_x, \quad (7.41)$$

$$\Phi = \hbar^2\kappa^2/2m \begin{pmatrix} \sin^2\theta & 0 \\ 0 & \sin^2(2\theta)/4 \end{pmatrix}, \quad (7.42)$$

$$V = \begin{pmatrix} V_1 & 0 \\ 0 & V_1\cos^2\theta + V_3\sin^2\theta \end{pmatrix}. \quad (7.43)$$

Contrary to previous discussion we assume at this point that  $V + \Phi = \Delta\sigma_z$ , with  $2\Delta = V_{11} + \Phi_{11} - V_{22} - \Phi_{22}$ . This arrangement leads hence to the effective Hamiltonian

$$H = \frac{1}{2m}(p_x - \kappa\sigma_x)^2 + \Delta\sigma_z \quad (7.44)$$

with eigenvalues

$$E_\pm = \frac{\hbar^2}{2m} \left( k^2 + \kappa^2 \pm 2\sqrt{\Delta^2 + k^2\kappa^2} \right), \quad (7.45)$$

and (unnormalized) eigenvectors

$$\Psi_\pm^T = \left( \frac{\Delta \pm \sqrt{\Delta^2 + k^2\kappa^2}}{k\kappa}, 1 \right). \quad (7.46)$$

In fig. 7.5 we depict the dispersion law  $E_\pm$ . Note that the finite  $\Delta$  opens a gap between the upper and the lower branch. Note also that for the lower branch there is a region of negative curvature and hence of negative mass, close to  $k = 0$ . This resembles the situation at the

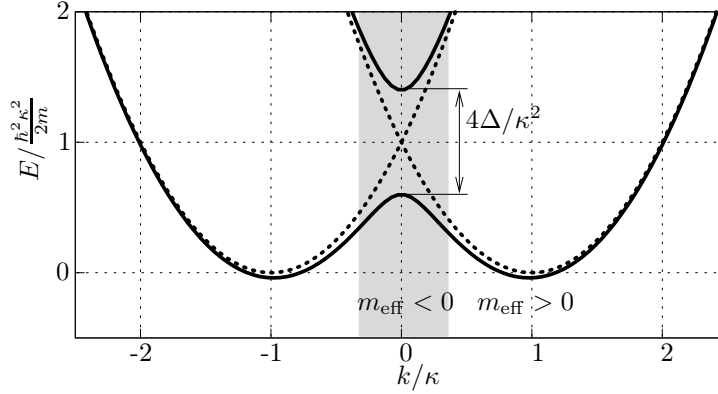


Fig. 7.5: Dispersion relation  $E_{\pm} = \frac{\hbar^2}{2m} (k^2 + \kappa^2 \pm 2\sqrt{\Delta^2 + k^2\kappa^2})$  for  $\Delta = 0.2$ . The dashed lines show the dispersion relation for  $\Delta = 0$ . The lower dispersion branch supports in a region centered at  $k = 0$  a negative effective mass  $m^*$ .

border of the Brillouin zone for atoms in optical lattices [Mey01]. For the lower dispersion branch the effective mass  $m^*$  is given by

$$\frac{1}{m^*} = \frac{1}{\hbar^2} \frac{\partial^2 E_-}{\partial k^2} = \frac{1}{m} \left( 1 - \frac{\kappa^2}{\sqrt{\Delta^2 + k^2\kappa^2}} + \frac{k^2\kappa^2}{(\Delta^2 + k^2\kappa^2)^{3/2}} \right). \quad (7.47)$$

At  $k \simeq 0$  we have  $m^*/m = |\Delta|/(|\Delta| - \kappa^2)$ . Hence,  $|\Delta| < \kappa^2$  is needed to obtain a negative mass at  $k = 0$ .

In the following we will consider the situation in which a (quasi-)condensate is prepared in the region of negative mass of the lower branch. Following our discussion of sec. 7.3, we introduce interactions and consider the spinor Gross-Pitaevskii equation

$$i\hbar\dot{\Psi}(x, t) = \left[ \frac{1}{2m} (p_x - \kappa\sigma_x)^2 + \Delta\sigma_z + g\Psi(x, t)^* \cdot \Psi(x, t) \right] \Psi(x, t). \quad (7.48)$$

For  $k$  close to zero and assuming only population of the lowest branch we may approximate the Gross-Pitaevskii equation as

$$i\hbar\dot{\Psi}(x, t) = \left[ \frac{-\hbar^2}{2m^*} \partial_x^2 + g|\Psi(x, t)|^2 \right] \Psi(x, t). \quad (7.49)$$

The existence of the soliton may be understood by considering a Gaussian ansatz for the atomic wavefunction:

$$\Psi(x) = \frac{1}{\sqrt{\sqrt{\pi}\sigma}} e^{-\frac{x^2}{2\sigma^2}}. \quad (7.50)$$

The kinetic energy is then

$$E_{\text{kin}} = -\frac{\hbar^2}{2m^*} \int_{-\infty}^{\infty} \Psi^*(x) \partial_x^2 \Psi(x) dx = \frac{\hbar^2}{4\sigma^2 m} \frac{|\Delta| - \kappa^2}{|\Delta|} \quad (7.51)$$

and the interaction energy

$$E_{\text{int}} = gN \int_{-\infty}^{\infty} |\Psi|^4 dx = \frac{gN}{\sqrt{2\pi}\sigma}. \quad (7.52)$$

Derivating with respect to the Gaussian width  $\sigma$ , we find an extremal point for

$$\sigma = \frac{\hbar^2 \kappa^2 - |\Delta| \sqrt{2\pi}}{2m |\Delta| gN}. \quad (7.53)$$

Actually the energy is strictly maximized, but due to the negative mass, the system behaves as “moving backwards in time”, and hence this extremal value of  $\sigma$  is actually the equilibrium width of the soliton as shown below. We have simulated numerically, by evolving eq. (7.49) in imaginary time (which is a well-established method to find ground state solutions). In the following we employ energy units of  $\frac{\hbar^2 \kappa^2}{2m}$  and length units of  $1/\kappa$ . Figure 7.6 shows the imaginary time evolution for an initial Gaussian wavepacket with  $\Delta = 0.25$  and  $gN = 0.03$ . The parameters are chosen in such a way, that the function in momentum space is well within the above mentioned range of negative curvature, and such that the effective mass is constant within the momentum space wavepacket. Furthermore the energy of the wavepacket is smaller than the gap, so that we do not have significant mixing with the upper branch. Clearly, the wavepacket width gets into an equilibrium solutions with a width  $\sigma \simeq 256.8$  in very good agreement with our Gaussian ansatz solution  $\sigma = \frac{|\Delta|-1}{|\Delta|} \frac{\sqrt{2\pi}}{gN} \approx 250$ . The slight departure is due to the fact that the actual soliton shape is not a Gaussian but rather a sech function.

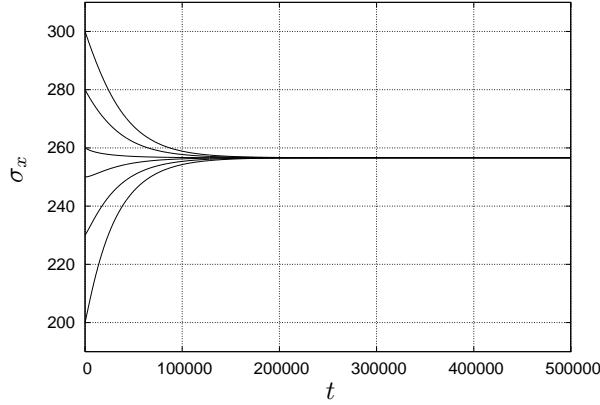


Fig. 7.6: The width  $\sigma$  of the density  $|\Psi(x)|^2$  vs. time in the imaginary time evolution. The calculations start with a Gaussian of widths  $\sigma$  equal to 200, 230, 250, 260, 280, and 300.

Hence, the modification of the dispersion law induced by the “simple” non-Abelian gauge field may induce a significant modification of the nonlinear properties of a quasi-BEC. Indeed the nonlinear physics of BECs in the presence of artificial electromagnetism (both Abelian and non-Abelian) is a fascinating topic of future research. Although a detailed discussion of these

possibilities lies beyond the scope of this thesis, we would like to mention that inhomogeneous electromagnetic fields may lead to intriguing vortex lattice patterns, and possibly to novel types of modulational instabilities.



# Chapter 8

## Conclusions

In this thesis we have investigated the basic physics governing atoms in the presence of artificial electromagnetism and, more specifically, novel phenomena appearing in atom optics under the influence of non-Abelian gauge fields.

In **Chapter 2** we explained different ways of inducing artificial electromagnetism, with a specific emphasis on the method employing dark state techniques. For the tripod laser scheme we established general conditions that the arrangement must fulfill to provide a non-Abelian gauge field. We then discussed particular arrangements that allow for a simple constant non-Abelian gauge (which we have denoted as the *simple* gauge), the non-Abelian version of the Landau gauge, and the non-Abelian version of the symmetric gauge.

In **Chapter 3** we discuss the physics of atomic wavepackets in the presence of the *simple* gauge, demonstrating that the wavepacket propagation may show effects that are intrinsically due to the non-Abelian character of the fields. We analyzed as well a tweezer atomic interferometer which may allow for the observation of the non-Abelian Aharonov-Bohm effect.

In **Chapter 4** we pointed out that the Landau level structure is significantly modified in the presence of a non-Abelian Landau gauge field. In particular, the degeneracy of the levels is broken and the gap between different Landau levels is filled by additional states. Hence, a sufficiently large non-Abelian part in the potential may completely destroy the Landau level structure. This destruction may be actually observed in Fermi gases in time-of-flight experiments by means of the de Haas-van Alphen-effect. In the same chapter we considered the modification of the Fock-Darwin spectrum in the presence of a non-Abelian symmetric gauge, involving the observation of a changed density profile for Fermi gases.

We extend our discussion in **Chapter 5** towards quasi-relativistic physics induced in cold gases by the *simple* gauge. For low momenta, the Hamiltonian becomes Dirac-like, resembling the case of electrons in graphene. This scenario opens the possibility of achieving Veselago superlensing in cold atomic gases, as for electrons in graphene.

In **Chapter 6** we explored further the remarkable effects that such *simple* non-Abelian gauge field may have in atom optics. We showed in detail that atomic reflection at a laser barrier may be significantly distorted, leading to the occurrence of double reflection including also the possibility of negative reflection.

Finally, in **Chapter 7** we considered the case of trapped gases in the presence of the *simple* gauge, showing that strict condensation is actually forbidden in the thermodynamical limit. For finite size systems, we have discussed that the quasi-condensate density presents a striking oscillatory character, which may be traced to a condensation in Mexican-hat like effective potential in momentum space. Last of all, we have introduced interactions using the theory

of spinor gases, and discussed some particularly interesting perspectives for interacting Bose gases in non-Abelian gauge fields, for both the nonlinear physics of quasi-condensates (as e.g. solitons) and the particularly exciting physics of strongly interacting systems in these non-Abelian fields.

We would like to mention that the vast majority of the arrangements discussed in this thesis are readily feasible within the current experimental state of the art, and in particular the *simple* gauge. Actually, recent progresses [LCP<sup>+</sup>09] allow to foresee exciting experimental perspectives for artificial electromagnetism in the next future.



# Bibliography

- [AA87] Y. Aharonov and J. Anandan. *Phase Change during a Cyclic Quantum Evolution*. Phys. Rev. Lett. **58**, 1593–1596, 1987. doi:10.1103/PhysRevLett.58.1593.
- [AAK<sup>+</sup>88] A. Aspect, E. Arimondo, R. Kaiser, N. Vansteenkiste, and C. Cohen-Tannoudji. *Laser Cooling below the One-Photon Recoil Energy by Velocity-Selective Coherent Population Trapping*. Phys. Rev. Lett. **61**, 826, 1988. doi:10.1103/PhysRevLett.61.826.
- [AB59] Y. Aharonov and D. Bohm. *Significance of Electromagnetic Potentials in the Quantum Theory*. The Phys. Rev. **115(3)**, 485–491, 1959. doi:10.1103/PhysRev.115.485.
- [ABLM82] S. V. Andreev, V. I. Balykin, V. S. Letokhov, and V. G. Minogin. *Radiative slowing and reduction of the energy spread of a beam of sodium atoms to 1.5 K in an oppositely directed laser beam*. JETP Lett. **34**, 442–445, 1982.
- [ABS94] R. Anderson, H. R. Bilger, and G. E. Stedman. *Sagnac effect: A century of Earth-rotated interferometers*. Am. J. Phys. **62**, 975–985, 1994. doi:10.1119/1.17656.
- [AEM<sup>+</sup>95] M. H. Anderson, J. R. Ensher, M. R. Matthews, C. E. Wieman, and E. A. Cornell. *Observation of Bose-Einstein Condensation in a Dilute Atomic Vapor*. Science **269**, 198, 1995. doi:10.1126/science.269.5221.198.
- [AHS90] J. Avron, J. Howland, and B. Simon. *Adiabatic Theorems for Dense Point Spectra*. Commun. Math. Phys. **128**, 497–507, 1990. doi:10.1007/BF02096869.
- [AK98] B. P. Anderson and M. A. Kasevich. *Macroscopic Quantum Interference from Atomic Tunnel Arrays*. Science **282**, 1686, 1998. doi:10.1126/science.282.5394.1686.
- [And64] A. F. Andreev. *The thermal conductivity of the intermediate state in superconductors*. Sov. Phys. JETP **19**, 1228, 1964.
- [ANVA<sup>+</sup>99] M. Arndt, O. Nairz, J. Voss-Andreae, C. Keller, G. van der Zouw, and A. Zeilinger. *Wave-particle duality of C<sub>60</sub>*. Nature **401**, 680–682, 1999. doi:10.1038/44348.
- [AO76] E. Arimondo and G. Orriol. *Nonabsorbing atomic coherences by coherent two-photon transitions in a three-level optical pumping*. Lettere Al Nuovo Cimento **17**, 333, 1976.
- [APSH06] A. S. Arnold, M. J. Pritchard, D. A. Smith, and I. G. Hughes. *Double-impulse magnetic focusing of launched cold atoms*. New J. Phys. **8**, 53, 2006. doi:10.1088/1367-2630/8/4/053.

- [ASB<sup>+</sup>93] C. G. Aminoff, A. M. Steane, P. Bouyer, P. Desbiolles, J. Dalibard, and C. Cohen-Tannoudji. *Cesium atoms bouncing in a stable gravitational cavity*. Phys. Rev. Lett. **71**, 3083, 1993. doi:10.1103/PhysRevLett.71.3083.
- [ASRVK01] J. R. Abo-Shaeer, C. Raman, J. M. Vogels, and W. Ketterle. *Observation of Vortex Lattices in Bose-Einstein Condensates*. Science **292**, 476, 2001. doi:10.1126/science.1060182.
- [ASY87] J. Avron, R. Seiler, and L. G. Yaffe. *Adiabatic Theorems and Applications to the Quantum Hall Effect*. Commun. Math. Phys. **110**, 33–49, 1987. doi:10.1007/BF01209015. [ERRATUM: Commun. Math. Phys. 156, 649-650 (1993)].
- [Bar04] L. D. Barron. *Molecular Light Scattering and Optical Activity*. Cambridge University Press, Cambridge, England, 2004.
- [BBB<sup>+</sup>99] K. Bongs, S. Burger, G. Birkl, K. Sengstock, W. Ertmer, K. Rzażewski, A. Sanpera, and M. Lewenstein. *Coherent Evolution of Bouncing Bose-Einstein Condensates*. Phys. Rev. Lett. **83**, 3577, 1999. doi:10.1103/PhysRevLett.83.3577.
- [BBD<sup>+</sup>99] S. Burger, K. Bongs, S. Dettmer, W. Ertmer, K. Sengstock, A. Sanpera, G. V. Shlyapnikov, and M. Lewenstein. *Dark Solitons in Bose-Einstein Condensates*. Phys. Rev. Lett. **83**, 5198, 1999. doi:10.1103/PhysRevLett.83.5198.
- [BCF<sup>+</sup>01] S. Burger, F. S. Cataliotti, C. Fort, F. Minardi, and M. Inguscio. *Superfluid and Dissipative Dynamics of a Bose-Einstein Condensate in a Periodic Optical Potential*. Phys. Rev. Lett. **86**, 4447, 2001. doi:10.1103/PhysRevLett.86.4447.
- [BDZ08] I. Bloch, J. Dalibard, and W. Zwerger. *Many-body physics with ultracold gases*. Rev. Mod. Phys. **80**, 885, 2008. doi:10.1103/RevModPhys.80.885.
- [Bee06] C. W. J. Beenakker. *Specular Andreev Reflection in Graphene*. Phys. Rev. Lett. **97**, 067007, 2006. doi:10.1103/PhysRevLett.97.067007.
- [BEM87] T. Bergeman, G. Erez, and H. J. Metcalf. *Magnetostatic trapping fields for neutral atoms*. Phys. Rev. A **35**, 1535–1546, 1987. doi:10.1103/PhysRevA.35.1535.
- [Ber84] M. V. Berry. *Quantal Phase Factors Accompanying Adiabatic Changes*. Proc. R. Soc. A **392**, 45, 1984. doi:10.1098/rspa.1984.0023.
- [Ber97] P. Berman, editor. *Atom Interferometry*. Academic, San Diego, 1997.
- [BF28] M. Born and V. Fock. *Beweis des Adiabatenatzes*. Zeitschrift für Physik **51**, 165–180, 1928. doi:10.1007/BF01343193.
- [BG05] I. Bloch and M. Greiner. *Exploring Quantum Matter with Ultracold Atoms in Optical Lattices*. Adv. At. Mol. Opt. Phys. **52**, 1, 2005.
- [BLOS87] V. I. Balykin, V. S. Letokhov, Y. B. Ovchinnikov, and A. I. Sidorov. *Reflection of an atomic beam from a gradient of an optical field*. JETP Lett. **45**, 353, 1987.

- 
- [BLOS88] V. I. Balykin, V. S. Letokhov, Y. B. Ovchinnikov, and A. I. Sidorov. *Quantum-State-Selective Mirror Reflection of Atoms by Laser Light*. Phys. Rev. Lett. **60**, 2137, 1988. doi:10.1103/PhysRevLett.60.2137.
- [BLP82] V. V. Beresteckii, E. M. Lifshitz, and L. P. Pitaevskii. *Quantum Electrodynamics*. Oxford, Butterworth Heinemann, 1982.
- [BMK<sup>+</sup>03] A. Bohm, A. Mostafazadeh, H. Koizumi, Q. Niu, and J. Zwanziger. *The Geometric Phase in Quantum Systems: Foundations, Mathematical Concepts, and Applications in Molecular and Condensed Matter Physics*. Springer, 2003.
- [BMR99] J. Boudon, R. Mathevet, and J. Robert. *Atomic interferometry*. J. Phys. B **32**, R173–R195, 1999.
- [Bor89] C. J. Bordé. *Atomic interferometry with internal state labelling*. Phys. Lett. A **140**, 10, 1989. doi:10.1016/0375-9601(89)90537-9.
- [Bos24] S. Bose. *Plancks Gesetz und Lichtquantenhypothese*. Zeitschrift für Physik **26**, 178, 1924. doi:10.1007/BF01327326.
- [BSSD04] V. Bretin, S. Stock, Y. Seurin, and J. Dalibard. *Fast Rotation of a Bose-Einstein Condensate*. Phys. Rev. Lett. **92**, 050403, 2004. doi:10.1103/PhysRevLett.92.050403.
- [BSTH95] C. C. Bradley, C. A. Sackett, J. J. Tollett, and R. G. Hulet. *Evidence of Bose-Einstein Condensation in an Atomic Gas with Attractive Interactions*. Phys. Rev. Lett. **75**, 1687, 1995. doi:10.1103/PhysRevLett.75.1687.
- [CBAC86] S. Chu, J. E. Bjorkholm, A. Ashkin, and A. Cable. *Experimental Observation of Optically Trapped Atoms*. Phys. Rev. Lett. **57**, 314, 1986. doi:10.1103/PhysRevLett.57.314.
- [CFA07] V. V. Cheianov, V. Fal’ko, and B. L. Altshuler. *The Focusing of Electron Flow and a Veselago Lens in Graphene p-n Junctions*. Science **315**, 1252, 2007. doi:10.1126/science.1138020.
- [CH82] R. J. Cook and R. K. Hill. *An electromagnetic mirror for neutral atoms*. Opt. Commun. **43**, 258, 1982. doi:10.1016/0030-4018(82)90392-3.
- [Chu98] S. Chu. *Nobel Lecture: The manipulation of neutral particles*. Rev. Mod. Phys. **70**, 685, 1998. doi:10.1103/RevModPhys.70.685.
- [CJ04] D. Chruscinski and A. Jamiolkowski. *Geometric Phases in Classical and Quantum Mechanics*. Birkhäuser Boston, 2004.
- [CT98] C. Cohen-Tannoudji. *Nobel Lecture: Manipulating atoms with photons*. Rev. Mod. Phys. **70**, 707, 1998. doi:10.1103/RevModPhys.70.707.
- [CW02] E. Cornell and C. E. Wieman. *Nobel Lecture: Bose-Einstein condensation in a dilute gas, the first 70 years and some recent experiments*. Rev. Mod. Phys. **74**, 875, 2002. doi:10.1103/RevModPhys.74.875.

- [Dar30] C. G. Darwin. *The diamagnetism of the free electron*. Proc. Cambridge Philos. Soc. **27**, 86, 1930. doi:10.1017/S0305004100009373.
- [dB37] L. de Broglie. *La physique nouvelle et les Quanta*. Flammarion, 1937.
- [DCT89] J. Dalibard and C. Cohen-Tannoudji. *Laser cooling below the Doppler limit by polarization gradients: Simple theoretical models*. J. Opt. Soc. Am. B **6**, 2023, 1989.
- [DGPS99] F. Dalfovo, S. Giorgini, L. P. Pitaevskii, and S. Stringari. *Theory of Bose-Einstein condensation in trapped gases*. Rev. Mod. Phys. **71**, 463, 1999. doi:10.1103/RevModPhys.71.463.
- [DHW<sup>+</sup>99] L. Deng, E. W. Hagley, J. Wen, M. Trippenbach, Y. Band, P. S. Julienne, J. E. Simsarian, K. Helmerson, S. L. Rolston, and W. D. Phillips. *Four-wave mixing with matter waves*. Nature **398**, 218, 1999. doi:10.1038/18395.
- [DMA<sup>+</sup>95] K. B. Davis, M. O. Mewes, M. R. Andrews, N. J. van Druten, D. S. Durfee, D. M. Kurn, and W. Ketterle. *Bose-Einstein Condensation in a Gas of Sodium Atoms*. Phys. Rev. Lett. **75**, 3969, 1995. doi:10.1103/PhysRevLett.75.3969.
- [DPR<sup>+</sup>96] M. B. Dahan, E. Peik, J. Reichel, Y. Castin, and C. Salomon. *Bloch Oscillations of Atoms in an Optical Potential*. Phys. Rev. Lett. **76**, 4508–4511, 1996. doi:10.1103/PhysRevLett.76.4508.
- [DSF<sup>+</sup>00] J. Denschlag, J. E. Simsarian, D. L. Feder, C. W. Clark, L. A. Collins, J. Cubizolles, L. Deng, E. W. Hagley, K. Helmerson, W. P. Reinhardt, S. L. Rolston, B. I. Schneider, and W. D. Phillips. *Generating Solitons by Phase Engineering of a Bose-Einstein Condensate*. Science **287**, 97–101, 2000. doi:10.1126/science.287.5450.97.
- [DSH<sup>+</sup>02] J. H. Denschlag, J. E. Simsarian, H. Häffner, C. McKenzie, A. Browaeys, D. Cho, K. Helmerson, S. L. Rolston, and W. D. Phillips. *A Bose-Einstein condensate in an optical lattice*. J. Phys. B **35**, 3095, 2002.
- [Ein24] A. Einstein. *Quantentheorie des einatomigen idealen Gases*. Sitzber. Kgl. Preuss. Akad. Wiss., Phys. Math. Kl. Bericht **22**, 261, 1924.
- [Ein25] A. Einstein. *Quantentheorie des einatomigen idealen Gases II*. Sitzber. Kgl. Preuss. Akad. Wiss., Phys. Math. Kl. Bericht **3**, 18, 1925.
- [FMB<sup>+</sup>02] F. Ferlaino, P. Maddaloni, S. Burger, F. S. Cataliotti, C. Fort, M. Modugno, and M. Inguscio. *Dynamics of a Bose-Einstein condensate at finite temperature in an atom-optical coherence filter*. Phys. Rev. A **66**, 011604, 2002. doi:10.1103/PhysRevA.66.011604.
- [Foc28] V. Fock. *Bemerkung zur Quantelung des harmonischen Oszillators im Magnetfeld*. Zeitschrift für Physik **47**, 446, 1928. doi:10.1007/BF01390750.

- 
- [FWGF89] M. P. A. Fisher, P. B. Weichman, G. Grinstein, and D. S. Fisher. *Boson localization and the superfluid-insulator transition*. Phys. Rev. B **40**, 546–570, 1989. doi:10.1103/PhysRevB.40.546.
- [GBM<sup>+</sup>01] M. Greiner, I. Bloch, O. Mandel, T. W. Hänsch, and T. Esslinger. *Exploring Phase Coherence in a 2D Lattice of Bose-Einstein Condensates*. Phys. Rev. Lett. **87**, 160405, 2001. doi:10.1103/PhysRevLett.87.160405.
- [GCY<sup>+</sup>09] K. J. Günter, M. Cheneau, T. Yefsah, S. P. Rath, and J. Dalibard. *Practical scheme for a light-induced gauge field in an atomic Bose gas*. Phys. Rev. A **79**, 011604(R), 2009. doi:10.1103/PhysRevA.79.011604.
- [GDSB01] R. Godun, M. D’Arcy, G. Summy, and K. Burnett. *Prospects for atom interferometry*. Contemporary Physics **42(2)**, 77–95, 2001. doi:10.1080/00107510118044.
- [GF06] A. Ghosh and P. Fischer. *Chiral Molecules Split Light: Reflection and Refraction in a Chiral Liquid*. Phys. Rev. Lett. **97**, 173002, 2006. doi:10.1103/PhysRevLett.97.173002.
- [GLJP88] P. L. Gould, P. D. Lett, P. S. Julienne, and W. D. Phillips. *Observation of associative ionization of ultracold laser-trapped sodium atoms*. Phys. Rev. Lett. **60**, 788–791, 1988. doi:10.1103/PhysRevLett.60.788.
- [GME<sup>+</sup>02] M. Greiner, O. Mandel, T. Esslinger, T. W. Hänsch, and I. Bloch. *Quantum phase transition from a superfluid to a Mott insulator in a gas of ultracold atoms*. Nature **415**, 39, 2002. doi:10.1038/415039a.
- [GMHB02] M. Greiner, O. Mandel, T. W. Hänsch, and I. Bloch. *Collapse and revival of the matter wave field of a Bose-Einstein condensate*. Nature **419**, 51, 2002. doi:10.1038/nature00968.
- [GML95] D. M. Giltner, R. W. McGowan, and S. A. Lee. *Atom Interferometer Based on Bragg Scattering from Standing Light Waves*. Phys. Rev. Lett. **75**, 2638, 1995. doi:10.1103/PhysRevLett.75.2638.
- [GN07] A. K. Geim and K. S. Novoselov. *The rise of graphene*. Nature Materials **6**, 183, 2007. doi:10.1038/nmat1849.
- [GO79] D. M. Greenberger and A. W. Overhauser. *Coherence effects in neutron diffraction and gravity experiments*. Rev. Mod. Phys. **51**, 43, 1979. doi:10.1103/RevModPhys.51.43.
- [GR01] G. Grynberg and C. Robilliard. *Cold atoms in dissipative optical lattices*. Phys. Rep. **355**, 335, 2001. doi:10.1016/S0370-1573(01)00017-5.
- [GW88] J. Garrison and E. Wright. *Complex geometrical phases for dissipative systems*. Physics Letters A **128**, 177–181, 1988. doi:10.1016/0375-9601(88)90905-X.
- [HHB<sup>+</sup>01] W. K. Hensinger, H. Häffner, A. Browaeys, N. R. Heckenberg, K. Helmerson, C. McKenzie, G. J. Milburn, W. D. Phillips, S. L. Rolston, H. Rubinsztein-Dunlop, and B. Upcroft. *Dynamical tunnelling of ultracold atoms*. Nature **412**, 52, 2001.

- [HN93] F. Hasselbach and M. Nicklaus. *Sagnac experiment with electrons: Observation of the rotational phase shift of electron waves in vacuum*. Phys. Rev. A **48**(1), 143–151, 1993. doi:10.1103/PhysRevA.48.143.
- [Hof76] D. R. Hofstadter. *Energy levels and wave functions of Bloch electrons in rational and irrational magnetic fields*. Phys. Rev. B **14**, 2239, 1976. doi:10.1103/PhysRevB.14.2239.
- [Hor86] P. A. Horváthy. *Non-Abelian Aharonov-Bohm effect*. Phys. Rev. D **33**, 407, 1986. doi:10.1103/PhysRevD.33.407.
- [HS75] T. W. Hänsch and A. L. Schawlow. *Cooling of gases by laser radiation*. Opt. Commun. **13**, 68, 1975. doi:10.1016/0030-4018(75)90159-5.
- [Hua87] K. Huang. *Statistical Mechanics*. Wiley & Sons, 1987.
- [JBC<sup>+</sup>98] D. Jaksch, C. Bruder, J. I. Cirac, C. W. Gardiner, and P. Zoller. *Cold Bosonic Atoms in Optical Lattices*. Phys. Rev. Lett. **81**, 3108, 1998. doi:10.1103/PhysRevLett.81.3108.
- [JD96] P. S. Jessen and I. H. Deutsch. *Optical lattices*. Adv. At. Mol. Opt. Phys. **37**, 95, 1996.
- [JO04] G. Juzeliūnas and P. Öhberg. *Slow Light in Degenerate Fermi Gases*. Phys. Rev. Lett. **93**, 033602, 2004. doi:10.1103/PhysRevLett.93.033602.
- [JO05] G. Juzeliūnas and P. Öhberg. *Creation of an Effective Magnetic Field in Ultracold Atomic Gases Using Electromagnetically Induced Transparency*. Optics and Spectroscopy **99**, 357–361, 2005. doi:10.1134/1.2055927.
- [JP07] R. Jackiw and S.-Y. Pi. *Chiral Gauge Theory for Graphene*. Phys. Rev. Lett. **98**, 266402, 2007. doi:10.1103/PhysRevLett.98.266402.
- [JRL<sup>+</sup>08] G. Juzeliūnas, J. Ruseckas, M. Lindberg, L. Santos, and P. Öhberg. *Quasirelativistic behavior of cold atoms in light fields*. Phys. Rev. A **77**, 011802(R), 2008. doi:10.1103/PhysRevA.77.011802.
- [JRO05] G. Juzeliūnas, J. Ruseckas, and P. Öhberg. *Effective magnetic fields induced by EIT in ultra-cold atomic gases*. J. Phys. B: At. Mol. Opt. Phys. **38**, 4171–4183, 2005. doi:10.1088/0953-4075/38/23/001.
- [JROF06] G. Juzeliūnas, J. Ruseckas, P. Öhberg, and M. Fleischhauer. *Light-induced effective magnetic fields for ultracold atoms in planar geometries*. Phys. Rev. A **73**, 025602, 2006. doi:10.1103/PhysRevA.73.025602.
- [JROK05] G. Juzeliūnas, J. Ruseckas, P. Öhberg, and A. Klein. *Effective magnetic fields in degenerate atomic gases induced by light beams with orbital angular momenta*. Phys. Rev. A **71**, 053614, 2005. doi:10.1103/PhysRevA.71.053614.
- [Juz09] G. Juzeliūnas. *Artificial magnetism for ultracold atoms*. Physics **2**, 25, 2009. doi:10.1103/Physics.2.25.

- 
- [JZ03] D. Jaksch and P. Zoller. *Creation of effective magnetic fields in optical lattices: the Hofstadter butterfly for cold neutral atoms*. New J. Phys. **5**, 56, 2003. doi:10.1088/1367-2630/5/1/356.
- [JZ05] D. Jaksch and P. Zoller. *The cold atom Hubbard toolbox*. Annals of Physics **315**, 52–79, 2005. doi:10.1016/j.aop.2004.09.010.
- [Kat50] T. Kato. *On the Adiabatic Theorem of Quantum Mechanics*. J. Phys. Soc. Jpn. **5**, 435–439, 1950.
- [Ket02] W. Ketterle. *Nobel lecture: When atoms behave as waves: Bose-Einstein condensation and the atom laser*. Rev. Mod. Phys. **74**, 1131, 2002. doi:10.1103/RevModPhys.74.1131.
- [KMP00] G. M. Kavoulakis, B. Mottelson, and C. J. Pethick. *Weakly interacting Bose-Einstein condensates under rotation*. Phys. Rev. A **62**, 063605, 2000. doi:10.1103/PhysRevA.62.063605.
- [KNG06] M. I. Katsnelson, K. S. Novoselov, and A. K. Geim. *Chiral tunnelling and the Klein paradox in graphene*. Nature Physics **2**, 620, 2006. doi:10.1038/nphys384.
- [KSF+02] L. Khaykovich, F. Schreck, G. Ferrari, T. Bourdel, J. Cubizolles, L. D. Carr, Y. Castin, and C. Salomon. *Formation of a Matter-Wave Bright Soliton*. Science **296**, 1290, 2002. doi:10.1126/science.1071021.
- [Lan30] L. Landau. *Diamagnetismus der Metalle*. Zeitschrift für Physik **64**, 629–637, 1930. doi:10.1007/BF01397213.
- [LCP99] J. Long, H. Chan, and J. Price. *Experimental status of gravitational-strength forces in the sub-centimeter regime*. Nucl. Phys. B **539**, 23–34, 1999. doi:10.1016/S0550-3213(98)00711-1.
- [LCP+09] Y.-J. Lin, R. L. Compton, A. R. Perry, W. D. Phillips, J. V. Porto, and I. B. Spielman. *Bose-Einstein Condensate in a Uniform Light-Induced Vector Potential*. Phys. Rev. Lett. **102**, 130401, 2009. doi:10.1103/PhysRevLett.102.130401.
- [LL02] L. D. Landau and E. M. Lifshitz. *Statistical Physics Part 1*. Butterworth-Heinemann, Oxford, 2002.
- [Lon38] F. London. *The  $\lambda$ -phenomenon of liquid helium and the Bose-Einstein degeneracy*. Nature **141**, 643, 1938. doi:10.1038/141643a0.
- [LSA+07] M. Lewenstein, A. Sanpera, V. Ahufinger, B. Damski, A. S. De, and U. Sen. *Ultracold atomic gases in optical lattices: mimicking condensed matter physics and beyond*. Advances in Physics **56**, 243, 2007. doi:10.1080/00018730701223200.
- [LWWP88] P. D. Lett, R. N. Watts, C. I. Westbrook, and W. D. Phillips. *Observation of Atoms Laser Cooled below the Doppler Limit*. Phys. Rev. Lett. **61**, 169–172, 1988. doi:10.1103/PhysRevLett.61.169.

- [Mag05] M. Maggiore. *A Modern Introduction to Quantum Field Theory*, p. 55. Oxford University Press, Oxford, 2005.
- [MAH<sup>+</sup>99] M. R. Matthews, B. P. Anderson, P. C. Haljan, D. S. Hall, C. E. Wieman, and E. A. Cornell. *Vortices in a Bose-Einstein Condensate*. Phys. Rev. Lett. **83**, 2498, 1999. doi:10.1103/PhysRevLett.83.2498.
- [Max65] J. C. Maxwell. *A Dynamical Theory of the Electromagnetic Field*. Philosophical Transactions of the Royal Society of London **155**, 459–512, 1865. doi:10.1098/rstl.1865.0008.
- [MCH93] J. D. Miller, R. A. Cline, and D. J. Heinzen. *Far-off-resonance optical trapping of atoms*. Phys. Rev. A **47**, R4567 – R4570, 1993. doi:10.1103/PhysRevA.47.R4567.
- [MCM<sup>+</sup>02] O. Morsch, M. Cristiani, J. H. Müller, D. Ciampini, and E. Arimondo. *Free expansion of a Bose-Einstein condensate in a one-dimensional optical lattice*. Phys. Rev. A **66**, 021601, 2002. doi:10.1103/PhysRevA.66.021601.
- [MCWD00] K. W. Madison, F. Chevy, W. Wohlleben, and J. Dalibard. *Vortex Formation in a Stirred Bose-Einstein Condensate*. Phys. Rev. Lett. **84**, 806, 2000. doi:10.1103/PhysRevLett.84.806.
- [MdS99] H. Metcalf and P. V. der Straten. *Laser Cooling and Trapping*. Springer Verlag, New York, 1999.
- [Mes90] A. Messiah. *Quantenmechanik Band 1 & 2*. Walter de Gruyter, 1990.
- [Mey01] P. Meystre. *Atom Optics*. Springer Verlag, New York, 2001.
- [MF06] E. McCann and V. I. Fal’ko. *Landau-Level Degeneracy and Quantum Hall Effect in a Graphite Bilayer*. Phys. Rev. Lett. **96**, 086805, 2006. doi:10.1103/PhysRevLett.96.086805.
- [MMC<sup>+</sup>01] O. Morsch, J. H. Müller, M. Cristiani, D. Ciampini, and E. Arimondo. *Bloch Oscillations and Mean-Field Effects of Bose-Einstein Condensates in 1D Optical Lattices*. Phys. Rev. Lett. **87**, 140402, 2001. doi:10.1103/PhysRevLett.87.140402.
- [MP00] N. Manini and F. Pistolesi. *Off-Diagonal Geometric Phases*. Phys. Rev. Lett. **85(15)**, 3067, 2000. doi:10.1103/PhysRevLett.85.3067.
- [MP07] A. Matulis and F. M. Peeters. *Appearance of enhanced Weiss oscillations in graphene: Theory*. Phys. Rev. B **75**, 125429, 2007. doi:10.1103/PhysRevB.75.125429.
- [MPP<sup>+</sup>85] A. L. Migdall, J. V. Prodan, W. D. Phillips, T. H. Bergeman, and H. J. Metcalf. *First Observation of Magnetically Trapped Neutral Atoms*. Phys. Rev. Lett. **54**, 2596, 1985. doi:10.1103/PhysRevLett.54.2596.
- [MRG<sup>+</sup>92] C. Miniatura, J. Robert, O. Gorceix, V. Lorent, S. L. Boiteux, J. Reinhardt, and J. Baudon. *Atomic Interferences and the Topological Phase*. Phys. Rev. Lett. **69(2)**, 261–264, 1992. doi:10.1103/PhysRevLett.69.261.



- 
- [MS93] N. Mukunda and R. Simon. *Quantum kinematic approach to the geometric phase*. Ann. Phys. **228**, 205, 1993. doi:10.1006/aphy.1993.1093.
- [MSM<sup>+</sup>03] D. McGloin, G. C. Spalding, H. Melville, W. Sibbett, and K. Dholakia. *Applications of spatial light modulators in atom optics*. Opt. Express **11**, 158, 2003.
- [MSS53] L. Marton, J. A. Simpson, and J. A. Suddeth. *Electron Beam Interferometer*. Phys. Rev. **90**, 490, 1953. doi:10.1103/PhysRev.90.490.
- [Mue04] E. J. Mueller. *Artificial electromagnetism for neutral atoms: Escher staircase and Laughlin liquids*. Phys. Rev. A **70**, 041603(R), 2004. doi:10.1103/PhysRevA.70.041603.
- [NGM<sup>+</sup>05] K. S. Novoselov, A. K. Geim, S. V. Morozov, D. Jiang, M. I. Katsnelson, I. V. Grigorieva, S. V. Dubonos, and A. A. Firsov. *Two-dimensional gas of massless Dirac fermions in graphene*. Nature **438**, 197, 2005. doi:10.1038/nature04233.
- [NJZ<sup>+</sup>07] K. S. Novoselov, Z. Jiang, Y. Zhang, S. V. Morozov, H. L. Stormer, U. Zeitler, J. C. Maan, G. S. Boebinger, P. Kim, and A. K. Geim. *Room-Temperature Quantum Hall Effect in Graphene*. Science **315**, 1379, 2007. doi:10.1126/science.1137201.
- [OBS<sup>+</sup>05] K. Osterloh, M. Baig, L. Santos, P. Zoller, and M. Lewenstein. *Cold Atoms in Non-Abelian Gauge Potentials: From the Hofstadter "Moth" to Lattice Gauge Theory*. Phys. Rev. Lett. **95**, 010403, 2005. doi:10.1103/PhysRevLett.95.010403.
- [PC00] J. Pachos and S. Chountasis. *Optical Holonomic Quantum Computer*. Phys. Rev. A **62**, 052318, 2000. doi:10.1103/PhysRevA.62.052318.
- [Pei33] R. Peierls. *Zur Theorie des Diamagnetismus von Leitungselektronen*. Zeitschrift für Physik **80**, 763–791, 1933. doi:10.1007/BF01342591.
- [Pen00] J. B. Pendry. *Negative Refraction Makes a Perfect Lens*. Phys. Rev. Lett. **85**, 3966, 2000. doi:10.1103/PhysRevLett.85.3966.
- [Pen04] J. B. Pendry. *A Chiral Route to Negative Refraction*. Science **306**, 1353, 2004. doi:10.1126/science.1104467.
- [Pen07] J. B. Pendry. *Negative Refraction for Electrons?* Science **315**, 1226, 2007. doi:10.1126/science.1140178.
- [Phi98] W. D. Phillips. *Nobel Lecture: Laser cooling and trapping of neutral atom*. Rev. Mod. Phys. **70**, 721, 1998. doi:10.1103/RevModPhys.70.721.
- [PM82] W. D. Phillips and H. Metcalf. *Laser Deceleration of an Atomic Beam*. Phys. Rev. Lett. **48**, 596, 1982. doi:10.1103/PhysRevLett.48.596.
- [Pri83] D. E. Pritchard. *Cooling Neutral Atoms in a Magnetic Trap for Precision Spectroscopy*. Phys. Rev. Lett. **51**, 1336–1339, 1983. doi:10.1103/PhysRevLett.51.1336.

- [PS02] C. J. Pethick and H. Smith. *Bose-Einstein Condensation in Dilute Gases*. Cambridge University Press, 2002.
- [PS04] L. P. Pitaevskii and S. Stringari. *Bose-Einstein condensation*. Clarendon Press, 2004.
- [PZR00] J. Pachos, P. Zanardi, and M. Rasetti. *Non-Abelian Berry connection for quantum computation*. Phys. Rev. A **61**, 010305, 2000. doi:10.1103/PhysRevA.61.010305.
- [RAB<sup>+</sup>95] T. M. Roach, H. Abele, M. G. Boshier, H. L. Grossman, K. P. Zetie, and E. A. Hinds. *Realization of a Magnetic Mirror for Cold Atoms*. Phys. Rev. Lett. **75**, 629, 1995. doi:10.1103/PhysRevLett.75.629.
- [RDJ02] J. Ruostekoski, G. V. Dunne, and J. Javanainen. *Particle Number Fractionalization of an Atomic Fermi-Dirac Gas in an Optical Lattice*. Phys. Rev. Lett. **88**, 180401, 2002. doi:10.1103/PhysRevLett.88.180401.
- [RJO05] J. Ruseckas, G. Juzeliūnas, P. Öhberg, and M. Fleischhauer. *Non-Abelian Gauge Potentials for Ultracold Atoms with Degenerate Dark States*. Phys. Rev. Lett. **95**, 010404, 2005. doi:10.1103/PhysRevLett.95.010404.
- [RKWH91] F. Riehle, T. Kisters, A. Witte, and J. Helmcke. *Optical Ramsey Spectroscopy in a Rotating Frame: Sagnac Effect in a Matter-Wave Interferometer*. Phys. Rev. Lett. **67**(2), 177–180, 1991. doi:10.1103/PhysRevLett.67.177.
- [ROB<sup>+</sup>95] E. M. Rasel, M. K. Oberthaler, H. Batelaan, J. Schmiedmayer, and A. Zeilinger. *Atom Wave Interferometry with Diffraction Gratings of Light*. Phys. Rev. Lett. **75**, 2633, 1995. doi:10.1103/PhysRevLett.75.2633.
- [RPC<sup>+</sup>87] E. L. Raab, M. Prentiss, A. Cable, S. Chu, and D. E. Pritchard. *Trapping of Neutral Sodium Atoms with Radiation Pressure*. Phys. Rev. Lett. **59**, 2631, 1987. doi:10.1103/PhysRevLett.59.2631.
- [Rus44] J. S. Russell. *Report on waves*. In *Report of the fourteenth meeting of the British Association for the Advancement of Science*, pages 311–390. 1844.
- [SAG08] T. D. Stanescu, B. Anderson, and V. Galitski. *Spin-orbit coupled Bose-Einstein condensates*. Phys. Rev. A **78**, 023616, 2008. doi:10.1103/PhysRevA.78.023616.
- [SB88] J. Samuel and R. Bhandari. *General Setting for Berry’s Phase*. Phys. Rev. Lett. **60**(23), 2339–2342, 1988. doi:10.1103/PhysRevLett.60.2339.
- [SCE<sup>+</sup>04] V. Schweikhard, I. Coddington, P. Engels, V. P. Mogendorff, and E. A. Cornell. *Rapidly Rotating Bose-Einstein Condensates in and near the Lowest Landau Level*. Phys. Rev. Lett. **92**, 040404, 2004. doi:10.1103/PhysRevLett.92.040404.
- [Sim83] B. Simon. *Holonomy, the Quantum Adiabatic Theorem, and Berry’s Phase*. Phys. Rev. Lett. **51**(24), 2167–2170, 1983. doi:10.1103/PhysRevLett.51.2167.

- 
- [SMB<sup>+</sup>98] M. Snadden, J. McGuirk, P. Bouyer, K. Haritos, and M. Kasevich. *Measurement of the Earth's Gravity Gradient with an Atom Interferometer-Based Gravity Gradiometer*. Phys. Rev. Lett. **81**(5), 971–974, 1998. doi:10.1103/PhysRevLett.81.971.
- [SPE<sup>+</sup>00] E. Sjöqvist, A. K. Pati, A. Ekert, J. S. Anandan, M. Ericsson, D. K. L. Oi, and V. Vedral. *Geometric Phases for Mixed States in Interferometry*. Phys. Rev. Lett. **85**, 2845–2849, 2000. doi:10.1103/PhysRevLett.85.2845.
- [SPTH02] K. E. Strecker, G. B. Partridge, A. G. Truscott, and R. G. Hulet. *Formation and propagation of matter-wave soliton trains*. Nature **417**, 150, 2002. doi:10.1038/nature747.
- [STB<sup>+</sup>03] K. Singh, D. M. Tong, K. Basu, J. L. Chen, and J. F. Du. *Geometric phases for nondegenerate and degenerate mixed states*. Phys. Rev. A **67**, 032106, 2003. doi:10.1103/PhysRevA.67.032106.
- [TK96] T. Takekoshi and R. J. Knize. *CO<sub>2</sub> laser trap for cesium atoms*. Optics Letters **21**, 77–79, 1996. doi:10.1364/OL.21.000077.
- [TSK<sup>+</sup>00] Y. Torii, Y. Suzuki, M. Kozuma, T. Sugiura, and T. Kuga. *Mach-Zehnder Bragg interferometer for a Bose-Einstein condensate*. Phys. Rev. A **61**(4), 041602(R), 2000. doi:10.1103/PhysRevA.61.041602.
- [UFSB98] R. G. Unanyan, M. Fleischhauer, B. E. Shore, and K. Bergmann. *Robust Creation and Phase-sensitive Probing of Superposition States via Stimulated Raman Adiabatic Passage with Degenerate Dark States*. Opt. Commun. **155**, 144, 1998. doi:10.1016/S0030-4018(98)00358-7.
- [Uhl86] A. Uhlmann. *Parallel transport and quantum holonomy along density operators*. Reports on Mathematical Physics **24**, 229–240, 1986. doi:10.1016/0034-4877(86)90055-8.
- [Uhl95] A. Uhlmann. *Geometric phases and related structures*. Reports on Mathematical Physics **36**, 461–481, 1995. doi:10.1016/0034-4877(96)83640-8.
- [USB99] R. G. Unanyan, B. W. Shore, and K. Bergmann. *Laser-driven population transfer in four-level atoms: Consequences of non-Abelian geometrical adiabatic phase factors*. Phys. Rev. A **59**, 2910, 1999. doi:10.1103/PhysRevA.59.2910.
- [Ves68] V. G. Veselago. *The electrodynamics of substances with simultaneously negative values of  $\epsilon$  and  $\mu$* . Sov. Phys. Usp. **10**, 509, 1968. doi:10.1070/PU1968v010n04ABEH003699.
- [WBM<sup>+</sup>96] S. R. Wilkinson, C. F. Bharucha, K. W. Madison, Q. Niu, and M. G. Raizen. *Observation of Atomic Wannier-Stark Ladders in an Accelerating Optical Potential*. Phys. Rev. Lett. **76**, 4512–4515, 1996. doi:10.1103/PhysRevLett.76.4512.
- [WC05] G. Whyte and J. Courtial. *Experimental demonstration of holographic three-dimensional light shaping using a Gerchberg-Saxton algorithm*. New J. Phys. **7**, 117, 2005. doi:10.1088/1367-2630/7/1/117.

- [WD75] D. Wineland and H. Dehmelt. *Proposed  $10^{14} \Delta\nu < \nu$  Laser Fluorescence Spectroscopy on  $Tl^+$  Mono-Ion Oscillator III*. Bull. Am. Phys. Soc. **20**, 637, 1975.
- [WG00] N. K. Wilkin and J. M. F. Gunn. *Condensation of Composite Bosons in a Rotating BEC*. Phys. Rev. Lett. **84**, 6, 2000. doi:10.1103/PhysRevLett.84.6.
- [WS89] F. Wilczek and A. Shapere. *Geometric Phases in Physics*. World Scientific Publishing, Singapore, 1989.
- [WZ84] F. Wilczek and A. Zee. *Appearance of Gauge Structure in Simple Dynamical Systems*. Phys. Rev. Lett. **52**, 2111, 1984. doi:10.1103/PhysRevLett.52.2111.
- [ZR99] P. Zanardi and M. Rasetti. *Holonomic Quantum Computation*. Phys. Lett. A **264**, 94–99, 1999. doi:10.1016/S0375-9601(99)00803-8.
- [ZWD07] S. L. Zhu, B. G. Wang, and L. M. Duan. *Simulation and Detection of Dirac Fermions with Cold Atoms in an Optical Lattice*. Phys. Rev. Lett. **98**, 260402, 2007. doi:10.1103/PhysRevLett.98.260402.

# List of Publications

The results of the present thesis have generated the following publications:

- *Double and negative reflection of cold atoms in non-Abelian gauge potentials*  
G. Juzeliūnas, J. Ruseckas, A. Jacob, L. Santos, P. Öhberg  
Physical Review Letters **100** 200405 (2008)
- *Landau levels of cold atoms in non-Abelian gauge fields*  
A. Jacob, P. Öhberg, G. Juzeliūnas, L. Santos  
New Journal of Physics **10** 045022 (2008)
- *Cold atom dynamics in non-Abelian gauge fields*  
A. Jacob, P. Öhberg, G. Juzeliūnas, L. Santos  
Applied Physics B **89** 439-445 (2007)



# Acknowledgements

This thesis would not have been possible without the help of a number of people whom I would like to thank here. First of all I would like to express my gratitude to Prof. Dr. Luis Santos for giving me the opportunity to work in his broadly interested and very active research group over the past few years. I thank him for the quality of his guidance, his patience and his trust.

Furthermore, I would like to thank our co-workers, especially the group of Dr. Patrik Öhberg, Michael Merkl and Frank Zimmer, for their hospitality while working in Edinburgh. I thank Prof. Dr. Gediminas Juzeliūnas for the inspiring collaborations throughout the years. I am grateful to Prof. Dr. Eberhard Tiemann who supported me in the European Graduate College *Interference and Quantum Applications*. I would also like to thank Prof. Dr. Ernst Maria Rasel for his questions from an experimental point of view and for being the co-referee for my thesis, as well as Prof. Dr. Manfred Lein for being the chairman for the disputation.

I thank my colleagues from the University of Stuttgart and University of Hannover who created a pleasant as well as inspiring atmosphere. Of my Stuttgart colleagues I especially thank Subhasis Sinha and Stefano Giovanazzi for their company and some awesome dinners. In particular I have to thank Rejish Nath, it was always fun to work with you. As for the Hannover team, I am grateful to the whole group: Rejish Nath, Michael Klawunn, Garu Gebreyesus, Karen Rodriguez, Giovanni Mazzeola, Ulrich Ebling and Philipp Hyllus. Thank you for your feedback, suggestions and just being around. I am also thanking the relatively new members of our group, Maria Colomé-Tatché, Frank Deuretzbacher, Kazimierz Łakomy and Alexander Pikovski for their nice company and interesting discussions, and of course all the people I got to know at the Institute of Quantum Optics, especially Yesh Pal Singh, Naceur Gaaloul and Andreas Gerdes. I thank Carsten von Zobeltitz and Alex Cojuhovski for keeping the computers running, Tobias Wirth and Martin Paech for their help with tricky latex problems, as well as Alexander Seel. Furthermore, I am grateful to Mirjam Krause and Ralf Jacob for reading the draft.